A THERANOSTIC BIO-DEVICE FOR BIOMEDICAL APPLICATIONS

A THESIS SUBMITTED TO

THE GRADUATE SCHOOL OF ENGINEERING AND SCIENCE

OF BILKENT UNIVERSITY

IN PARTIAL FULFILLMENT OF THE REQUIREMENTS FOR

THE DEGREE OF

MASTER OF SCIENCE

IN

MATERIALS SCIENCE AND NANOTECHNOLOGY

By

NEDIM HACIOSMANOĞLU

August 2019

A THERANOSTIC BIO-DEVICE FOR BIOMEDICAL APPLICATIONS

By Nedim Hacıosmanoğlu

August 2019

We certify that we have read this dissertation and that in our opinion it is fully adequate, in scope and in quality, as a thesis for the degree of Master of Science.

Urartu Özgür Şafak Şeker (Advisor)

Sreeparna Banerjee

Serkan İsmail Göktuna

Approved for the Graduate School of Engineering and Science:

Ezhan Karaşan
Director of the Graduate School

ABSTRACT

A THERANOSTIC BIO-DEVICE FOR BIOMEDICAL APPLICATIONS

Nedim Hacıosmanoğlu

M.S in Materials Science and Nanotechnology

Advisor: Urartu Özgür Şafak Şeker

August, 2019

Biological systems are programmable by their nature. With using the abilities of these systems, scientists have designed, engineered and repurposed living machines for various tasks including biological sensing, recording of cellular events, drug production and disease treatment. Compared to the current methodology for these tasks, engineering biological systems provide a promising tool for the future of medicine, especially in the case of disease treatment. Type II Diabetes Mellitus (T2DM) is a medical condition which occurs by the deficiency of insulinotropic hormones inside the body, and affects nearly half billion people worldwide. Treatment strategies for this disease includes monitoring patient for blood glucose levels, fine production of insulinotropic hormones and providing dose-controlled treatment for the patients. All these operations increase the cost of the treatment and cause a global problem for both medical professionals and the patients. In this thesis, we propose novel systems for developing theranostic strategies for T2DM by using synthetic biology principles and genetically controlled sense-and-response cascades inside living cells. Proposed systems include a whole-cell glucose biosensor module, which can detect glucose

concentrations by using internal glycolysis machinery of a probiotic *Escherichia coli* (*E. coli*) bacteria, and a release module, which can controllably secrete therapeutic molecules from the *E. coli* cell surface. To do that, we engineered an enzyme based biosensor module which takes the pyruvate synthesized as a result of glycolysis and turns that molecule into hydrogen peroxide via SpxB pyruvate oxidase enzyme to later detect that signal with an optimized hydrogen peroxide biosensor. In order to later incorporate this biosensor with a release mechanism, we designed and engineered an Antigen-43 (Ag43) autotransporter based peptide release system. In that system, we used Ag43 autotransporter fused GLP-1 peptide, an insulinotropic hormone for the type II diabetes treatment that is controllably displayed on the cell surface. Another Ag43 fused protein, TEV protease, with a different control mechanism is also cooperated in the system to release GLP-1 from the surface by cutting the peptide from its recognition site. Taking the ability of glucose sensing and the successfully engineered release mechanisms, our proposed system has a huge potential to be used as an alternative system for treatment of the T2DM.

Keywords: Synthetic biology, Whole cell biosensor, Protein release, Living therapeutics

ÖZET

BİYOMEDİKAL UYGULAMALAR İÇİN TEŞHİS VE TEDAVİ BİYO-ARACI

Nedim Hacıosmanoğlu

Malzeme Bilimi ve Nanoteknoloji, Yüksek Lisans

Danışman: Urartu Özgür Şafak Şeker

Ağustos, 2019

Biyolojik sistemler doğaları gereği programlanabilirdir. Bilim insanları bu sistemlerin yeteneklerini kullanarak biyolojik teşhis, hücresel olayların kaydedilmesi, ilaç üretimi ve hastalık tedavisi gibi konular için "yaşayan sistemler" tasarlamış, geliştirmiş ve bu ilaçları yeniden amaçlandırmıştır. Bu amaçlar için kullanılan güncel yöntemlerle kıyaslandığında biyolojik sistemler mühendisliği tıbbın ve özellikle hastalık tedavisinin geleceği için umut verici bir araç sunmaktadır. Tip 2 diyabet (T2D) vücutta insülinotropik hormonların eksikliğinden kaynaklanan ve dünya genelinde yarım milyar insanı etkileyen bir hastalık durumudur. Bu hastalığın tedavi stratejileri hasta kanındaki glikoz seviyelerinin izlenmesini, insülinotropik hormonların ilaç kalitesinde üretilmesini ve hastaya dozaja göre uygulanmasını kapsar. Tüm bu operasyonlar tedavinin fiyatını arttırmakta ve hem sağlık profesyonelleri hem de hastalar için global bir problem oluşturmaktadır. Bu tez çalışmasında biz, T2D için sentetik biyoloji prensipleri ve genetik mühendisliğine dayalı hücre içi duyu ve cevap yolaklarını kullanan özgün sistemler önermekteyiz. Önerilen stratejiler, *Escherichia coli* (*E. coli*) bakterisinin hücre içi glikoliz mekanizmasını kullanan ve glikoz miktarını

belirleyebilen bir tüm hücre biyosensör modülünü, ve hücre yüzeyinden kontrollü şekilde tedavi edici moleküler salgılayabilen bir salınım modülü içermektedir. Bu amaçla glikoliz sonucu üretilen piruvatı hidrojen perokside çeviren piruvat dehidrogenaz enzimi SpxB kullanılmış ve sonrasında üretilen hidrojen peroksiti algılayabilen geliştirilmiş bir tüm hücre biyosensörü oluşturulmuştur. Bu biyosensörün oluşturduğu sinyalin ise daha sonraki aşamalarda hücre içerisinde ilişkilendirilmesi için Antijen-43 (Ag43) ototransporterine bağlı hücresel salınım sistemi geliştirilmiştir. Bu sistemde T2D tedavisinde kullanılan insülinotropik GLP-1 hormonu ile birleştirilmiş Ag43 ototransporteri kontrollü olarak hücre yüzeyinde ifade edilmiş, farklı orijinli bir model Ag43 ototransporterinin kontrolüyle ise birleştirildiği TEV proteaz enzimi ile GLP-1 hormonunun TEV tanınma bölgesinden kesilip ortama salınması sağlanmıştır. Glukoz tespit sistemi ve başarıyla çalıştırılan cevap mekanizması göz önüne alındığında oluşturduğumuz sistem T2D tedavisi için büyük bir potansiyel taşımaktadır.

Anahtar Kelimeler: Sentetik biyoloji, Tüm hücre biyosensörleri, Protein salımı, Yaşayan ilaçlar

Acknowledgements

I would first like to thank to my thesis advisor, Dr. Urartu Özgür Şafak Şeker, for his guidance and mentorship, also providing me an opportunity to work in Synthetic Biosystems Lab (SBL) and providing us a scientific environment that we can compete with world-class research. I would also like to thank Bilkent University's Materials Science and Nanotechnology (MSN) Graduate Program members and staff for their continuous support during my study. In addition, I would like to thank Dr. Sreeparna Banerjee and Dr. Serkan İsmail Göktuna for their valuable time and being jury members in my thesis defence. Besides, I would like to thank Dr. Ömür Çelikbıçak for his assistance and guidance during mass spectrometry analyses that we operated in HUNITEK.

I am grateful and delighted to meet all the senior researchers of our laboratory including Dr. Esra Yuca, Dr. Ebuzer Kalyoncu, Dr. Tolga Tarkan Ölmez and Dr. Elif Duman. I am thankful for their continuous support during troubleshooting the problems in my experiments, and also supporting me morally to continue my research. I would like to thank every member of SBL for being such smart and hardworking researchers. During the time, I spend in SBL, all these brilliant scientists worked so hard, helped me for every kind of my problems, and show amazing skills of creativity, although most of the time fighting alongside with living and health problems on their own. I wish best for all these people for the rest of their lives, and I am already excited to be colleagues with them in the future. In person, I would like to thank Recep Erdem Ahan and Ebru Şahin Kehribar for being such great researchers and helping me on biological design, alongside being such good friends. I would like to specially thank Behide Saltepe

for sharing her research experiences with me during the first years of my study, and later our resulted and (almost) published work. I would also like to thank Cemile Elif Özçelik, Efe Musa Işılak, Büşra Merve Kırpat, Sıla Köse, Özge Begli, and Merve Yavuz for their friendship and support during my thesis. I can write a whole page of my gratitudes for all these people individually, but I want to say that I will always be grateful for all of them to make me believe that we can compete with the scientists from around globe in the topic of synthetic biology. I would also like to thank new members of our lab, Julian Ostaku, Zafer Koşar, Merve Erden, Eray Ulas Bozkurt and Gökçe Özkul for their friendship for the last year. I believe that after their thesis, they will be great researchers.

Before finish, I would like to thank all my family members, especially my father Hilmi Hacıosmanoğlu and my mother Filiz Hacıosmanoğlu, for their endless support during their only son's adventure into the unknown world of molecular biology. Besides, I would also like to thank beloved members of Kutanis family from always being my greatest moral support during my education. Without them, this thesis would never have an end. Lastly, I would like to thank our Great Leader and Eternal Commander Mustafa Kemal Atatürk for his great vision on young Turkish Republic. His ideals turned Ankara from a small city of Anatolia to a world capital which resulted with founding top universities of our country here, and a world-class research environment that gave me a chance to pursue my dreams. My loyalty to his ideas will always be an honour for me.

This study is supported by Turkish Academy of Sciences, Science Academy.

Table of Contents

List of Figures

List of Tables

CHAPTER 1

INTRODUCTION

Repurposing biological elements is the newest form of engineering since it harbours many of the well-known principles from the field. From an analytical perspective, insights of molecular biology shows most prominent examples of cellular structures and chemical reactions where design and engineering meets in a highly optimized and effective manner. After the emergence of biotechnology in the late 80's and development of screening and testing tools, scientists started to use knowledge derived from living systems for the sake of humanity, and recently, this knowledge increased enough to redesign and create complex systems for many different tasks. Starting from bio-mining to biological computing (Figure 1), synthetically designed living systems emerged on many different fields to contribute human good [1-3].

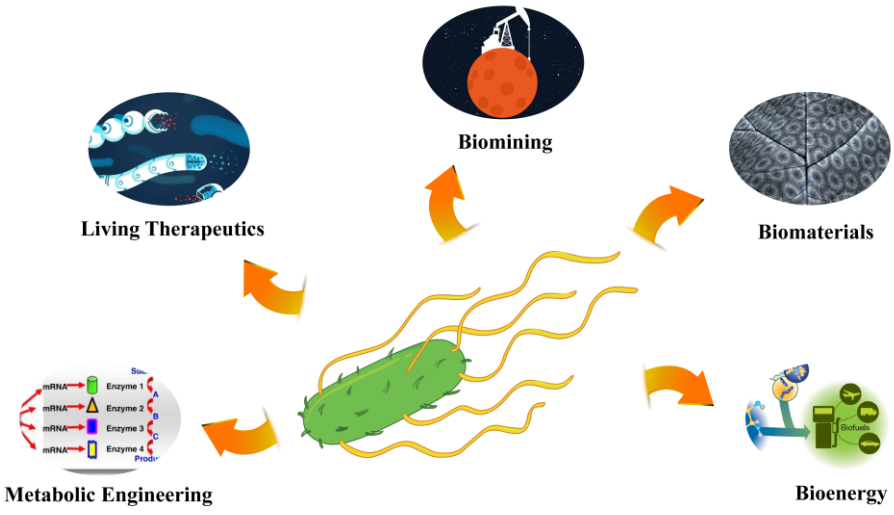

Figure 1: Application fields of synthetic biology

Among these fields, a concept named as “living medicines” or “living therapeutics” has gained huge attention since the overall perspective may provide a cheaper and better alternative for the all known therapies for different diseases [4, 5]. Main power of this new approach lies on the principles of synthetic biology, and applied smart-design principles which eventually creates theranostic bio-devices [6, 7]. Synthetic biology is a newly developed research field which is aiming to discover, redesign and utilize biological elements by combining them separately as parts of an electronic device [8, 9]. This utilization creates amazing flexibility to the researchers which can eventually resulted by development of optimized biological parts such as biological sensors, genetic recorders, production and delivery systems (Figure 2) in addition to chassis development strategies like biological containment and genome modifications [10-15].

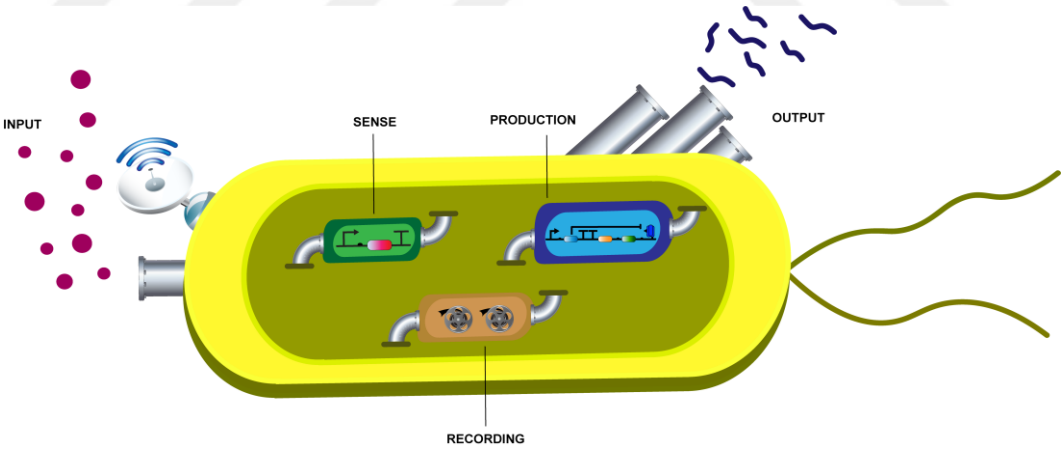

Figure 2: Main design elements on living therapeutics that are representing special duties assigned to biological systems

These genetic tools or modules can be separately used or may incorporated for high level machineries. As for derived from them, living organisms are the main chassis to plug and play those modules and their variety is ranging from

prokaryotes to archaea and mammalian cells, although this is also about to change by cell-free systems. When it comes to probiotics among these chassis, our ability to engineer them becomes more and more important with the emerging genetic technologies. Probiotics could simply be described as microorganisms that are living residents in our body and contribute to the many health benefits for us. As a very hot topic on current research, human probiotics and human microbiota gained huge attention since their positive effects including immune system boosting, defending body against pathogens and synthesizing some of the supplementary molecules revealed clearly [16, 17]. If we could see those probiotics from the side of a biological designer, they provide an amazing chassis for further operations due to their natural abilities including naturally colonizing gastrointestinal system and being invisible for the immune system [18, 19]. Besides, biological tools which are designed for wild type bacterial strains can also be used for the probiotics, and for many cases, these tools can be used between different bacterial strains [20, 21]. As micro-scale machineries that can mainly colonize human gastrointestinal system and having a large portfolio of genetic modules, probiotics are the most suitable organisms to transform medicine and the fate of diseases. From the perspective of medicine, problems on disease treatment has entered a new era that cost of diagnostics and modulation of treatment strategies becomes a challenging task for the medical professionals. Evolving of infectious diseases and lack of optimized or personalized therapy for the patients is a huge problem that humanity is about to face with in the future. Among the recent effort (Figure 3) on optimization for the disease treatment, living medicines are the ones which showing great diversity on the application

scale [22]. Although the probiotics are mainly inhabiting the gastrointestinal tract, they can be implemented against metabolic, infectious and, autoimmune diseases, and even against cancer [23]. For instance, in a recent study on hypertension, a probiotic strain (*Lactobacillus plantarum* NC8) engineered to secrete a modified peptide and that treatment successfully reduced blood pressure in rats [24]. In an another work, engineered *Lactobacillus lactis* equipped with a sensor module to sense metabolic molecules from an enterotoxic bacteria, *Enterococcus faecalis*, and respond this stimulus with a bacteriocin that can kill *E. faecalis* [25]. On the other hand, *Bifidobacterium longum* probiotic is also engineered to deliver proliferation inhibiting drugs for the cancer treatment [26].

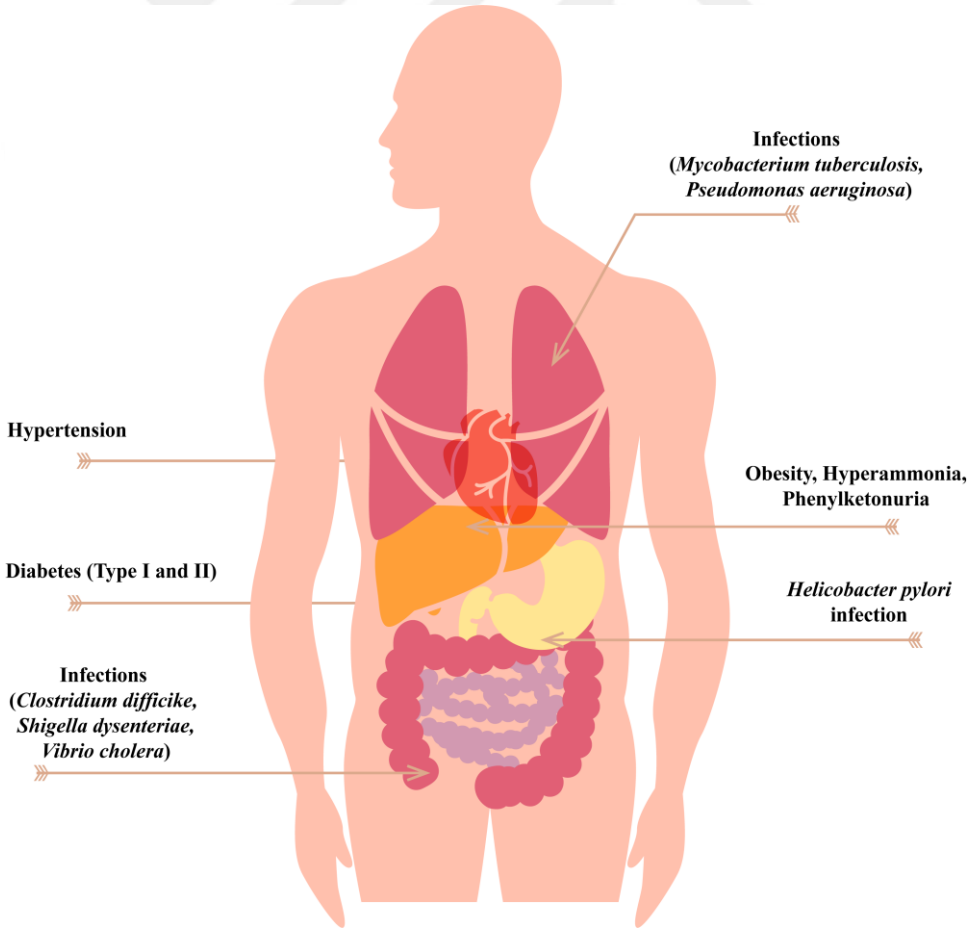

Figure 3: Different diseases that are targeted by living therapeutics

1.1. Escherichia Strain Probiotics: *Escherichia coli* Nissle 917

Among these probiotic strains that are showing some of the state-of-art examples of living therapeutics design, one probiotic strain is having the title of "workhorse" since its ability to harbour most of the well-characterized genetic modules, and being handy for genetic manipulations with variety of tools. *Escherichia coli* (*E.coli*) Nissle 1917 (EcN) is a bacterial strain which is isolated and used as a probiotic since the beginning of 1920's [27]. In addition to that, this strain could be presented in the feces in a very high concentration since its ability to adopt gut microflora by metabolic characteristics. Despite being presented in high amounts in large intestine, EcN is reported to be safe for the human body from the site of causing any inflammatory effects. In the literature, EcN is encountered for various tasks as a suitable chassis candidate for a living therapeutic due to above mentioned properties. In recent works, EcN reported to be used for the prevention of *Vibrio cholerae* virulence, to target pathogens with antimicrobial peptides, and for killing colorectal cancer cells [28-30]. As mentioned, all these studies showing that EcN is a very useful chassis for developing novel systems and using the well-characterized tools of synthetic biology to achieve complicated operations which never operated from a complex cascade before. Besides, flexible and well-characterized engineering techniques could allow us to develop personalized living medicines with probiotic bacterial strains in a shorter time compared to the current production and treatment strategies.

1.2. Type II Diabetes: Current Therapies and Advancements

Diabetes mellitus is a metabolic disorder that is caused from deficiency of insulin secretion or decreasing/demolishing of insulin action in the body. There are two main forms of diabetes mellitus known as Type I diabetes mellitus (T1DM), and Type II diabetes mellitus (T2DM), which is observed in 95% of the diabetes cases [31, 32]. The problem in T2DM generally encounters with the mismatch in insulin production with lipid, carbohydrate and protein metabolism, and eventually, emergence serious health problems for the individuals [33]. There are many factors which are influencing T2DM development in the patients. Although the mechanism is not clearly understood, genetic content is considered as one of the major influences [34]. Research on certain genetic regions with genome wide association studies showing that there is a high correlation for genes involving β-cell development and metabolic regulation [35]. In addition, living style is also a very important factor for the development of T2DM [35]. Recently, it is also shown by metagenome-wide association studies that gut microbiota has showing characteristic changes in T2DM patients, and this change leads to development of the disease by altering vitamin and carbohydrate metabolism [36].

By the 2050, it is estimated that there will be half billion patients who are suffering from T2DM or the complications, and these life-quality decreasing medical conditions include cardiovascular diseases, retinopathy, neuropathy, nephropathy, and even different types of cancer [37-39]. When all these conditions and their possible load for the global medical care considered, adopting

the concept of living medicines as an alternative treatment or preventive strategy for the T2DM becomes very important for the future of humanity. Current treatment strategies for T2DM include non-insulinotropic drugs (including Glucagon-like peptide 1 (GLP-1)) and Insulin or Insulin analogs. Detailed information about medical treatment standarts and usage of these drugs can be found at "Standards of Medical Care in Diabetes" published by American Diabetes Association [40]. Among these drugs, usage of Insulin and GLP-1 is a debated topic among different applications since they provide the most efficient treatment strategies. In their action, insulin works on body homeostasis by acting on his cognate receptor, and GLP-1 is an effector that promotes insulin secretion [41]. Current research on treatment strategies for T2DM includes combinatorial therapies with both insulin and GLP-1, viral therapies for insulin and other. In addition to these strategies, there are also some examples from the literature that are aiming to generate new technologies for T2DM therapy by using synthetic biology and living therapeutics. In the literature, probiotics including *Lactobacillus gasseri*, and *Lactobacillus paracasei* engineered before to produce GLP-1 inside human body [42, 43]. Advantage of using GLP-1 for the treatment of T2DM is coming from its promising pharmacokinetics that is preventing hyperglycemia and other side effects [44]. Current research and therapies are lacking a theranostic strategy that can adjust delivered drug levels and ability to be useful for combinatorial therapies. Our strategy is suitable for solving both of these issues in T2DM due to highly utilized genetic modules that are derived from current synthetic biology repertoire.

1.3. Genetic Tools to Design a Bio-Device: Whole Cell Biosensors

By the definition, “biosensor” is a device which can sense the environmental signals by using biological elements [45]. Living systems are good examples of biosensors since giving response to the signals coming from the environment is very crucial for their survival. When a living organism itself used as a biosensor device by employing its whole cellular machinery, it is known as a “whole-cell biosensor”. With the emergence of biotechnology, scientists started discovering and engineering core elements that are responsible from this sensing function and later, whole cell biosensors emerged as better alternatives for other sensing technologies. Core element of a whole-cell biosensor is known as “promoter”, and a promoter is simply a deoxyribonucleic acid (DNA) part that is naturally controlling the expression of a gene inside the genome [46]. By driving the expression to a reporter, which is an analytically measurable biological molecule (i.e., fluorescent or luminescent proteins), whole-cell biosensors can report various chemicals in their environment [47]. From the side of living therapeutics, this is a huge advantage since very few of the current treatment strategies are incorporating drug production and detection strategies with the treatment in a single, autonomous device. There are three main strategies to design a whole cell biosensor, and all of these strategies mined from the living systems. In this thesis, we will discuss and use two of these strategies including two component systems (TCS) and transcription factor (TF) based biosensors.

1.4. Two Component Systems

In living systems, signalling pathways are used to convert chemical or biological signal to the messages that can downstream genetic machinery can understand and respond. This strategy forms the basic function of life. Due to that, there are many mechanisms that are specifically developed for signal transduction. Two-component systems are well-known signalling pathways that are presented with many different forms in prokaryotes to eukaryotes [48, 49]. Generally, a two-component system is composed of a kinase, which is generally located in outer or inner membrane to receive specific molecules, emit signal to downstream pathway by changing its kinase activity and phosphorylating the effector, and an effector molecule, which gets the signal from kinase and activates a specific promoter by binding its cognate promoter region. TCSs have many different applications as sensor modules due to their simplicity and well-characterized function. For instance, TCSs used in the literature for many different applications including optogenetics and heavy metal sensing [50, 51]. Most of these studies using engineered version of EnvZ TCS kinase. In his pioneering work, Dr. James Baumgartner engineered bacterial EnvZ-OmpR two component system with a periplasmic glucose binding protein and its effector to detect changing glucose concentrations in *E. coli* bacteria [52]. This study later repeated by Dr. Jan T. Panteli to utilize the design for the same purpose [53]. Although having low specificity that causes false signals, complex design that causes metabolic burden and narrow dynamic range that limits detection, these two studies are showing the potential of TCSs as biosensor systems.

1.5. Transcription Factor Based Biosensors

Transcription Factors are protein molecules that can interact with a specific promoter and assist promoter to control transcription of specific gene/gene clusters. In addition to these, they can respond to specific molecules by binding, changing conformation and by altering their activity. Just like an electrical circuit, by changing the types of promoters and TFs with plug-and-play fashion, these molecules can be used to generate or multiplex many different whole cell biosensors. In theory, one TF can be used to engineer one biosensor, and in nature, thousands of different TFs working inside cells to regulate metabolism by controlling and transmitting cellular signals [54]. This flexibility and diversity allow scientists to engineer many different TF based whole-cell biosensors. Although TFs are widely used systems for biosensors, they have some limitations due to their nature. Firstly, although the diversity is high, there is only a limited number of TFs available for specific molecules [55]. Secondly, off-target activity of TFs upon different promoters may cause serious problems for the TF based biosensor operations [56]. Finally, same TF can be activated by different inducers. With the emergence of synthetic biology, second and final problem about TF based biosensors resolved by engineering internal promoter elements (transcription initiation region, TF binding region etc.) and ribosome binding sites (RBSs) or engineering TFs [57]. For the first problem, Libis and colleagues developed a unique approach that involves enzymes to convert molecules that cannot recognized by TFs to molecules that have a defined TF-promoter couple [55]. With that, this study doubled the known repertoire of TF based biosensors. This strategy promises a great opportunity to design unique sensor and response

systems for living therapeutics, if coupled with release systems and designer proteins.

1.6. Genetic Tools to Design a Bio-Device: Designer Proteins

Proteins are the building blocks of biology. Depending on the organism, pathway or genetic combination, they can occupy different functions inside cells. With the development of cloning and sequencing techniques, scientist characterized functions of various proteins by adopting different strategies including deletion, fusion and sequence shuffling to identify functions of the specific regions of the proteins [58]. These proteins are also known as recombinant proteins. After that, these characterized regions again used for many different applications to give proteins new functions and properties. One of the well-known example of this technique is generation of antibodies with different chains to obtain enhanced functions and therapeutics [59]. In addition to binding properties, different functions can be introduced to proteins by fusing specific proteins or protein tags. This strategy allows scientists to relocalize, live-track, release, and process proteins in a controllable fashion [60, 61]. Knowing the principles of these processing strategies could build the response molecules for living therapeutics with state-of-art strategies.

1.7. Fusion Proteins and Release Strategies

Releasing specific proteins with a controllable manner from the bacterial cells is a long lasting goal of scientists since the overall idea can simplify protein

purification processes dramatically. Tremendous effort has been shown to characterize and design proteins, protein tags and other systems (membrane leakage, cell lysis etc.) to release proteins from the cells as final products [62]. Recent technologies have also evolved to use these genetic tools as modules to incorporate in biological design. From the side of living therapeutics design, release systems are critical tools to build a response module to incorporate with processed signal. In *E. coli*, there are highly optimized tools for protein or peptide release to the extracellular environment [63]. Many of these strategies involve fusion of target proteins with either specific transporter proteins from SEC or TAT transportation systems, or naturally secretable proteins such as YebF [63, 64]. Although these tools provide useful strategies to send target proteins to the extracellular environment, they are generally lack of precise control and titratable release strategies. Recently, a different class of proteins known as autotransporters employed to design cell display and release strategies, in order to solve the above mentioned problems. Naturally, this class of proteins are transported to the periplasmic space and later translocated on outer membrane by folding. By designing fusion proteins with an autotransporter, display of different proteins can be achieved [65]. As an additional tool, site-specific proteases also incorporated in recent studies to precisely control protein release from displayed autotransporters [66]. Overall, protease mediated release strategy from autotransporter fusion proteins could compose one of the best response modules to drive biosensor responses to design sense-and-response cascades for future living therapeutics. Besides, these strategy could be best suited for multiplexing the type of released products.

1.8. Protein Processing with Site Specific Proteases

Proteases are the class of proteins which are known with their ability of cutting or degrading different proteins and/or peptides. Among these proteins, a subclass known as site-specific proteases (SSPs) are gained attention due to their ability of recognizing specific amino acid sequences and cutting the peptide bond from a specific point [67]. This property have applications ranging from affinity tag removal to transcription control, and also promising a special tool for designing protein release strategies [68, 69]. Tobacco Etch Virus (TEV) protease is a well-known example of SSPs which derived from viruses and used to cut peptide bond among proteins between Arginine (Q) and Glycine (G) amino acids of ENLYFQG recognition site [70]. In a very recent study, Ag43 fused TEV protease co-expressed with Ag43 fused cargo proteins to successfully deliver target proteins to the environment with a self-actuated, logic gate embedded protein delivery machinery [66]. Considering autotransporter mediated display and TEV protease controlled release strategies, this strategy promises a prominent tool to design controllable release strategies if fused with biological sensors or other control strategies

1.9. Characterization of Fusion Proteins via Folding Tools

In addition to wet lab experiments, there are also many in silico tools to characterize fusion proteins before embedding into the living systems. These computational methods could provide useful information about protein folding

and ligand binding before cloning the engineered constructs. Swiss-Model is a widely used, web-based server to determine homology models of designed protein structures [71]. Although the server is useful to predict small tags with a short run time, it is not useful for larger fusion proteins which does not have crystal structures. I-TASSER is considered as a better alternative for structure prediction of large fusion proteins due to its optimized energy-minimization algorithm for folding pattern prediction [72]. After design and in silico folding for designed proteins, docking studies may require to predict their activity and modification-dependent conformational changes. Docking is a computational method to send target molecules on native or designed proteins to calculate binding energies and estimate affinity for a specific molecule. Autodoc Vina is the most cited docking software in the literature which uses a hybrid scoring system and optimized energy minimization for scoring the binding candidates [73]. As an alternative, web based docking tool, Swiss-Dock and HPEPDOCK servers can be used for fast estimations of binding molecules [74, 75]. With its user-friendly interface and interconnected library with chemical databases, Swiss-Dock could provide a preliminary platform to easy test designed constructs for their ligand binding score. HPEPDOCK is on the other hand, a peptide docking server that can use peptide sequence as an input and derives successful docking strategies by using iterative model generation to give docking results on protein-peptide interactions. As an alternative strategy, computational techniques could be very useful tools to make intelligent guesses on biological design preliminary to production steps and also to discover alternative regulation strategies for fusion proteins in addition to be be less expensive and more analytical characterization techniques.

1.10. The Aim of Study

Although there are different attempts to generate living therapeutics for the T2DMs, literature is lacking of high specificity, theranostic and multiplexible modules for biological design. In this thesis, we are aiming to generate engineered genetic circuits that can measure glucose levels in human gut and that can be controlled to release therapeutic GLP-1 hormone to the cellular environment. To achieve this, cellular modules of glucose biosensor and peptide release system defined and different strategies proposed to equip bacteria with these modules. Our first module aimed to detect glucose concentrations in physiological levels by measuring the hydrogen peroxide generation inside the cell as a product of glucose consumption. In that system, it is aimed to use SpxB enzyme which can convert glycolysis product of glucose, pyruvate, to hydrogen peroxide, for later detecting this signal with an engineered hydrogen peroxide biosensor part. On the other hand, our second module is aimed to release therapeutic peptide molecules by an engineered, Ag43 autotransporter protein based release strategy which produces Ag43 fused TEV protease to release again controllably displayed, Ag43 fused GLP-1 peptide. By these proposed strategies, we are aiming to contribute synthetic biology toolbox to build a living therapeutic for the treatment of T2DM.

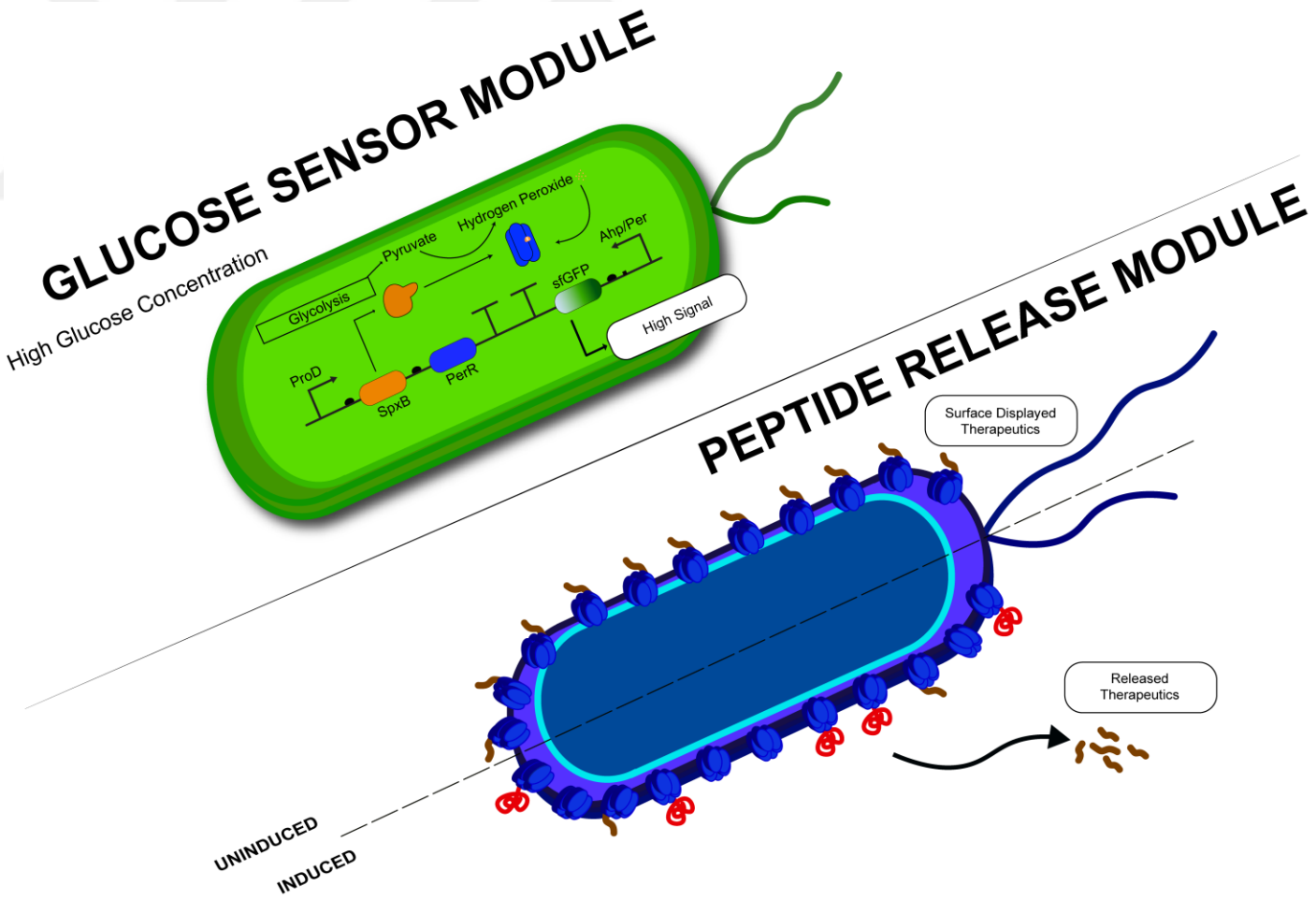

Figure 4: Main design strategy of our proposed systems; glucose sensing module and release system module illustrated together

CHAPTER 2

MATERIALS AND METHODS

2.1. Bacterial Strains, Growth and Maintenance

For cloning and characterization purposes, *Escherichia coli* (*E. coli*) DH5α strain used as the main chassis. Primary cell stocks are stored in -80 ˚C with storage medium (Lysogeny Broth, LB (Appendix E1) with 25% Glycerol). This bacterial strain is specially developed for cloning purposes by mutating some of the endonucleases, and provide a better alternative for long term storage with plasmid vectors. For the production of proteins and T7 promoter induction experiments, *E. coli* BL21(DE3) strain used. Different from the other strain contains, this strain has T7 polymerase and LacI repressor, which are necessary to activate and control T7 promoter upon induction with IPTG (Isopropyl ß-D-1-thiogalactopyranoside). In addition to that, strain is knocked out for some proteases for protein overproduction. *E. coli* JW3367-7 is a knockout strain that is purchased from Coli Genetic Stock Center and has ΔenvZ738::kan mutation. Probiotic strain *E. coli* Nissle 1917 is isolated from Mutaflor® pill by dissolving pill powder in 10 mL distilled and autoclaved water, streaking the dissolved powder on LB Agar plate (Appendix E1) to obtain a single colony and by selecting a single colony to grow overnight in LB medium for preparing primary stocks to proceed with further experiments. Isolation of *E. coli* Nissle 1917 cells verified by a strain specific PCR (Polymerase Chain Reaction) as previously described [76].

2.2. Chemical Transformation of Bacterial Cells

Bacterial cells are chemically transformed to clone, test and maintain plasmid constructs. To prepare chemically competent cells, primary cell stocks grown in LB medium at 37 ˚C, 200 rpm for 16 hours. After that, cells inoculated in 1:100 volume of fresh LB medium and grown until an OD_{600} of 0.2-0.4 value. Then, cells cooled in ice for 10 minutes, and centrifuged down in 3000 rpm for another 10 minutes. Finally, supernatant removed from the centrifuged cells and cell pellet dissolved in 1:10 growth volume of TSS buffer (Appendix E2). Cells stored in -80 ˚C for further experiments. For the transformation of plasmids, competent cells ice thawed for 20 minutes and gently mixed with 1-100 ng plasmids, or with ligation mix for the T4 ligation (Appendix E3), or with Gibson Assembly Mix (Appendix E4) for the cloning. After inoculation for 30 minutes, heat shock applied at 42 ˚C for 30 seconds. Then, cells inoculated on ice for 2 more minutes before addition of 1 mL SOC (Super Optimal Broth with Catabolite Repression) medium (Appendix E5). As final step, cells grown with SOC medium for 1 hour, centrifuged down at 8000 rpm for 5 minutes and spreaded on LB Agar plates with relevant antibiotics.

2.3. Cloning of Plasmid Vector Constructs

In order to clone pET22B-T7-Ag43-GLP1 construct, template plasmid pET22B-Ag43-αβ40 (built before by our lab member Cemile Elif Özçelik) digested with AflIII and SpeI to obtain 7.9 kb plasmid backbone. In order to obtain GLP-1 insert, Ag43 gene with TEV cut site amplified with forward REA21 and reverse

Ag43-GLP1-FOR-1, Ag43-GLP1-FOR-2, Ag43-GLP1-FOR-3 primers to obtain Ag43-GLP-1 gene by extension PCR as 2729, 2765 and 2800 bp fragments. pET22B-Ag43-αβ40 plasmid again use as template for 1st step of extension PCR with Ag43 gene. After that without visualizing fragments, GLP-1 insert amplified from this construct with GLP1-Lig-For and GLP1-Lig-Rev, as 183 bp fragment and digested with AflIII and SpeI to obtain 132 bp insert. Then this insert ligated to the backbone by T4 Ligase (NEB) by using 1:5 insert-backbone ratio. Backbone and insert visualized in 1% agarose gel by running in 140V for 30 minutes in 1XTAE buffer (Appendix E6). After that, fragments isolated from agarose gel and joined together with Gibson Assembly mix as described. Resulted Gibson mix transformed in *E. coli* DH5α for further characterizations by previously described chemical transformation method. Then, two colonies selected from resulted transformation plate, plasmid isolation protocol operated and plasmid samples send to the sequencing.

For cloning pET22B-T7-sfGLP1 construct, sequence verified pET22B-T7-Ag43-GLP1 plasmid digested with SpeI and 8 kb fragment directly used as backbone. To insert sfGFP, gene amplified from pET22B-T7-Ag43-sfGFP plasmid (previously built by Recep Erdem Ahan) with sfGLP1-F and sfGLP1-R primers as a 775 bp amplicon. DNA parts visualized in 1% agarose gel by running in 140V for 30 minutes in 1XTAE buffer. After that, fragments isolated from agarose gel as described. Backbone and insert joined together by Gibson assembly with using 1:3 backbone to insert ratio. Gibson mix transformed into *E. coli* DH5α cells by previously described method. Two colonies selected after transformation, grown for plasmid isolation with described procedure and plasmids send to the Sanger

sequencing for verification. To clone alternative GLP-1 analogs in pET22B-T7-Ag43-Exentin-4-Penetratin, pET22B-T7-Ag43-mGLP1-Penetratin, and pET22B-T7-Ag43-mGLP1-His plasmids, pET22B-Ag43-GLP1 plasmid digested before with AflIII and SpeI enzymes and 7.9 kb fragment used as backbone. Inserts that encoding Exentin-4-Penetratin (293), mGLP1-Penetratin (266 bp) and mGLP1-His (238 bp) genes ordered from IDT with backbone overlaps and inserted to the plasmid backbone by Gibson assembly with using 1:10 backbone-insert ratio. Gibson mix chemically transformed into *E. coli* DH5α. Plasmid isolation procedure operated as previously described and samples from two colonies send to the Sanger sequencing.

In order to clone pSR59.4-Trz1 plasmid, partial Trg receptor gene amplified from *E. coli* MG1655 genome by using NH1 and NH5-NW primers and 825 bp insert obtained. To obtain backbone, pSR59.4 plasmid (Addgene/63175, Dr. Jeffrey Tabor's lab) amplified with NH4-NW and NH6 primers and 5.3 kb backbone fragment obtained. DNA parts visualized in 1% agarose gel by running in 140V for 30 minutes in 1XTAE buffer. After that, fragments isolated from agarose gel as described. Two fragments joined together by 1:3 backbone to insert ratio Gibson Assembly. Selected colonies send to the sequencing for verification.

In order to clone pET22B-T7-GoX-Trx plasmid, GoX-Trx gene ordered from IDT as 4 fragment pieces with Gibson assembly overlaps. 4 fragments mixed in water to use as PCR template and amplified with GOX-PET22B-FOR and GOX-PET22B-REV primers as a 2290 bp amplicon. Backbone to generate this plasmid obtained by using a previously built pET22B-T7 expression plasmid by digesting with XhoI-KpnI and using the 5.2 bp fragment as backbone. DNA parts visualized

in 1% agarose gel by running in 140V for 30 minutes in 1XTAE buffer. After that, fragments isolated from agarose gel as described. Two fragments joined together by gibson assembly with using 1:2 backbone to insert ratio. Selected colonies then send to the sequencing for verification

For cloning the pET22B-PROD-OxyR-sfGFP-AhpCp1 plasmid, a previously built biosensor plasmid (built and kindly provided by Recep Erdem Ahan) digested with BamHI-SpeI and 6 kb fragment used as backbone to insert OxyR gene which amplified by Oxy6-Oxy7 primers and obtained as a 998 bp amplicon. DNA parts visualized in 1% agarose gel by running in 140V for 30 minutes in 1XTAE buffer. After that, fragments isolated from agarose gel as described. 1:3 backbone-insert ratio applied for joining two fragments with Gibson assembly. After verification of OxyR gene with colony PCR as a 998 bp amplicon by using PFU polymerase, new plasmid digested with XhoI-EcoRI to use as 6.2 kb backbone. sfGFP gene amplified with NH-ECNKO forward primer and three step of reverse primers (AhpCp1-1, AhpCp1-2, AhpCp1-3) to attach AhpCp1 synthetic primer with extension PCR. Final 876 bp fragment visualized and isolated from agarose gel to join together with backbone by Gibson Assembly by using standard protocol. After cloning, plasmids isolated and send to the sequencing for verification with described procedures.

In order to clone pZA-PROD-PerR-Ahp/Per-sfGFP, pZA backbone with PROD promoter (2.9 kb) amplified with pZA-H2O2-S3-For and pZA-H2O2-S3-Rev primers. Then PerR gene insert amplified from Bacillus subtilis genome with PerR-For and PerR-Rev primers as 511 bp amplicon. DNA parts visualized in 1% agarose gel by running in 140V for 30 minutes in 1XTAE buffer. After that,

fragments isolated from agarose gel as described. Two fragments joined with Gibson assembly by using 1:3 backbone-insert ratio. After verification of PerR with colony PCR by using insert primers, PerR carrying backbone (2.5 kb) amplified with pZA-H2O2-R-Rev1 and pZA-H2O2-BB-F primers. DNA parts visualized in 1% agarose gel by running in 140V for 30 minutes in 1XTAE buffer. In order to generate Ahp/Per hybrid promoter, sfGFP attached insert amplified by a 3-step PCR with forward pZA-H2O2-R-For1 primer and three set of revers primers named as AhpCp1-PerR-R2 (875 bp), AhpCp1-PerR-R2 (913 bp), and pZA-H2O2-Insert-R (953 bp). DNA parts visualized in 1% agarose gel by running in 140V for 30 minutes in 1XTAE buffer. After that, fragments isolated from agarose gel as described. Two fragments joined together with Gibson assembly by using 1:3 backbone to insert ratio. Selected colonies send to the sequencing for verification.

In order to build pZA-PROD-SpxB-PerR-Ahp/Per-sfGFP plasmid, previously built pZA-PROD-PerR-Ahp/Per-sfGFP plasmid digested with BamHI and 3.2 kb fragment used as backbone. To obtain SpxB insert, SpxB gene amplified from iGEM 2019 distribution kit by SpxB-For and SpxB-Rev fragments and 2007 bp amplicon obtained. Backbone and insert visualized in 1% agarose gel by running in 140V for 30 minutes in TAE buffer. After that, fragments isolated from agarose gel as described. Two fragments joined together by Gibson assembly by using 1:3 backbone-insert ratio. Insert checked with colony PCR by using insert amplification primers. To clone pZA-PROD-PerR-Ahp/Per-SpxB-sfGFP plasmid, SpxB-M2-BB-For and SpxB-M2-BB-Rev primers used to amplify 3.3 kb backbone from previously built pZA-PROD-PerR-Ahp/Per-sfGFP. SpxB gene

amplified from iGEM 2019 distribution kit by using SpxB-M2-For and SpxB-M2-Rev primers. Obtained 1898 bp amplicon used as insert and joined with backbone by using Gibson Assembly and 1:3 bacbone-insert ratio. After that, two colonies selected for sequencing and standard procedure applied.

In order to build pZS-PROD-SpxB-Ag43-sfGLP1 plasmid, pZS backbone amplified by REA97 and REA98 primers. PROD-SpxB module as first insert amplified by pZS-PRODMC-Rev and SpxB-EF as 2004 bp amplicon and Ag43-sfGLP1 gene obtained by using PELB-SpxBE-rev and Ag43-sfGLP1-pZS-For primers as 3474 bp amplicon. DNA parts visualized in 1% agarose gel by running in 140V for 30 minutes in 1XTAE buffer. After that, fragments isolated from agarose gel as described. These three fragments joined together with Gibson Assembly by using 1:3:3 backbone-insert 1-insert 2 ratio. Colonies checked by fluorescence to determine functionality. In order to build pZA-PROD-PerR-Ahp/Per-Ag43-TEV plasmid, previously built pZA-PROD-PerR-Ahp/Per-sfGFP plasmid amplified to obtain 2.6 kb backbone by pZA-H2O2-R-Rev1 and pZA-V3-Rel-BB-For primers. In order to amplify Ag43-sfGLP1 insert, pZA-V3-Rel-For and pZA-V3-Rel-Rev primers and 3369 bp amplicon obtained. DNA parts visualized in 1% agarose gel by running in 140V for 30 minutes in 1XTAE buffer. After that, fragments isolated from agarose gel as described. Two fragments joined together by Gibson assembly with 1:3 backbone to insert ratio. Positive colonies selected by colony PCR with insert primers.

Unless the otherwise stated, Polymerase Chain Reaction (PCR) procedures operated with NEB Q5 High Fidelity DNA Polymerase. Standard procedure provided by the company used for setting reactions. On the other hand, colony

PCR procedure operated with Pfu polymerase. Melting temperature (Tm) values for primers calculated by using NEB Tm calculator (http://tmcalculator.neb.com/). Gibson assembly procedure operated by using standard 50 ng backbone DNA in Gibson mix and insert DNA with predetermined backbone to insert ratio. Reaction set in one tube and incubated in 50 ˚C for one hour. After that, gibson mix transformed to the competent bacteria by previously described method. NEB T4 Ligase used during the ligation procedure. Standardized protocol provided by the company used to set up the reactions. After ligation, ligation mix transformed to the competent cells by previously defined chemical transformation procedures. Enzymatic digests operated by using NEB restriction enzymes and company's standard reaction protocols used. Agarose gel electrophoresis used to visualize PCR and digestion products. During the procedure, 1-2% agarose gel prepared by using agarose (Sigma-Aldrich) as v/w, that is dissolved in TAE buffer and melted in a microwave. To visualize DNA in agarose gel, SYBR SAFE (Thermo Scientific) DNA dye used. Gel extraction of visualized DNA operated by MN Gel Extraction kit and standard procedures used that is given by the company.

2.4. Plasmid Isolation and Sequencing

Plasmid isolation after cloning for characterization and other purposes has been done by using Thermo Scientific GeneJet® plasmid isolation kit by using standardized protocol with some modifications. In order to isolate plasmids, 2-5 mL of cell overnight growth centrifuged down at 11000 rpm for 3 minutes. After that, supernatant discarded and cell pellet resuspended in 200 µL Resuspension Buffer. Then, 200 µL Lysis Buffer added, cells gently mixed by inverting sample

tube 6-8 times, and incubated for 5 minutes in room temperature. Next, 250 µL Neutralization Buffer added on samples, sample tubes gently mixed again by inverting sample tube 6-8 times and the samples centrifuged down at 11000 rpm for 10 minutes. In next step, supernatant carefully removed and transferred to a spin filter DNA binding column. By using a vacuum chamber, supernatant that contains plasmids filtered and binded to the column. After that, column washed 2 times with Washing Buffer and spin columns centrifuged down at maximum speed for 3 minutes to remove residual liquids. As final step, columns dried in heat block at 60 ˚C for 2 minutes to evaporate alcohol contaminants, and plasmids eluted by using 20-50 µL, double distilled, sterile H_2O addition to the column. Additional 5 minutes of incubation applied with water and elution step made by centrifuging down columna at maximum speed for 2 minutes. Plasmid DNA stored in -20 ˚C for further use. Characterization of DNA amount has been operated by using Nanodrop® microvolume spectrophotometer. By using Nanodrop 2000 software>Nucleic Acid Characterization section, concentration of the isolated plasmids measured as ng/µL. By inspecting 230/260 and 260/280 ratio to, contamination of phenolic compounds and alcohol also investigated respectively. Sequencing samples send to the Genewiz company by preparing 50-100 ng/µL sample in 10 µL volume and mixing with 5 µL OF 5 µM sequencing primer. Sanger Sequencing service selected for readouts.

2.5. Sequence Alignment and Design

All the construct designs and alignments made with online Benchling software (http://benchling.com). Sequence files obtained from sequencing services of

Genewiz company uploaded to the Genewiz server as .ab1 or .seq files. From the control panel of the server, alignment option selected and MAFFT (Multiple Alignment using Fast Fourier Transform) algorithm used for creating analyses. Standard parameters used during the analyses.

2.6. Glucose Oxidase: Expression and Hydrogen Peroxide Production Test

Glucose Oxidase (GoX) enzyme cloned under T7 promoter in pET22B plasmid with previously described workflow and protein sequence verified by Sanger sequencing. After that, production of the protein induced by auto-induction medium (recipe available in the reference) with 16h growth at 200 rpm, 30 ˚C [77]. In order to test and functionally characterize dthe produced hydrogen peroxide via GoX, an enzyme based assay operated as described below.

Hydrogen peroxide production by the addition of glucose tested by ABTS (2,2'-azino-bis(3-ethylbenzothiazoline-6-sulphonic acid)) method. In that method, overnight induced cultures of wild type *E. coli* and *E. coli* BL21(DE3) strain that harbors T7 controlled Glucose Oxidase production plasmid centrifuged down at 8000 rpm for 5 min and washed 2 times with 1X PBS Buffer (Phosphate Buffered Saline, Appendix E). After that, GOX test buffer (Appendix E) that contains ABTS added on cells AS 250 µL final volume in a 96-well plate. In that assay, and ABTS oxidation due to hyrdogen peroxide mediated and HRP (Horseradish Peroxidase) catalzied reaction cascade can be tracked due to colorimetric change in ABTS dye and measured with M5 spectramax as absorbance at 415 nm for 5 minutes.

2.7. Expression and Characterization of Surface Displayed Proteins and Peptides

Ag43 mediated surface display of GLP-1 analogues and sfGFP fused GLP-1 (sfGLP1) is induced by 1 mM IPTG to control protein expression from T7 promoter with BL21(DE3) strain. Characterization of the surface displayed sfGLP1 has been firstly done by heat release experiment. To do that, primary cell stock grown at 37 ˚C, 200 rpm for 16 hours in LB medium with relevant antibiotics. After that, cells inoculated in fresh LB medium as 1:100 diluted, induced with IPTG at OD_{600} 0.4-0.6, and grown at 30 ˚C, 200 rpm for 16 hours. In order to check surface display with heat release, overnight induced cells centrifuged down at maximum speed for 2 minutes and washed 3 times with 1x PBS and resuspended in 1x PBS. After that, cells heated at 60 ˚C for 5 minutes, while keeping a sample without heating. Finally, samples centrifuged down at maximum speed for 2 minutes and fluorescence of the supernatant for both heated and control samples measured by M5 Spectrophotometer with using 495 excitation and 510 emission values.

In order to check release of the sfGLP1 with purified TEV protease, overnight induced cells washed with TEV buffer (Appendix E) twice, resuspended in 250 µL TEV buffer and added 10 µg GST-TEV (produced by Recep Erdem Ahan, Büşra Kırpat and Gökçe Özkul) enzyme while adding PBS as negative control to the similar set of samples. Cells inoculated in +4 ˚C for 16 hours in rotator. In final step, 250 µL of cells centrifuged down at maximum speed for 2 minutes,

fluorescence of the supernatant for both GST-TEV added and control samples measured by M5 Spectrometer with using 495 excitation and 510 emission values.

2.8. SDS-PAGE Analyses

Sodium Dodecyl Sulfate Polyacrylamide Gel Electrophoresis (SDS-PAGE) applied to visualize protein samples. Biorad Mini-PROTEAN gel casting and electrophoresis system used during the analysis. TEV released protein samples heated at 95 ˚C for 5 minutes by mixing with 6X SDS loading dye (375 mM Tris-HCl, 9% Sodium deodecyl sulfate, 50% Glycerol, 9% Betamercatoethanol and 0.03% Bromophenol blue dye). After that, heated samples loaded into 12% SDS-PAGE gel (BioRad recipe) with Page Ruler (Sigma-Aldrich) protein marker. Gel run operated at 120 V inside running buffer for 1.5-2 hours. After that, SDS-PAGE gel stained by Coomassie Blue staining. To do that, gel soaked into Coomassie blue staining solution (0.1% Coomassie Brilliant Blue R250 dye, 50% Methanol and 10% glacial acetic acid) and heat-boiled for 45 seconds with microwave oven. Then, gel incubated for 20 minutes inside the solution on a shaker at room temperature. After that, gel transferred into destaining buffer (40% Methanol and 10% Glacial acetic acid) and again heat-boiled at microwave oven for 45 seconds. After 1 hours of incubation at room temperature in destaining buffer, gel transferred into fresh destaining buffer and incubated overnight. For visualizing the gel and analysis of protein bands, ImageLab software and ChemiDoc Imaging system (BioRad) used.

2.9. Genetically Controlled Protein and Peptide Release from Cell Surface

In order to genetically control the release of Ag43 displayed sfGLP1, *E. coli* BL21(DE3) cells carrying pET22B-T7-(Ag43-sfGLP1)-AmpR construct co-transformed with REA83 plasmid (constructed by Recep Erdem Ahan for Ahan et al, 2019 study and contains aTc, anhydrotetracycline, inducible tetO promoter that controls the expression of Ag43 mediated TEV protease display) that has chloramphenicol resistance. After co-transformation, a single colony selected and grown in dual antibiotic supplemented LB medium for overnight at 30 ˚C, 200 rpm for 16 hours. After that, cells transferred in 2x MOPS medium (recipe available in reference) with dual antibiotics as 1:100 dilution [78]. When cells reach to an OD600 value of 0.4, induced with 0.2 mM IPTG and grown overnight at 30 ˚C, 200 rpm for 16 hours. After that, cells centrifuged down at 2700 rpm for 10 minutes, medium renewed and 125 nM aTc added to induce Ag43-TEV expression. After 16 hours of aTc induction at 30 ˚C, 200 rpm, cells centrifuged down at maximum speed for 2 minutes and fluorescence of the supernatant for both aTc induced and control samples measured by M5 Spectrophotometer with using 495 excitation and 510 emission values.

2.10. Mass Spectrometry Analyses

Mass Spectrometry (MS) analysis has been operated at Hacettepe University's HUNITEK Analysis Laboratories by the assistance of Doç. Dr. Ömür Çelikbıçak by using MALDI-TOF (Matrix Assisted Laser Desorption Ionization Time of

Flight) MS instrument (Ultraflex Extreme MALDI-TOF, Bruker Daltonics). During the analyses, instrument operated with linear positive mode and ground steel used as target.

In addition, HCCA (Alpha-Cyano-4-Hydroxycinnamic acid) matrix used for peptide analysis, SA (Sinapinic acid) matrix used for peptide analysis. During the sample preparation, three different solutions used including Solution 1 (Saturated HCCA solution, 30:70 (v/v), Asetonitril: TFA 0.1% H2O), Solution 2 (Saturated SA solution prepared in ethanol) and Solution 3 (Saturated SA solution, 30:70 (v/v), Acetonitril : TFA 0.1% H2O). Each sample that is investigated for target peptides prepared by mixing sample with Solution 1 as 1:1 or 1:10 sample volume/matrix volume ratio and taking 0.5 µL of the solution to dry on target plate (dry droplet method). Similarly, each sample that is investigated for target proteins prepared by first drying 2 µL of Solution 2 as a thin layer on target plate, then mixing sample with Solution 3 as 1:1 or 1:10 sample volume/matrix volume ratio and taking 0.5 µL of this solution to dry on target plate as a second layer (double layer method). Calibration of the device made by using Bruker Peptide Calibration Mix (700-3500 Da).

MALDI-MS analyses operated by using 20 kV accelerating voltage for the real-time analysis of ion flight. Spectrums obtained by using SmartBeam laser at 355 nm and 1000 average laser pulse. Final data analysed by Bruker FlexAnalysis software. Calculations of sfGLP-1 and GLP-1 moleculer weights both made by MS device and Benchling protein analysis tool.

2.11. Modelling and Docking Studies

In order to determine binding affinities of the newly designed GLP-1 analogues and native human GLP-1, receptor structures investigated from Protein Data Bank (PDB) web server (http://www.rcsb.org). From the database, a structure named as 5OTT selected as the receptor candidate for peptide docking since it represents extracellular portion of GLP-1 Receptor bounded with a modified ligand. Structure edited by PyMol software to delete water ions and remove native peptide structure on the crystal. After that, modified receptor structure saved as .pdb file to later use as docking template. Peptide sequences derived from Benchling design and noted as plain text. Shortly, candidate sequences named as hGLP1 to represent human GLP-1(7-36), mGLP-1h to represent modified, his tagged human GLP-1(7-36). In final step, these informations loaded to the HPEPDOCK server (http://huanglab.phys.hust.edu.cn/hpepdock) to operate a global docking analysis with the candidate peptides. Results investigated with PyMol molecular viewing software after the analyses by using alignment function of the program. Aligned receptor-peptide complex images exported for visualization.

2.12. Biosensor Induction and Measurement

Biosensor measurements are operated for hydrogen peroxide, and glucose biosensor separately for either *E. coli DH5α* or *E. coli* Nissle 1917. For the hydrogen peroxide biosensors, candidate circuits in bacterial chassis grown from -80 ˚C stock for 16 hours in 37 ˚C, 200 rpm in LB medium supplemented with

relevant antibiotics. After that, cells transferred into fresh LB medium with 1:100 dilution ratio. Then, cells tracked to an OD_{600} value of 0.4 for the induction. Hydrogen Peroxide (H_2O_2) is purchased from Sigma Aldrich and 30% solution stock contains nearly 10 M H_2O_2. Experiments carried in both LB medium and 2X MOPS medium supplemented with Casamino Acid (0.2%) and Glucose (2%). For the glucose sensor measurements, again the cell stocks grown overnight in LB medium with relevant antibiotics at 37˚C, 200 rpm. After that, cells transferred in fresh LB or 2X MOPS medium that contains Casamino Acid (0.2%) and Glucose (2%). After cells reach an OD_{600} value of 0.4, cells induced with D(+)-Glucose by given concentrations. For all the biosensor measurements, fluorescent signal tracked in each hour by taking 1 mL sample from the growth, centrifuging down the sample at 14000 rpm for 1 minute, discarding supernatant, and washing the pellet for 2 times with 1 mL 1X PBS. As final step, cells resuspended in 250 µL 1X PBS and fluorescence measured with M5 Spectramax Spectrophotometer.

2.13. Biosensor Coupled Peptide and Protein Release from Cell Surface

Biosensor coupled release system is operated by using double transformed constructs that carrying Ag43-sfGLP1 protein that is continuously expressed and Ag43-TEV that is synthesized as the output of glucose sensor module. In the experiment, *E. coli* cells carrying only the Ag43-sfGLP1 used as negative control. At first, overnight grown cells inoculated in fresh LB or 2X MOPS (including 0.1% casamino acid and 2% glycerol) and grown in 30 ˚C until they reach an OD_{600} value of 0.4 or near. Then, glucose introduced on the medium as 2 and 10

mM concentrations. Uninduced cells again used as control. For each hour, 250 µL sample taken from the cells, centrifuged down at maximum speed for 2 minutes and supernatant taken for measuring fluorescence at M5 Spectramax Spectrophotometer.

All the biosensor and protein release experiments have at least three replicates. After the experiments, collected data analysed by using GraphPad analysis software. Whole cell fluorescence values divided into OD_{600} value in each measurement point to normalize the results with cell number.

CHAPTER 3

RESULTS AND DISCUSSION

3.1. Designing a Whole-Cell Glucose Biosensor

As our first module, we wanted to develop a whole-cell glucose biosensor for the future applications of detecting glucose levels in human body. With that, we will be able to develop response modules calibrated with the changing glucose levels.

3.1.1. Designing a Whole-Cell Glucose Biosensor; Two Component System

In our first design, we adopted two component system strategy that is first used by Baumgartner et al, 1994 study to sense glucose in *E. coli* cells [52]. In that system, a chimeric protein kinase built by fusing periplasmic domain of Trg protein and cytoplasmic domain of EnvZ sensor kinase together. Trg can naturally interact with Glucose Galactose Binding Protein (GGBP) in periplasm when glucose is presented and bound to GGBP. After in that system, Trg periplasmic domain transfer signal to EnvZ kinase for activation of OmpR effector protein to activate gene expression from pOmpC promoter in the presence of glucose as illustrated in Figure 5 [79]. Later, Dr. Jeffrey Tabor built an engineered system to build light switchable two component systems in *E. coli*, and deposited pSR59.4 plasmid to the Addgene repository. Here, we used that plasmid to change light switchable domain of chimeric EnvZ with Trg to build a glucose sensor module.

This plasmid contains OmpR expression module with pOmpB97 promoter and the chimeric kinase can control sfGFP expression by pOmpF146 promoter. Overall, we aimed to use Jeffrey Tabor's optimized two component system with the Baumgartner's chimeric EnvZ to build an effective whole cell glucose sensor for *E. coli* bacteria (Figure 6).

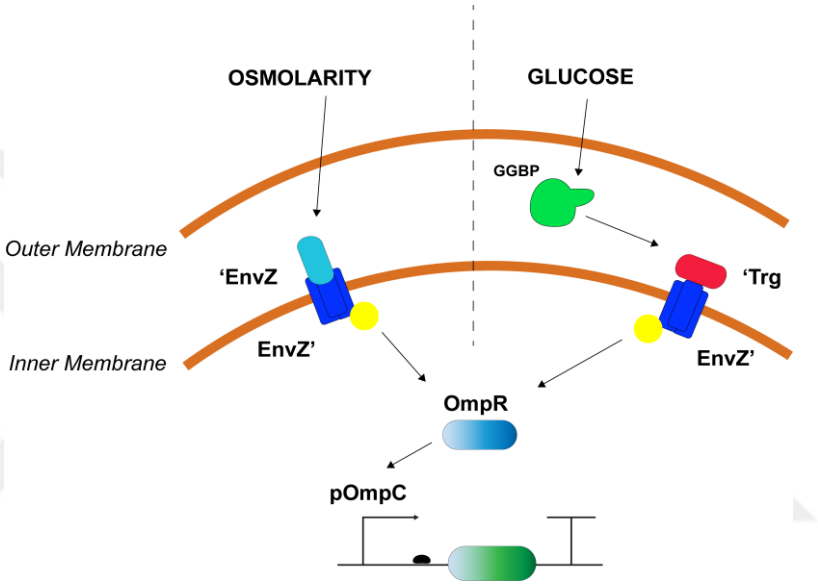

Figure 5: Illustration of Native and engineered EnvZ pathways.

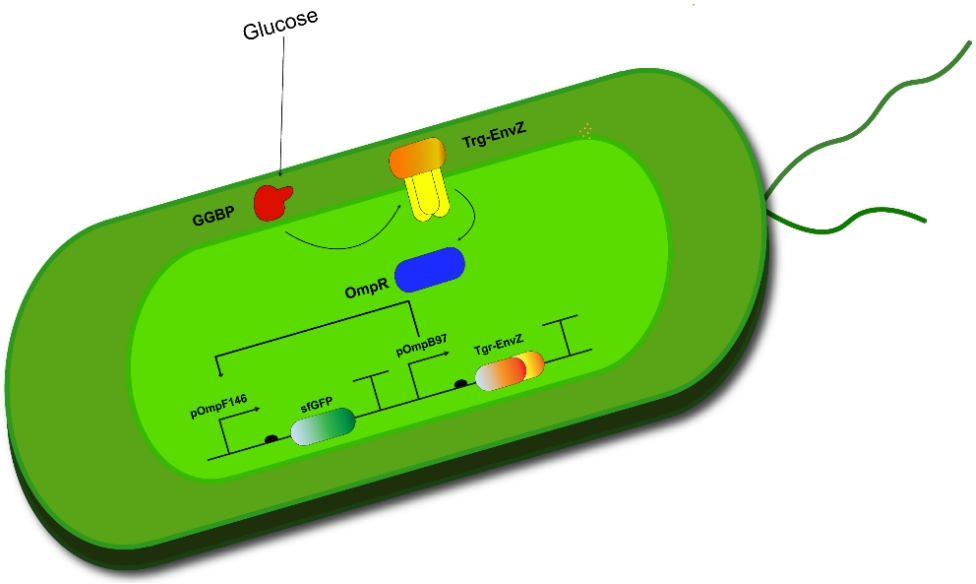

Figure 6: Illustration of Trg-EnvZ based whole-cell glucose biosensor mechanism.

3.1.2. Construction of pSR59.4-Trz1 Plasmid

In order to modify pSR59.4 plasmid as a glucose sensor construct, backbone of the plasmid which contains cytoplasmic segment of EnvZ and promoter regions amplified with NH4-NW and NH6 primers and 5.3 kb backbone fragment obtained as expected (Figure 7). After that, periplasmic region of Trg protein amplified from *E. coli* DH5α genome with NH1 and NH5-NW primers and an 825 bp insert obtained (Figure 7). After verification of the sequence by plasmid isolation for 2 colonies and sequencing (Appendix D6), existence of Trg gene fused to EnvZ confirmed, and cells transformed to an EnvZ deletion mutant *E. coli* strain (JW3367-7) purchased from Coli Genetic Stock Center.

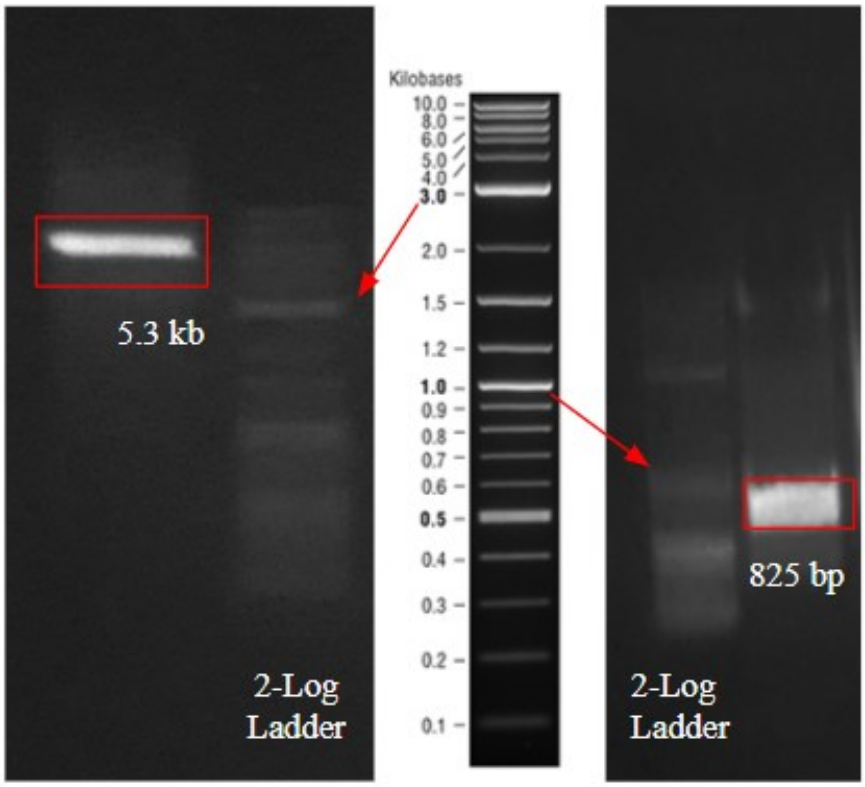

Figure 7: Agarose gel image for backbone of pSR59.4 (5.3 kb, left) visualized with 2-log (NEB, middle) DNA ladder and Trg periplasmic region (825 bp, right).

3.1.3. Characterization of pSR59.4-Trz1 Construct as Glucose Sensor Candidate

In order to characterize the glucose sensing abilities of the pSR59.4-Trz1 construct as a glucose sensor candidate, we adopted experimental procedure that is applied in Baumgartner et al, 1994 study and induced cells that growing at 37 ˚C with 100 µM glucose and observed the fluorescence increase for the next 2 hours. In the article, it is reported that 100 µM is the lowest concentration that is not affecting the growth of the cells in LB medium. After investigations, a low degree of fluorescence signal increase recorded in 2 hours (Figure 8), but in physiological level, this signal did not show any significant increase (data not shown).

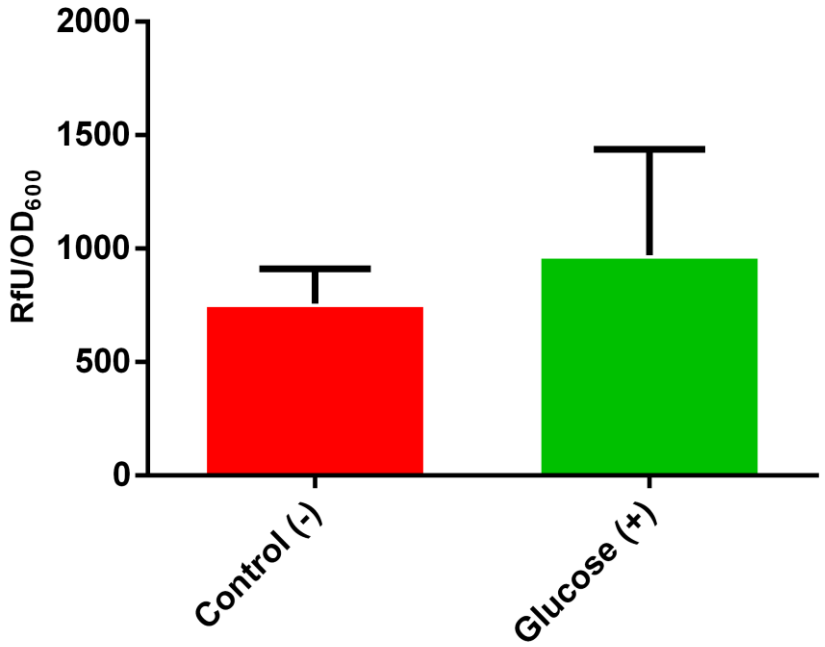

Figure 8: Glucose sensor candidate pSR59.4 characterized by 100 µM glucose in LB medium. Low degree of signal recorded for the samples after 2 hours.

Statistical Analysis made for triplicates of samples with Student's T-Test. Results minimized with wild type cell fluorescence.

3.2. Designing an Enzyme Based Whole-Cell Glucose Sensor System

Two components systems are hard to optimize and they require high level of metabolic burden for the bacterial cells. Besides, during the experiments, fold change of the signal remained low and we evaluated that as a possible problem for the future designs. Due to that, we changed our strategy to build a different whole cell biosensor which utilizes an enzyme to convert glucose to detectable metabolites in *E. coli* bacteria. During our literature search, we found that a class of enzymes known as Glucose Oxidases (from now on, this enzyme will be referred as GoX) can convert glucose to D-Glucano-1,5-Lactone and Hydrogen Peroxide. Besides, in the literature, we saw that there are many systems characterized specifically for measuring hydrogen peroxide concentrations by a whole cell biosensor mechanism in *E. coli* (Figure 9). Overall, we proposed that expressing glucose oxidase and a hydrogen peroxide biosensor construct together in *E. coli* could provide us a fast acting whole cell biosensor mechanism. With that purpose and as a first step to build proposed system, pET22B-T7-GoX construct build to express GoX gene in *E. coli* bacteria.

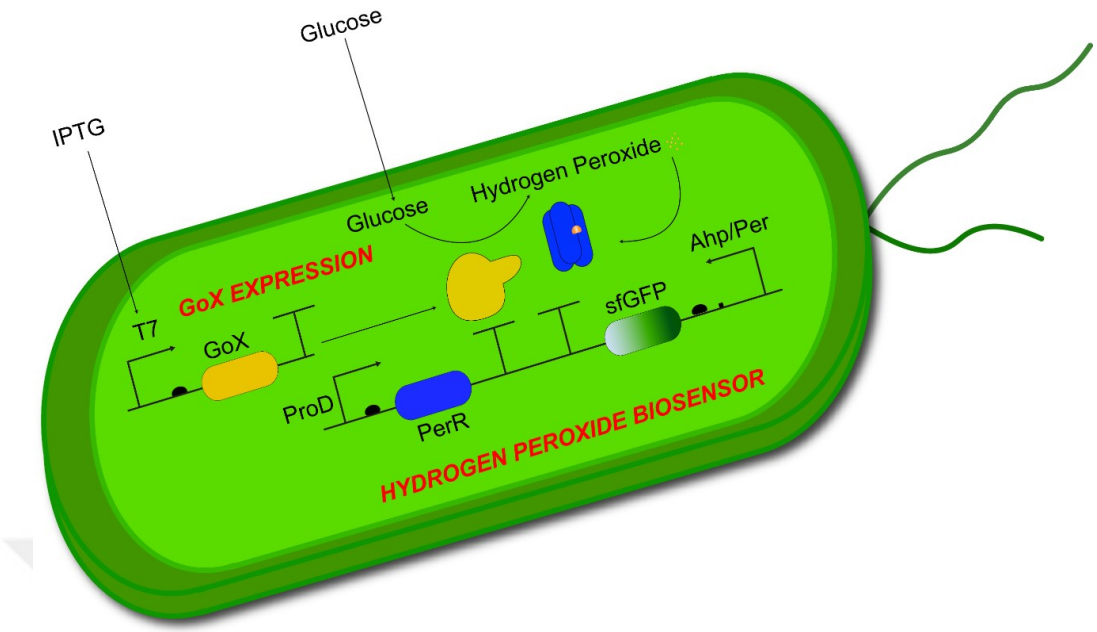

Figure 9: Illustration of GoX based whole-cell glucose sensor strategy.

3.2.1. Construction of pET22B-T7-GoX-Trx plasmid

For amplifying GoX gene derived from *Penicillium amagasakiense*, we ordered 4 different gene fragments that has sequential Gibson Assembly overlaps to form 2290 bp GoX gene fragment. In order to amplify this gene, 4 fragments mixed in distilled water as equal amounts and the 2.2 kb long gene amplified by PCR reaction with GOX-PET22B-FOR and GOX-PET22B-REV fragments (Figure 10). After that, this gene part joined together with pET22B-T7 backbone obtained as a 5.2 kb digest product of previously built pET22B-T7-RbmA plasmid (previously built by Musa Efe Işılak and kindly provided for this study) with XhoI and KpnI enzymes (Figure 11). Gibson mix prepared with using 1:2 backbone to insert ratio and resulted colonies transformed to *E. coli* DH5α. After that, two colonies selected from the cloning plate and plasmid isolation procedure operated to verify sequence with Sanger sequencing (Appendix D7).

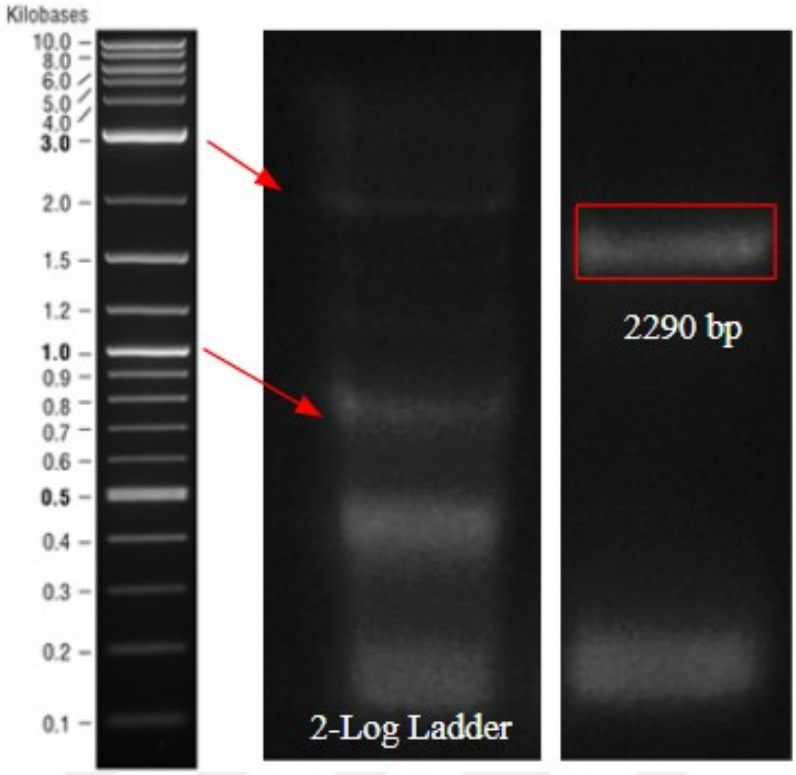

Figure 10: Agarose gel image for 2290 bp GoX gene amplified from synthesized gene fragments and visualized with 2-log (NEB) DNA ladder.

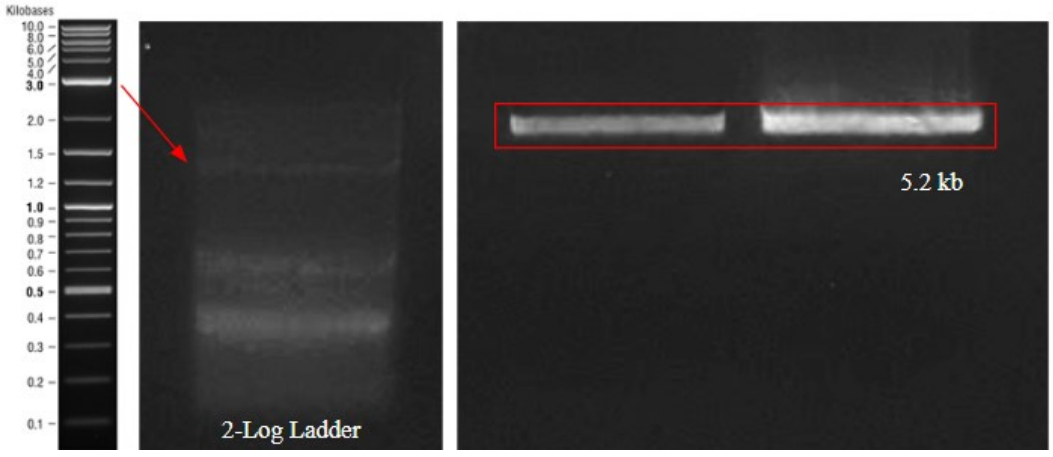

Figure 11: Agarose gel image for pET227-T7 backbone obtained from pET22B-T7-RbmA backbone by digestion with KpnI-XhoI. 5.2 kb fragment obtained as expected. 2-Log Ladder (left) used for the characterization.

3.2.2. Detection of Hydrogen Peroxide Produced by GoX

In order to detect hydrogen peroxide produced by expressed GoX, sequence verified plasmids transformed into *E. coli* BL21(DE3) cells with previously described chemical transformation method. Then, a single colony selected from the transformation plate and grown in LB medium supplemented with 1 mM IPTG. By using uninduced and wild type cells as control, hydrogen peroxide production by the addition of glucose tested with the previously described method (Figure 12).

From these results, it can be concluded that hydrogen peroxide could be produced by the bacterial cells coupled with the addition of glucose to the environment. Although GoX producing cells detected as the highest signal producing cells for hydrogen peroxide, other cells and even wild type cells detected as to producing hydrogen peroxide from glucose. In the literature, it is found that glucose addition may lead to the production of hydrogen peroxide naturally by glycolysis fallowing regeneration of NAD^+ from NADH [80]. Overall these results are indicating that addition of glucose could be converted to hydrogen peroxide in the bacterial systems with higher ratio when glucose oxidase is presented. Besides, visual inspection of the reaction after 5 minutes also showing the high degree of oxidation of the ABTS dye for GoX sample incubated with 50 mM glucose.

In addition to this experiment, hydrogen peroxide production with the changing amount of GoX also tested with ABTS assay (Figure 13), and it is observed that the oxidation state of the ABTS could remain steady with 1 mM IPTG induction which maximizes protein production from T7 promoter.

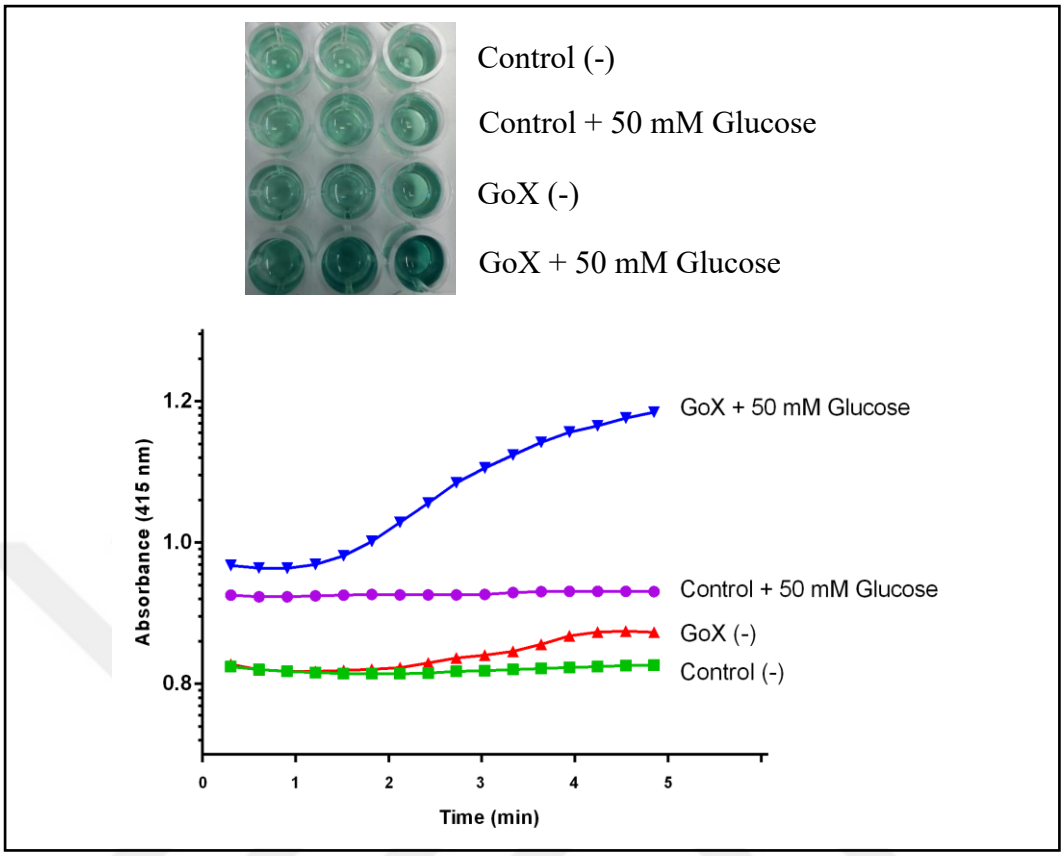

Figure 12: Hydrogen peroxide production test for GoX by ABTS assay including visual inspection of the reaction after 5 minutes (top).

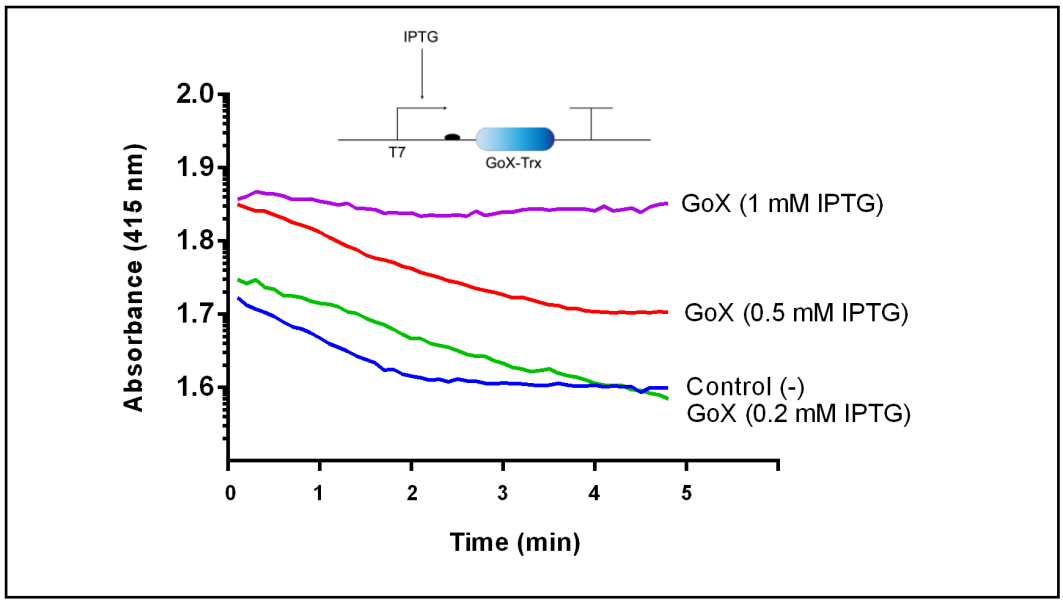

Figure 13: Hydrogen peroxide production test with ABTS assay by changing GoX expression rates. Genetic circuit to control GoX induction also illustrated (top).

3.3. Designing a Whole-Cell Hydrogen Peroxide Biosensor

After the characterization of GoX generated hydrogen peroxide, we continued with building a hydrogen peroxide biosensor as the second part of our glucose sensor design. From the literature, we checked internal mechanisms of the hydrogen peroxide resistance of the *E. coli* bacteria, and we realized that there is a transcriptional activator in the genome named as OxyR (Figure 14) which can be activated in the presence of hydrogen peroxide.[50]

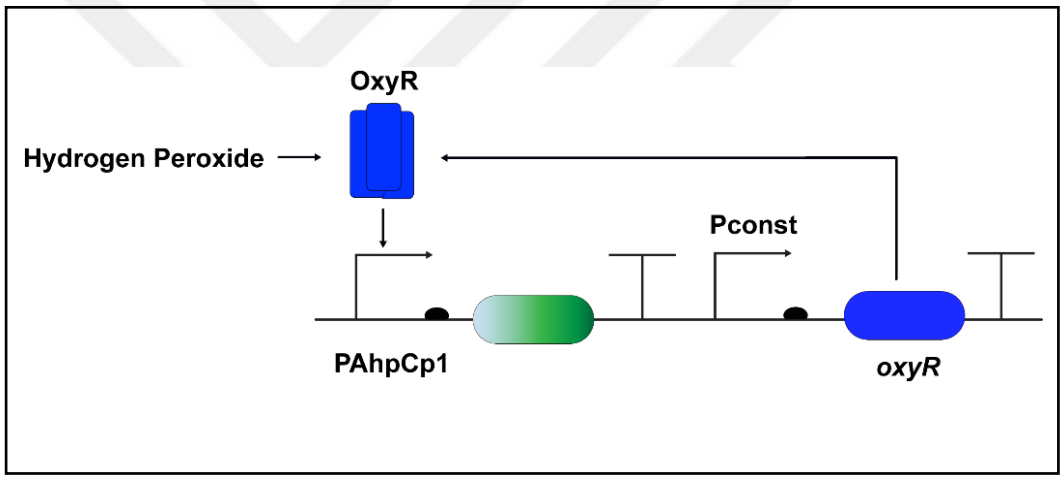

Figure 14: Illustration of OxyR based hydrogen peroxide biosensor mechanism

This natural mechanism of OxyR is discovered to be protecting bacteria on the effect of hydrogen peroxide by activating defence genes from the genome. Besides, we also realized that there is an engineered promoter in the Registry of Standard Biological Parts known as AhpCp1, and it is characterized on its activation by hydrogen peroxide. In order to use that module as hydrogen peroxide biosensor, we constructed pET22B-PROD OxyR-AhpCp1-sfGFP plasmid to couple with GoX as glucose sensor.

3.3.1. Construction of Hydrogen Peroxide Biosensor Plasmid; pET22B - PROD - OxyR - AhpCp1 - sfGFP

6 kb backbone fragment to generate pET22B-PROD-OxyR-AhpCp1-sfGFP plasmid obtained from a previously designed sensor plasmid by our lab member Sıla Köse, by digesting the plasmid with BamHI-SpeI enzyme (Figure 14). After that, OxyR fragment generated by PCR reaction operated with Oxy6-Oxy7 primers as a 998 bp amplicon (Figure 15). Two fragments joined together with Gibson Assembly and Gibson mix transformed in *E. coli* DH5α cells by previously described chemical transformation protocol. After that, 6 colonies selected from cloning plate and grown for plasmid isolation. Then, in order to detect the OxyR in the backbone, insert PCR repeated with same primers by but using PFu polymerase by using plasmids obtained from the colonies as templates. Resulted PCR fragments visualized in the agarose gel as described and positive colonies detected (Figure 16).

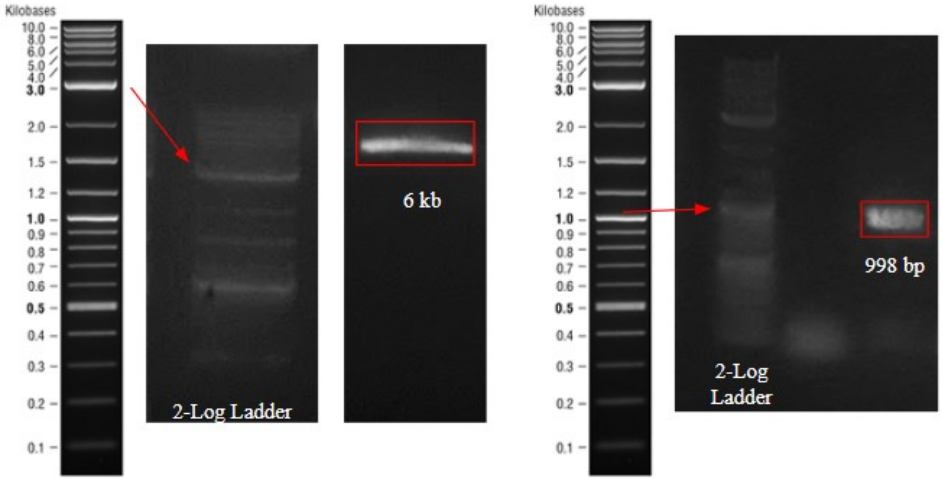

Figure 15: Agarose gel image for BamHI-SpeI digested backbone (6 kb, left) and OxyR insert (1 kb, right) visualized in agarose gel with 2-log (NEB) DNA ladder.

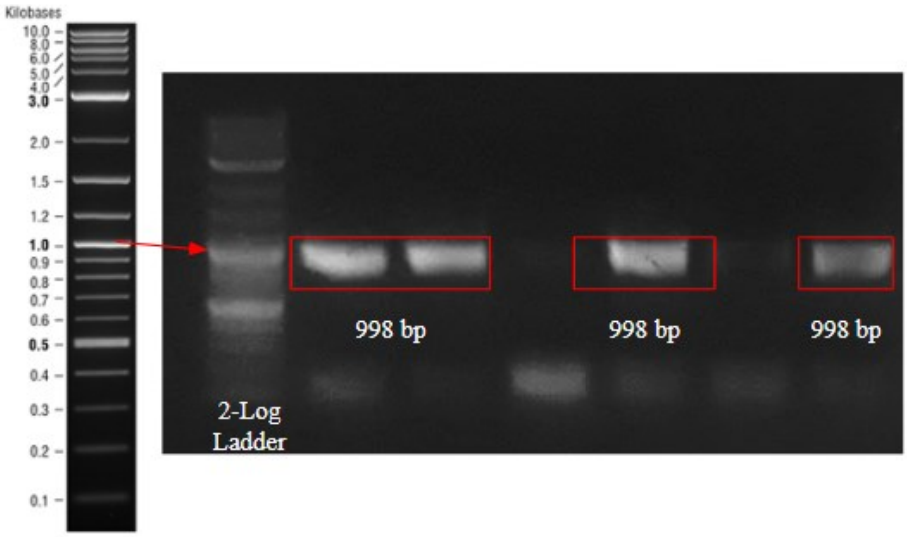

Figure 16: Agarose gel image for colony PCR of OxyR detection in colonies. Colony 1-2-4 and 6 (left to right) interpreted as positive. 2-log (NEB) DNA ladder used for characterization of amplicons on agarose gel.

After that, positive colony plasmids digested with XhoI-EcoRI to obtain 6.2 kb backbone (Figure 17) for final stage of cloning and isolated from the gel as described before. In order to introduce AhpCp1 promoter downstream of sfGFP, gene fragment amplified with NH-ECNKO forward primer and three different reverse primers named AhpCp1-1, AhpCp1-2, AhpCp1-3 sequentially. Resulted 876 bp PCR product visualized on agarose gel to be used as insert (Figure 17). After joining two fragments together with Gibson assembly, Gibson mix transformer in *E. coli* DH5α by using previously described methods. Resulted colonies identified by fluorescence and two colonies selected for sequence verification. After plasmid isolation procedure, samples send to the Sanger sequencing and results verified for AhpCp1 promoter (Appendix D8).

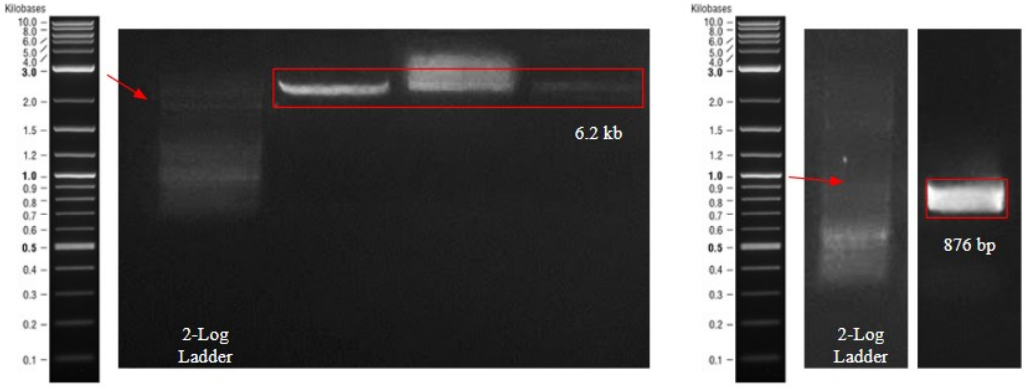

Figure 17: Agarose gel image for OxyR including pET22B backbone that is digested with EcoRI-XhoI (6.2 kb, left) and AhpCp1-sfGPF insert (876 bp, right) wit 2-log (NEB) DNA ladder on agarose gel.

3.3.3. Characterization of OxyR Based Hydrogen Peroxide Biosensor

In order to characterize OxyR based hydrogen peroxide biosensor introduced in pET22B-PROD-OxyR-AhpCp1-sfGPF plasmid, sequence verified cells grown and characterized with a gradient of hydrogen peroxide as described (Figure 18, 19). From the results it can be seen that our hydrogen peroxide biosensor shows analogue signal output with the applied inducer concentration. Besides, there is a fold change increase in fluorescence signal reported for every 1 mM increase in hydrogen peroxide concentration. Although the signal increase is sufficient to detect low levels of hydrogen peroxide, background signal is also interpreted as high for our future applications. In order to reduce background signal, we designed and cloned a modified version of this biosensor with following strategies.

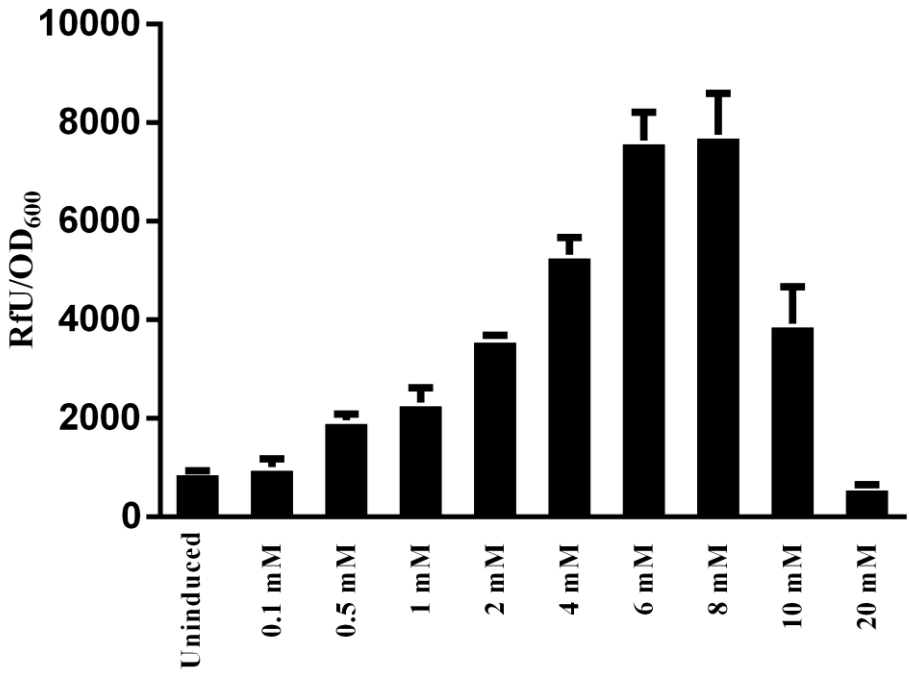

Figure 18: Characterization of pET22B - PROD - OxyR - AhpCp1 - sfGFP with hydrogen peroxide gradient by M5 Spectramax. Note that cells are dying after 10 mM of hydrogen peroxide and this causes the decay on sfGFP fluorescence in the graph.

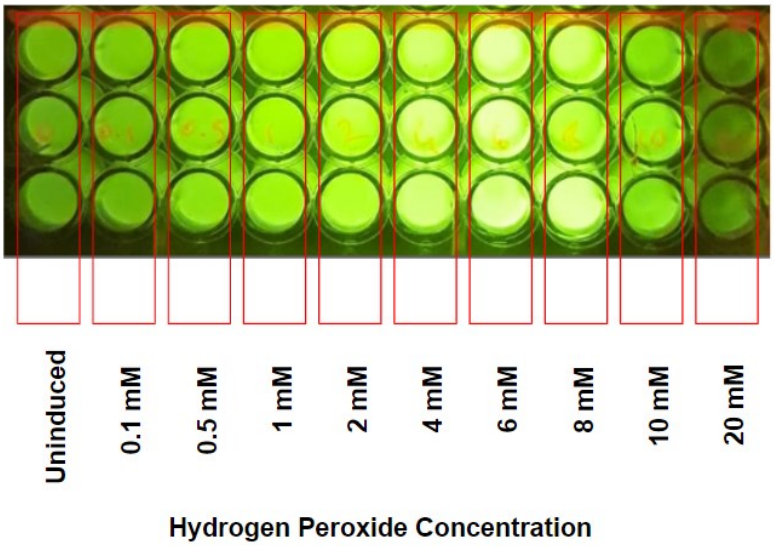

Figure 19: Fluorescence image of the hydrogen peroxide sensor characterization of pET22B - PROD - OxyR - AhpCp1 – sfGFP

3.3.4. Design Strategies for Reducing Background Signal for Hydrogen Peroxide Biosensor

Transcription based biosensor design incorporates two different transcription factors, activators or repressors. As a fundamental difference between these two design elements, activators generally cause high level of background signal since they can activate gene expression even in low amounts. In the case of living therapeutics, this may cause problems in the form of unintended therapeutic release from the cells. To prevent that, we modified our sensor design with a transcriptional repressor by searching the literature and built pZA-PROD-PerR-Ahp/Per-sfGFP plasmid for further experiments. In that plasmid there is a hybrid promoter engineered for this study named as Ahp/Per. This promoter constructed by inserting a PerR binding site to the -10 -35 region of the AhpCp1 promoter (Figure 20) as illustrated below and created a repressible promoter (Figure 21) for improving the leakage of AhpCp1. Main mechanism of PerR baseh hydrogen peroxide biosensor also illustrated below (Figure 22).

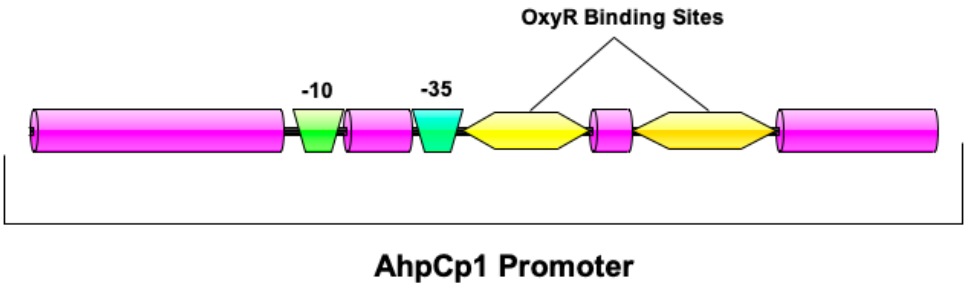

Figure 20: Illustration of genetic elements of the AhpCp1 promoter

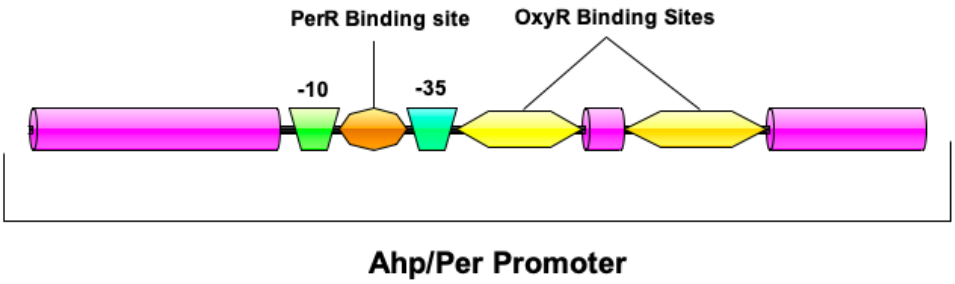

Figure 21: Illustration of genetic elements of the hybrid Ahp/Per promoter

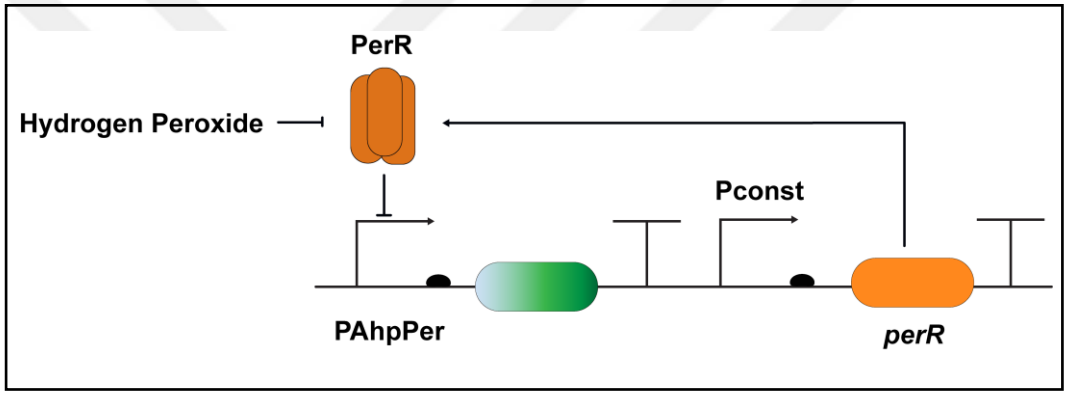

Figure 22: Illustration of PerR based hydrogen peroxide biosensor mechanism

3.3.5. Construction of pZA - PROD - PerR - Ahp/Per - sfGFP plasmid

For the construction of pZA - PROD - PerR - Ahp/Per - sfGFP plasmid, pZA-PROD backbone (2.9 kb) amplified from previously built sensor plasmid (built and kindly provided by Sıla Köse) with with pZA-H2O2-S3-For and pZA-H2O2-S3-Rev primers (Figure 23). In order to insert PerR gene to downstream of PROD, insert amplified from *Bacillus subtilis* genome by PerR-For and PerR-Rev primers as 511 bp fragment (Figure 23). Backbone and insert joined together as

described before, and PerR gene verified from the colonies by colony PCR with PFu polymerase (Figure 24). PerR verification followed by generation of hybrid Ahp/Per promoter by amplifying PerR containing backbone with pZA-H2O2-R-Rev1 and pZA-H2O2-BB-F primers (Figure 25) and sfGFP extended promoter and ribosome binding site (RBS) region with pZA-H2O2-R-For1 primer and three sequential reverse primers named as AhpCp1-PerR-R2 (875 bp), AhpCp1-PerR-R2 (913 bp), and pZA-H2O2-Insert-R (953). Obtained 953 bp fragment (Figure 25) joined with backbone by Gibson assembly, and characterized by Sanger sequencing (Appendix D9,10).

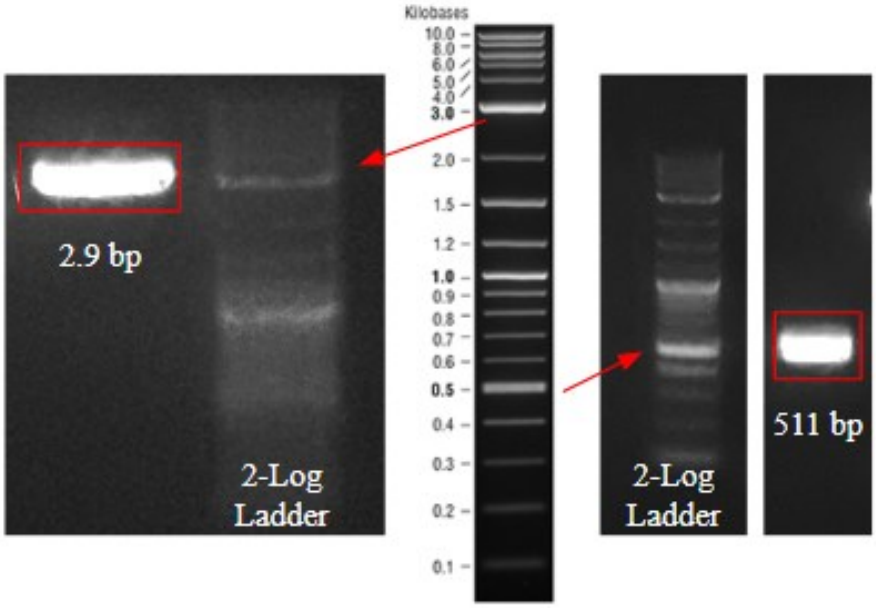

Figure 23: Agarose gel image for pZA-H202-PerR backbone (left, 3 kb) and PerR insert (511 bp, right) amplified with PCR and visualized on agarose gel with 2-log DNA ladder (NEB)

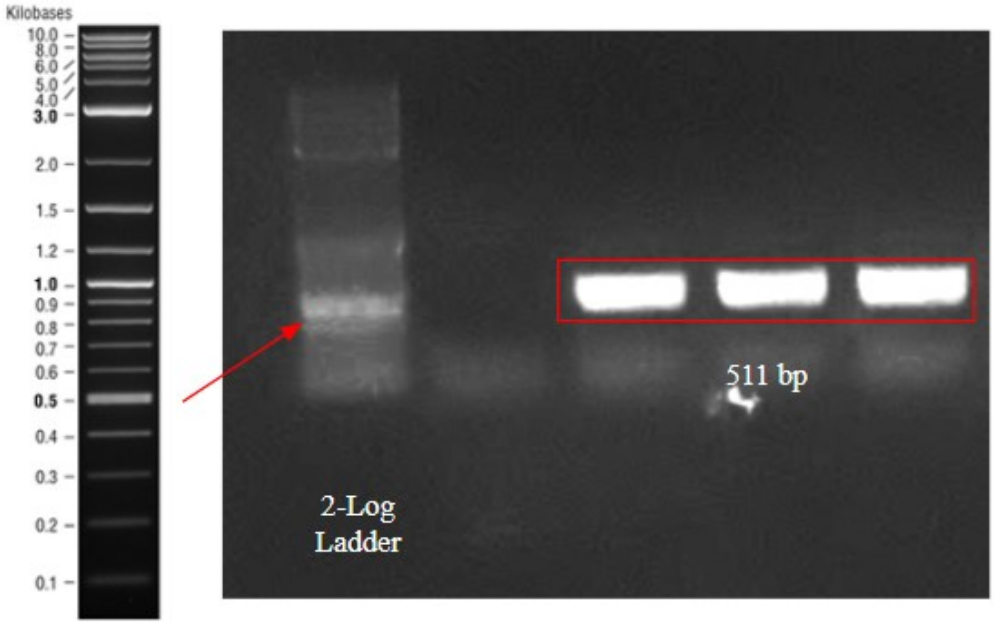

Figure 24: Agarose gel image for colony PCR verification of PerR. 511 bp amplicons obtained for colony 2-3-4 as expected.

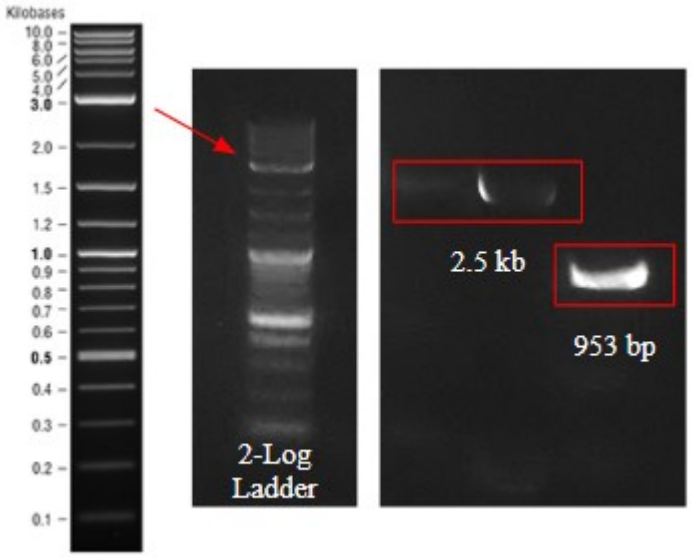

Figure 25: Agarose gel image for PCR results for pZA-PROD-PerR containing backbone (2.5 kb) and Ahp/Per-sfGFP insert (953 bp) visualized on agarose gel with 2-log (NEB) DNA ladder for characterization.

3.3.6. Characterization of PerR based Hydrogen Peroxide Biosensor

In order to characterize PerR based hydrogen peroxide biosensor, same experiments that are operated for OxyR based biosensor measurements operated and the following results are obtained (Figure 26 and 27)

From the results it can be seen that background signal reduced while the fold change for each milimolar of hydrogen peroxide added to the system is preserved. With these results, we are confident that we engineered a novel, low background hydrogen peroxide biosensor for the future applications.

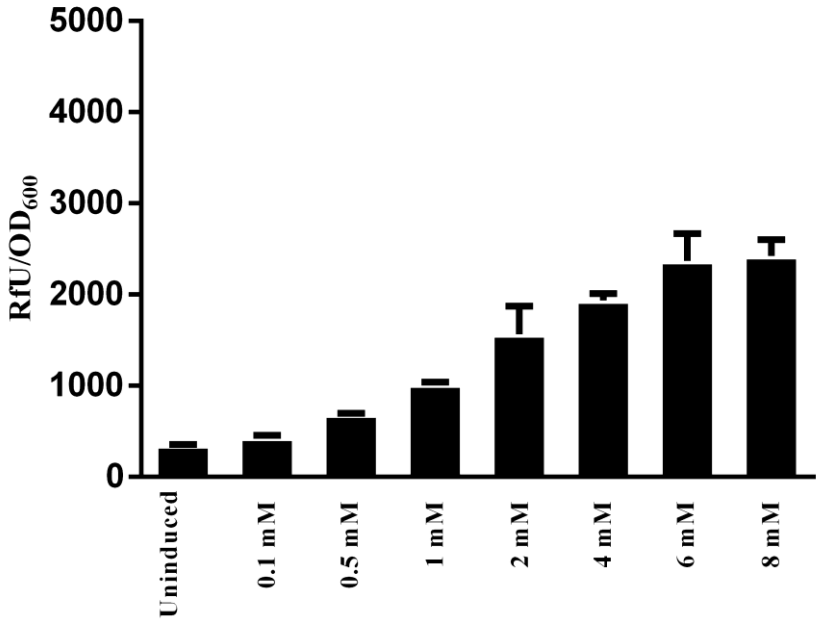

Figure 26: Characterization of cell fluorescence for of pZA - PROD - PerR - Ahp/Per - sfGFP with hydrogen peroxide gradient by M5 Spectramax.

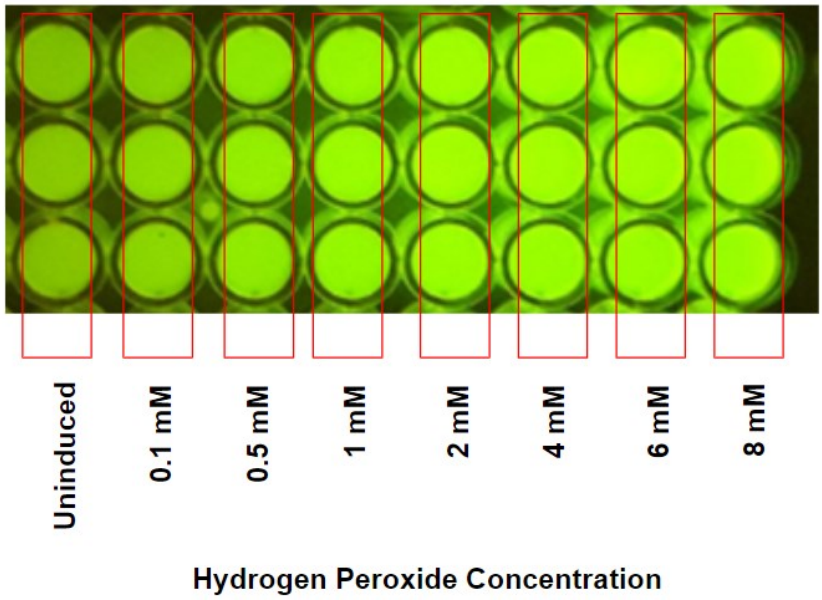

Figure 27: Fluorescence image of the hydrogen peroxide sensor characterization of pET22B - PROD - OxyR - AhpCp1 - sfGFP.

3.3.7. Co-Transformation and Characterization of Hydrogen Peroxide Biosensor Constructs with GoX

To build our glucose biosensor with previously proposed design, we co-transformed OxyR and PerR based biosensor plasmids with *E. coli* BL21(DE3) cells that harboring pET22B-T7-GoX-Trx plasmid. With that way, we are aiming to couple hydrogen peroxide production mediated by GoX with hydrogen peroxide biosensor to have a whole cell glucose biosensor. After co-transformation, cells harboring candidate glucose sensor systems tested for their response against glucose (Figure 28).

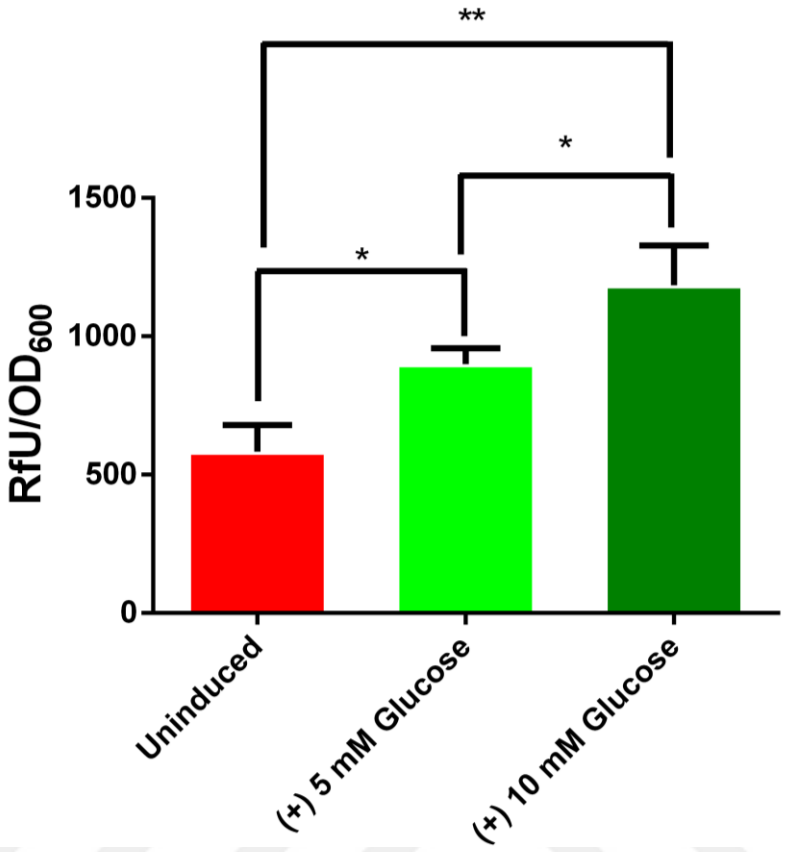

Figure 28: Results for GoX coupled hydrogen peroxide biosensor. Measurements operated by the addition of 5 or 10 mM glucose as the sensor input. Statistical Analysis made for triplicates of samples with Tukey's Multiple Comparison Test (*: $p<0.1$, (**: $p<0.01$). Results minimized with wild type cell fluorescence.

Although the results are showing a slight increase upon addition of glucose into the system, overall design requires optimization for achieving a high degree of signal upon induction. We suppose that low signal ratio in this design may be caused from low amount of hydrogen peroxide produced via GoX and maybe the resistance by integral hydrogen peroxide defense mechanisms.

3.4. Design Strategies for SpxB Based Whole-Cell Glucose Sensor

As an alternative strategy to GoX based glucose sensor and increase the overall signal strength, we designed a different strategy based on the production of pyruvate from glucose via internal glycolysis pathway. In that system, glucose consumption of bacteria resulted with the production of pyruvate as a product of glycolysis, and this pyruvate molecule then converted to the hydrogen peroxide via SpxB pyruvate oxidase. After that, optimized hydrogen peroxide biosensor detects its inducer to give the output signal as a function of glucose presented.

In this system, we designed two different approach (Figure 29) to build a SpxB based glucose sensor strategy. In first design, production of PerR and SpxB modulated by a constitutive promoter, PROD, to prepare system for glucose detection. Upon consumption of glucose via glycolysis, system planned to be triggered by the production of hydrogen peroxide and retardation in PerR function, which allows Ahp/Per hybrid promoter to produce sfGFP. This design named as simple regulation construct since it is inspired from the basic form of whole cell biosensor design (Figure 30).

In second strategy, we wanted to build a positive autoregulation circuit, which can trigger itself by the production of hydrogen peroxide from glucose consumption. In this system, SpxB gene transferred to the downstream of Ahp/Per promoter with sfGFP to reduce background coming from glycerol consumption during *E. coli* growth (Figure 31).

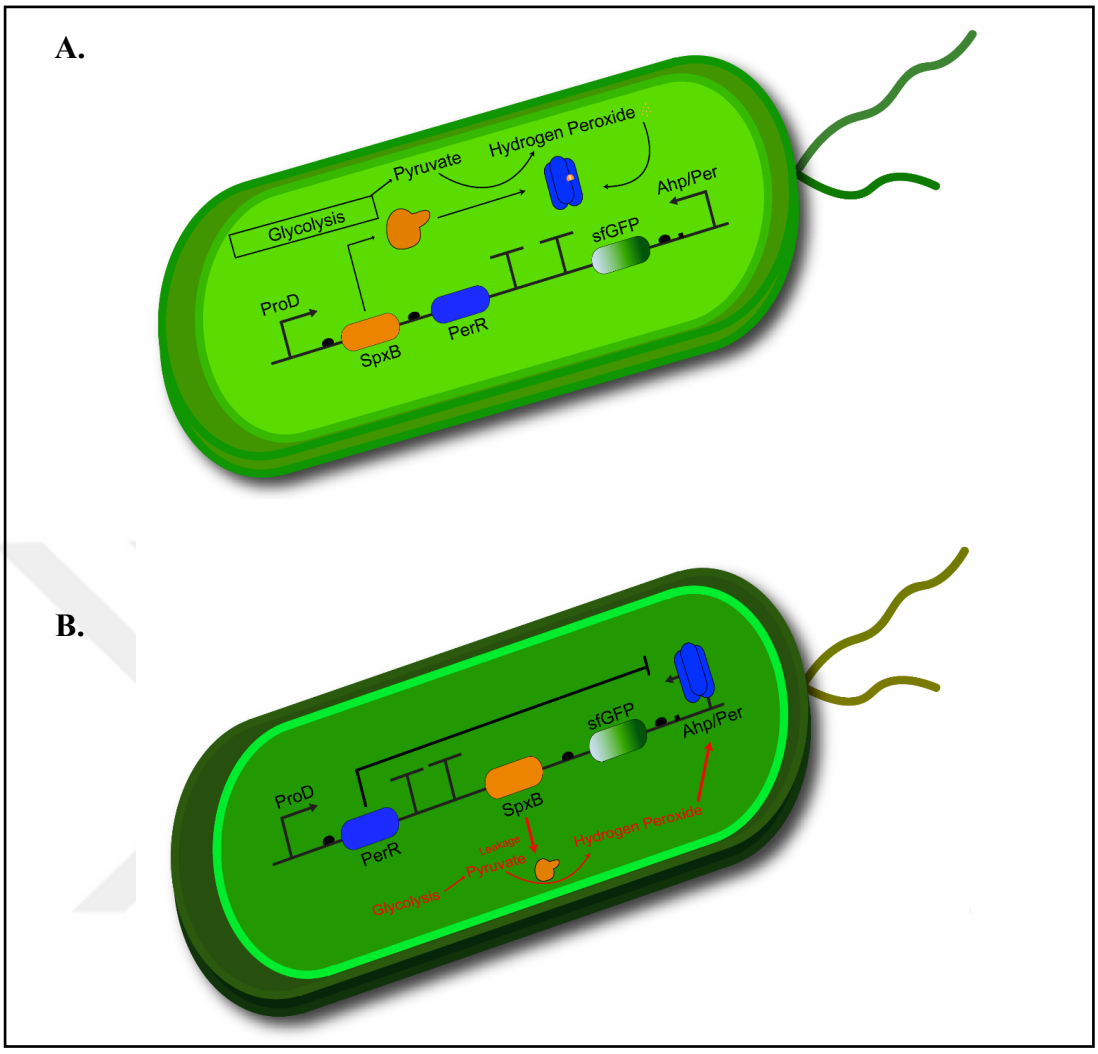

Figure 29: Illustration of SpxB based glucose biosensors. **A)** Simple Regulation Circuit, **B)** Positive Autoregulation Circuit)

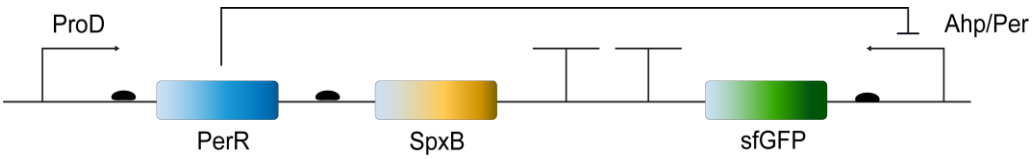

Figure 30: Circuit representation of simple regulation circuit for SpxB based glucose sensor

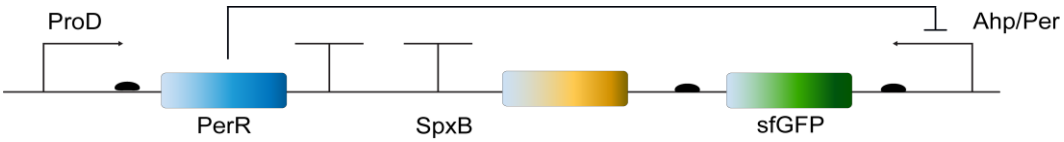

Figure 31: Circuit representation of positive autoregulation circuit for SpxB based glucose sensor

3.4.1. Cloning for Simple Regulation and Positive Feedback Constructs for SpxB Based Glucose Sensor

In order to clone simple regulation glucose sensor plasmid, PerR based hydrogen peroxide biosensor plasmid digested with BamHI and 3.2 kb fragment used as backbone (Figure 32). As insert, SpxB gene obtained from iGEM 2019 distribution kit by PCR amplification with SpxB-For and SpxB-Rev primers as a 2007 bp fragment (Figure 32). Two fragments joined together as previously described and SpxB gene checked by colony PCR (Figure 33).

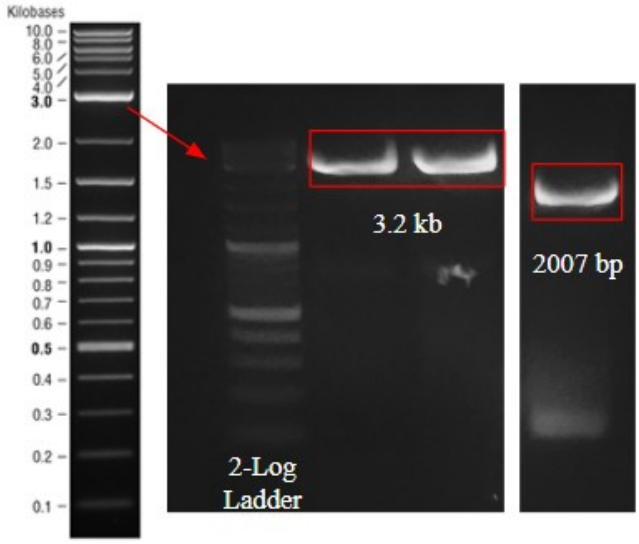

Figure 32: Agarose gel image for 3.2 kb backbone and 2007 bp SpxB insert amplified by PCR for cloning simple regulation circuit. Amplicons visualized on agarose gel with 2-log (NEB) DNA ladder.

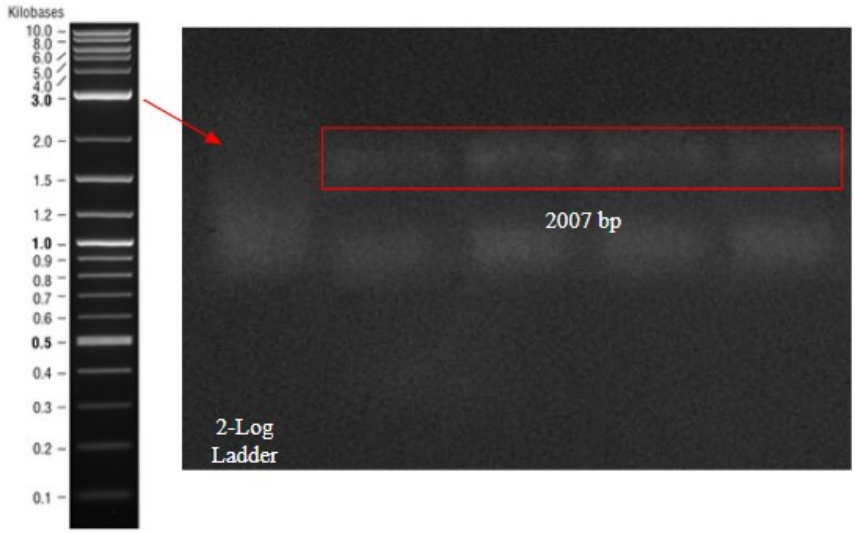

Figure 33: Agarose gel image for colony PCR to detect 2007 bp SpxB insert. Amplicons visualized on agarose gel with 2-log (NEB) DNA ladder.

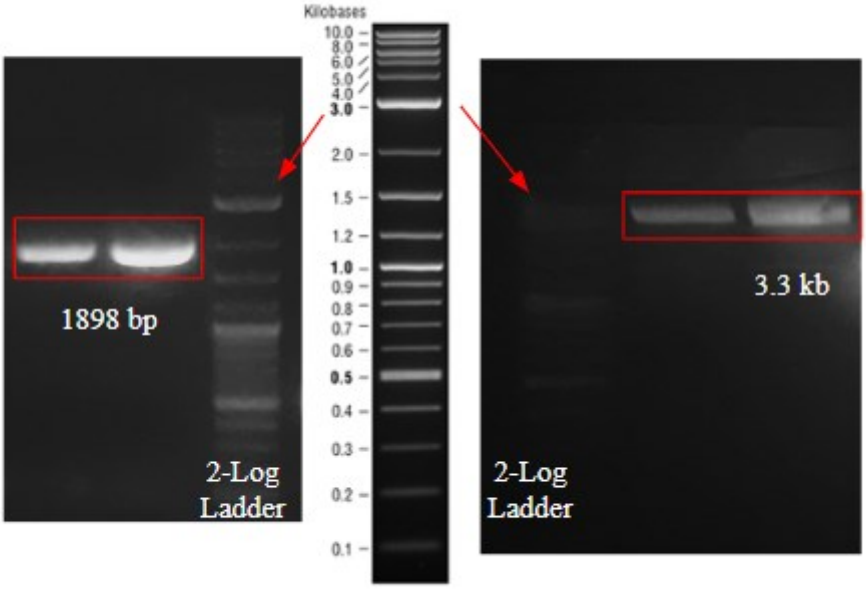

Figure 34: Agarose gel image for 3.3 kb backbone and 1898 bp SpxB insert amplified by PCR for cloning positive autoregulation circuit. Amplicons visualized on agarose gel with 2-log (NEB) DNA ladder.

For cloning the positive autoregulation construct, backbone (3.3 kb) amplified by PCR via SpxB-M2-BB-For and SpxB-M2-BB-Rev primers by using PerR based hydrogen peroxide biosensor as template (Figure 34). SpxB insert amplified again from iGEM 2019 distribution kit by SpxB-M2-For and SpxB-M2-Rev primers and 1898 by fragment used as insert to join two fragments as described before (Figure 34). SpxB gene initial region detected by Sanger Sequencing (Appendix D).

3.4.2 Characterization of SpxB Based Glucose Sensors with Probiotic Bacteria

In order to characterize two sensor constructs, we transformed simple regulation and positive autoregulation plasmids to the *E. coli* Nissle 1917 probiotic bacteria by previously described method. Overall procedure to isolate, characterize and transform *E. coli* Nissle 1917 operated as illustrated below (Figure 35);

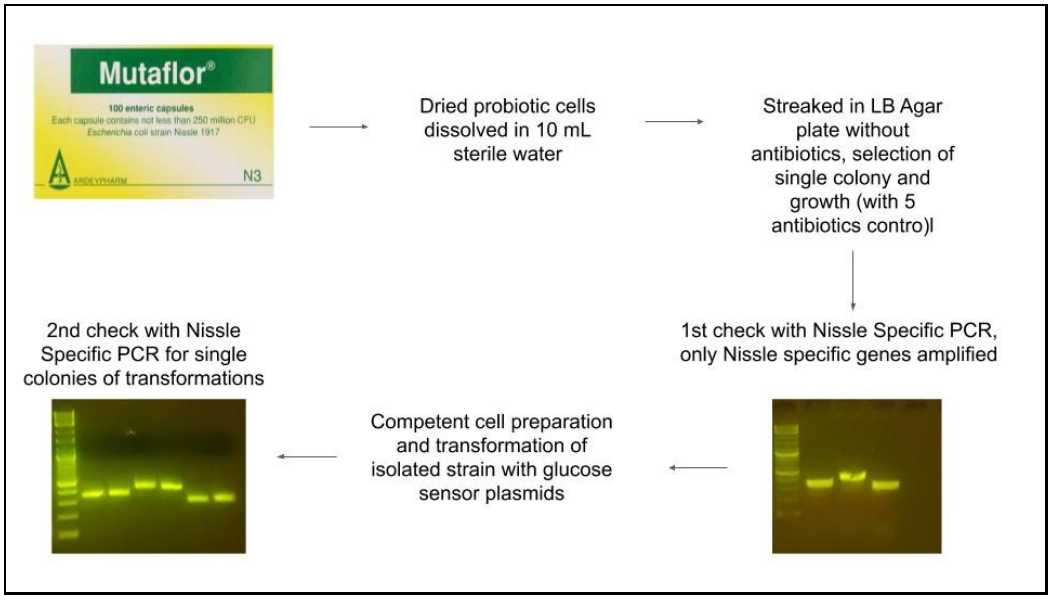

Figure 35: Experimental workflow to isolate and identify *E. coli* Nissle

After transformation into *E. coli* Nissle 1917 by chemical transformation, sensor constructs characterized by growing cells in LB medium at 37 ˚C, 200 rpm for overnight and inoculation in 2x MOPS (supplemented with 2% glycerol) medium to grow until an OD600 value of 0.4-0.5. Then, cells induced with given amounts of glucose to test system response. Biosensor measurements operated by standard procedures that are described before. As figures illustrate below (Figure 36, 37), up to 2.5 fold change in signal response recorded by simple regulation circuit and by positive autoregulation circuit. Considering that intestinal L-cells that are natural sources of GLP-1 hormone, are regulating their expression with 4-fold change in gene expression, these circuits are showing near ideal output for our designs. Signal outputs of the circuits are also distinguishable by naked eye under transilluminator device (Figure 36, 37).

As a comparison of three different whole-cell glucose biosensor strategies (Figure 38), we can conclude that we solved the detection problem by engineering enzyme based biosensor strategies with glucose or pyruvate oxidases. With glucose oxidase, we obtained 1-fold change for diabetic blood glucose levels, but at the same time, we had high background which can later cause instability for the therapeutics release. In our last strategy, we obtained a low background glucose biosensor which has up to 2.5-fold signal change with diabetic blood glucose levels. Besides, low background will provide o steadier and less leaky system in the future applications.

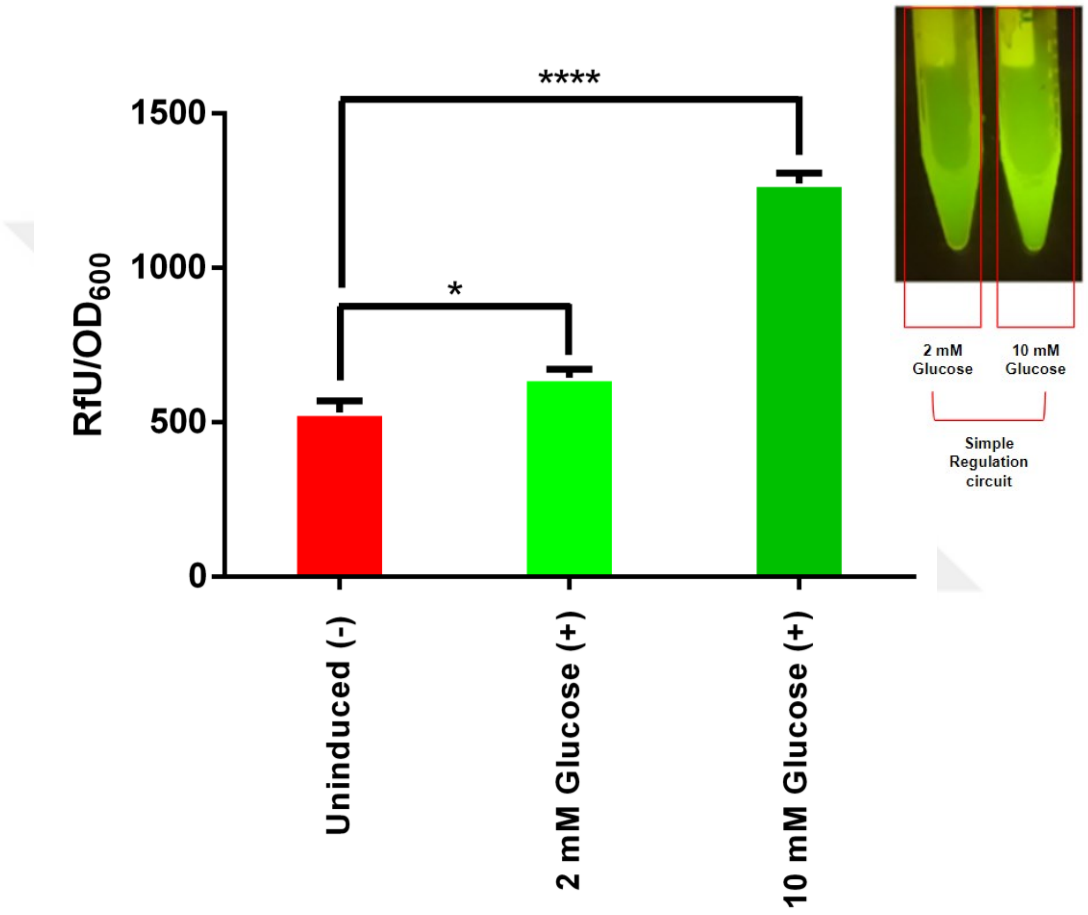

Figure 36: Characterization of simple regulation circuit with physiologic levels of glucose fluorescence analysis and visual fluorescence check. Analysis made for triplicates of samples with Tukey's Multiple Comparison Test (*: $p<0.1$, ***: $p<0.001$). Results minimized with wild type cell fluorescence.

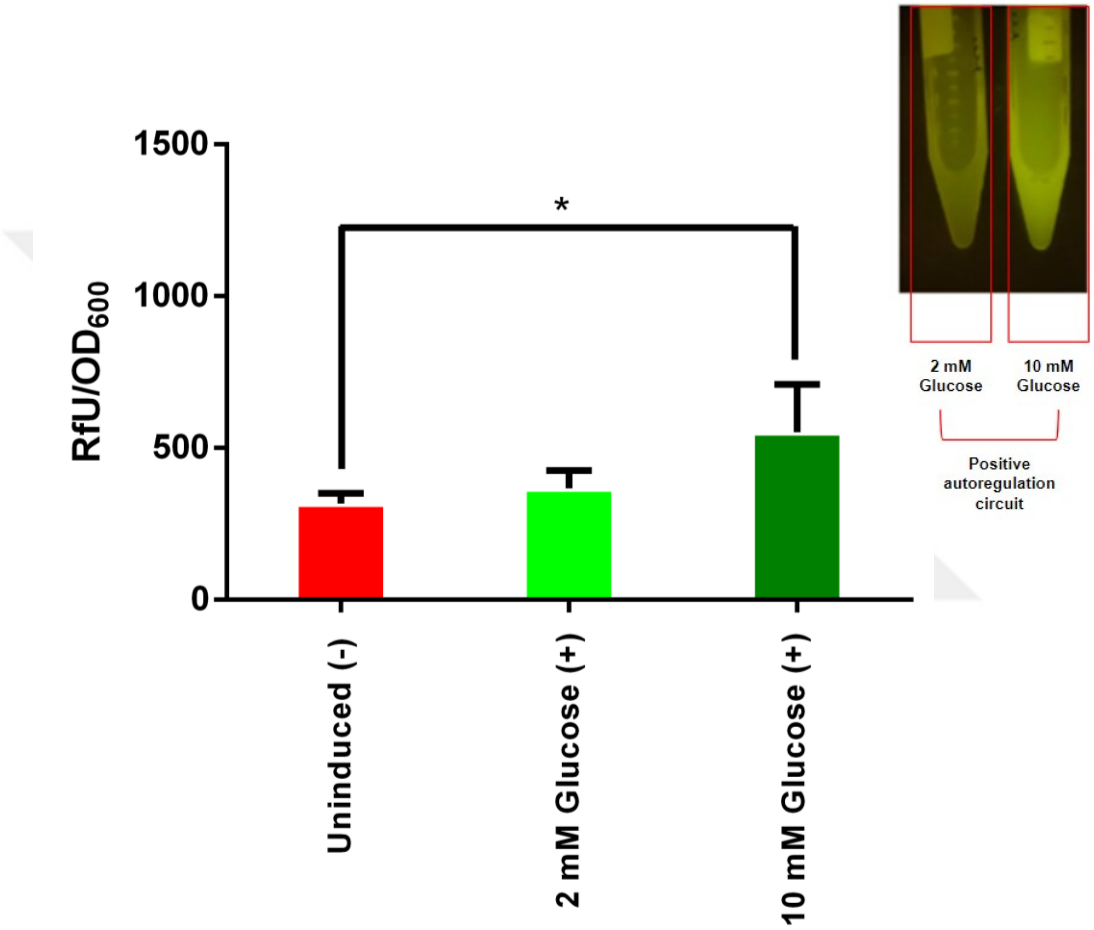

Figure 37: Characterization of positive autoregulation circuit with physiologic levels of glucose by fluorescence analysis and visual fluorescence check. Analysis made for triplicates of samples with Tukey's Multiple Comparison Test (*: $p<0.1$). Results minimized with wild type cell fluorescence.

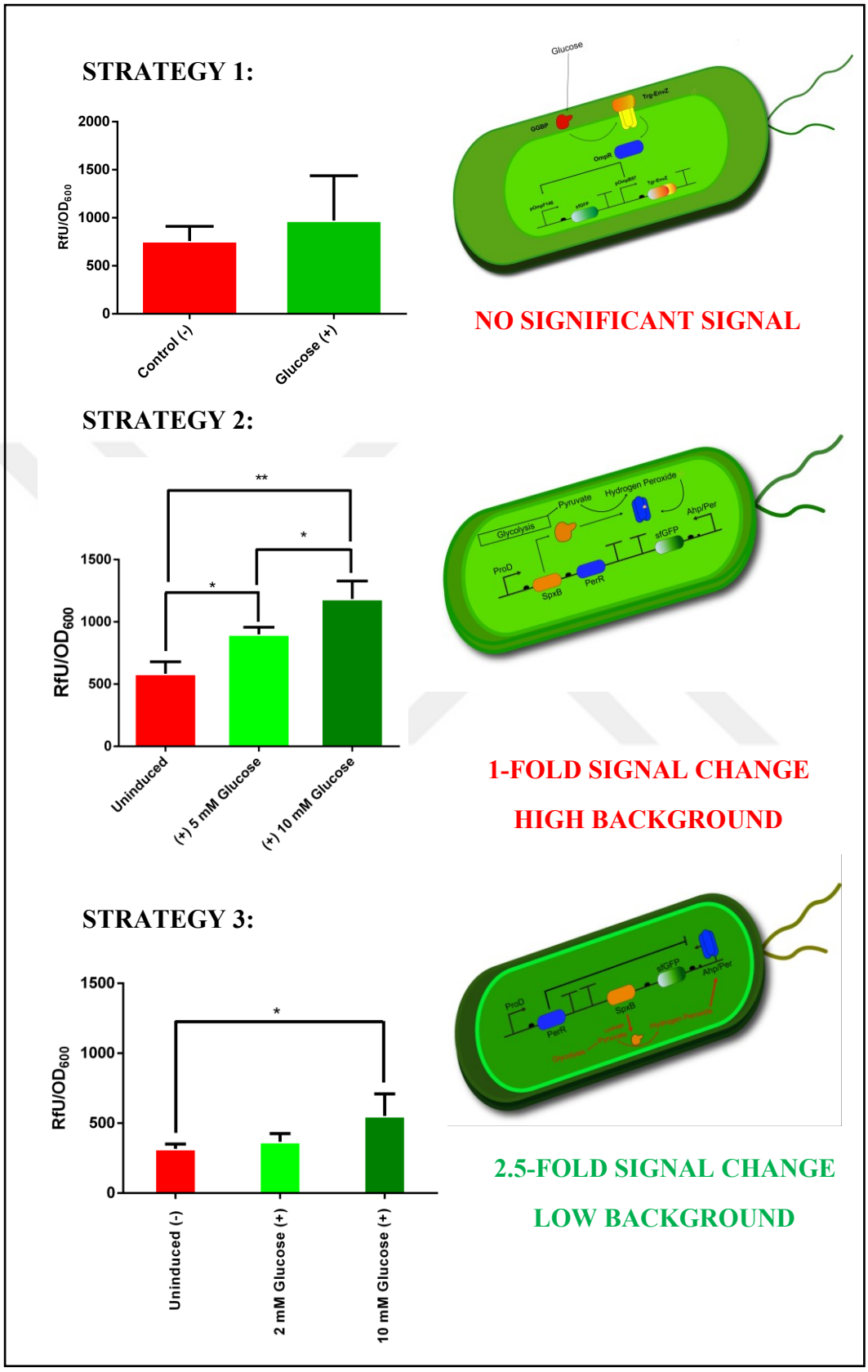

Figure 38: Comparison of three differend biosensor strategies

3.5. Displaying Wild Type and Mutant GLP-1 peptides on Cell Surface

In a recent study, it is shown that cargo protein that is incorporated between signal peptide and N-terminal passenger portion of Ag43 autotransporter can be displayed in the *E. coli* cell surface efficiently.[66] Besides, by adding a TEV recognition site between Ag43-alpha passenger domain and cargo protein can allow specific control on the release of the protein after the display. Overall topology and the strategy of the Ag43 mediated release design illustrated below (Figure 39).

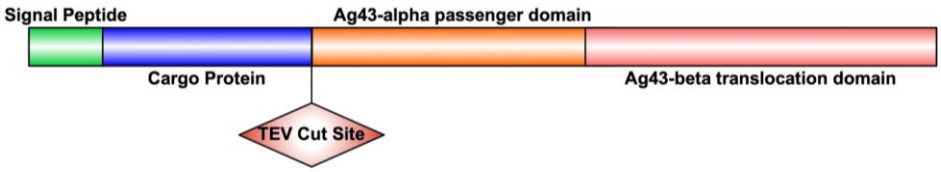

Figure 39: Structure of engineered Ag43 for the display and release of proteins from cell surface. TEV cut site specifically placed between cargo and alpha passenger domain to mediate release.

In our strategy, this system utilized to display active form of human GLP-1 peptide hormone (7-36 amino acids of native hormone) to build an inducer-dependant release machinery. With that purpose, pET22B - T7 - Ag43 - GLP1 plasmid built to display GLP-1(7-36) hormone at *E. coli* cell surface and later pET22B - T7 - Ag43 - sfGLP1 built by fusing sfGFP gene to GLP-1 peptide for further characterization. TEV recognition site also preserved at the constructs for

engineering controlled release strategies. Overall system illustrated below (Figure 40);

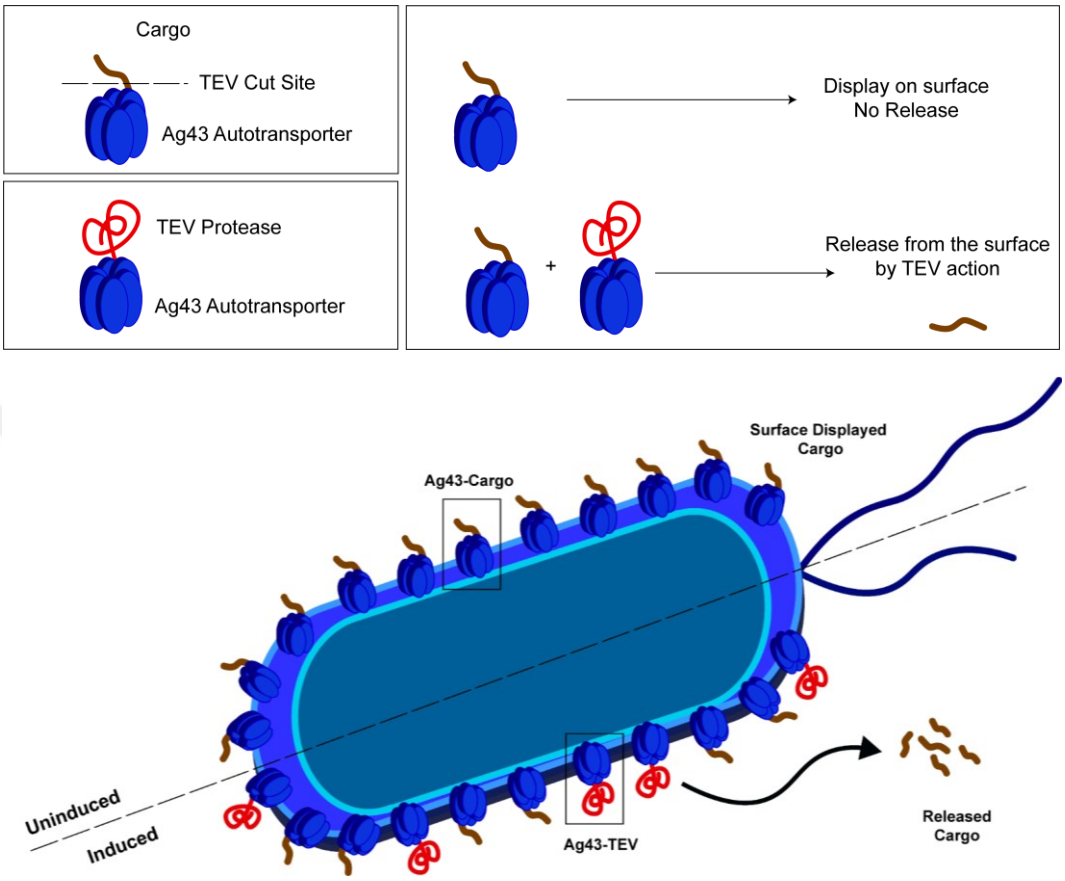

Figure 40: Illustration of overall strategy to release therapeutic peptides

3.5.1. Construction of pET22B - T7 - Ag43 - GLP1 and pET22B - T7 - Ag43 - sfGLP1 plasmids

In order to construct pET22B-T7-Ag43-GLP1 plasmid, backbone fragment obtained by digesting pET22B-T7-αβ40 plasmid (built by Cemile Elif Özçelik and kindly provided for this study) digested with AflIII and SpeI to obtain 7.9 kb expected backbone (Figure 41). GLP-1 gene obtained by amplifying with GLP1-Lig-For and GLP1-Lig-Rev primers. Ag43-GLP1 fragment amplified by extension PCR to add GLP-1 gene as described in methods used as template.

Finally, obtained GLP-1 gene fragment digested with AflIII and SpeI, visualized in 1% agarose gel with expected 132 bp length (Figure 41) and isolated from the gel with previously described methods. As a last step, digested GLP-1 gene and T7-Ag43 carrying pET22B backbone fused together with T4 Ligation. Later, DNA sequence verified with Sanger Sequencing (Appendix D1). Since peptide molecules are hard to identify and visualize in liquid solutions, we decided to fuse sfGFP protein for easy tracking the release of the peptide from the cell surface. To do that, pET22B-T7-Ag43-sfGLP1 plasmid constructed. As the backbone of that plasmid for direct usage, sequence verified pET22B-T7-Ag43-sfGLP1 plasmid digested with SpeI which has a cut site on N-terminal portion of GLP-1.

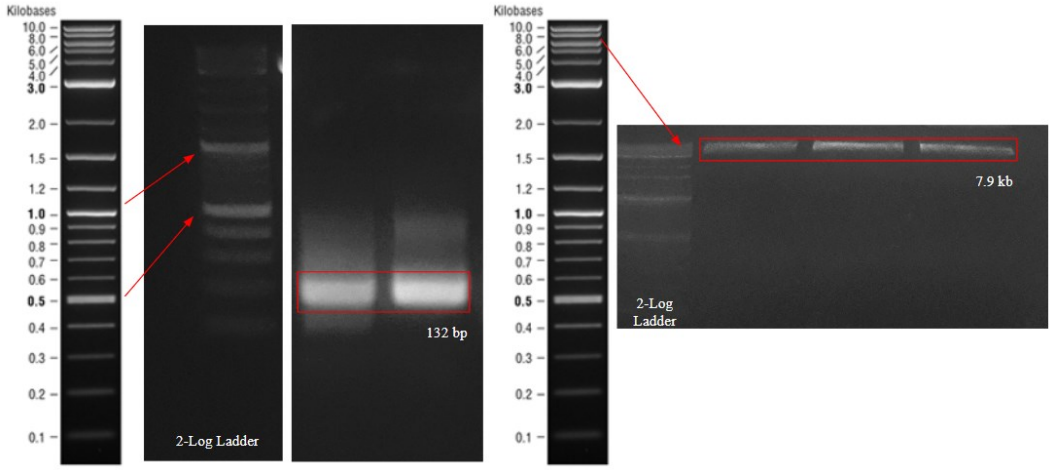

Figure 41: Agarose gel image for AflIII and SpeI digested GLP-1 fragment (132 bp) and 2-log ladder (NEB) at left. AflIII and SpeI digested backbone (7.9 kb) and 2-Log ladder (NEB) right.

sfGFP gene amplified from pET22B-T7-Ag43-sfGFP plasmid (previously built and kindly provided by Recep Erdem Ahan) by using sfGLP1-F and sfGLP1-R primers as an expected 775 bp amplicon (Figure 42) to fuse on this cut site with

Gibson assembly. After the transformation of *E. coli* DH5α, three colonies selected and plasmid isolation procedure applied for these colonies. Isolated plasmids chemically transformed in *E. coli* BL21(DE3) strain to induce protein production with T7 promoter, and colonies selected by visual inspection of fluorescence (Figure 41) during the growth in auto-induction medium , which prevents LacI repression on T7 promoter and keeps expression of this promoter open without induction. Lastly, visually characterized colonies grown for plasmid isolation from DH5α stock and plasmid sequences verified by Sanger sequencing (Appendix D2).

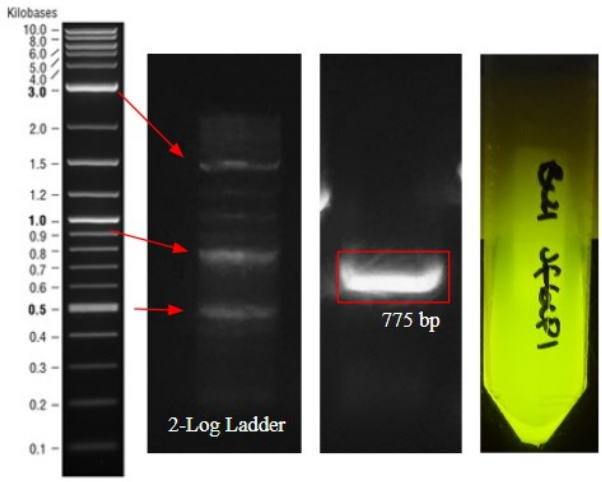

Figure 42: Agarose gel image for 2-Log ladder (NEB) left and sfGFP fragment with GLP-1 insert overlaps (775 bp amplicon) at middle, sfGLP1 fluorescence shown after transformation to the BL21(DE3) (left)

3.5.2. Characterization of Surface Displayed Proteins by Heat Release Assay

In order to characterize sfGFP fused GLP-1 display on surface (from now on fusion protein will be referred as sfGLP1), heat release assay applied. It is known

that while passing from the membrane, alpha-passenger domain is cleaved by internal protease of the autotransporter machinery and weak interaction between alpha-passenger and beta-translocation domain of Ag43 autotransporter keeps alpha-passenger domain on the surface [81]. It is also characterized that by briefly heating the cells, this weak interactions can be disrupted to detach alpha-passenger domain and attached cargo from the surface. With that aim, cells that display Ag43 mediated sfGLP1 protein grown in auto-induction medium at 30 ˚C, 200 rpm for overnight by using Ag43 mediated sfGFP displaying cells as positive control. After that, cells washed 2 times with 1x PBS by centrifuging down at 3000 rpm for 10 minutes. Finally, cells heated for 5 minutes at 60 ˚C in heat block to release proteins from the surface while keeping a set of non-treated cells as negative control. After that, cells centrifuged down and supernatant fluorescence measured by M5 Spectramax (Figure 43).

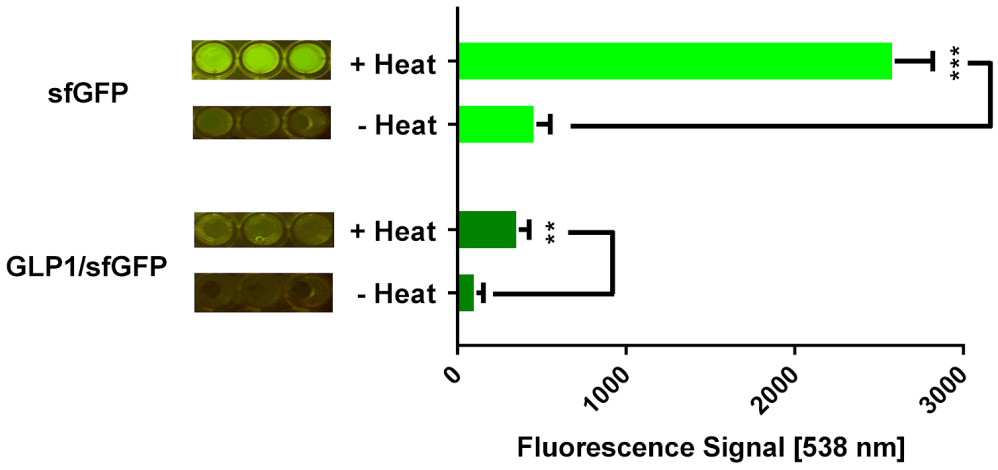

Figure 43: Fluorescence measurement by heat release of sfGLP1. Statistical analyses made for triplicates of experimental samples with Student's T-Test. (***: $p<0.001$, **: $p<0.01$)

It can be seen that supernatant fluorescence increases for both positive control and sfGLP1 construct, which is an indicator of the detachment of alpha-passenger domain from the cell surface. Although this assay is a useful way to prove surface display, results are not showing indications about TEV controlled release. Besides, in that strategy, cargo protein remains attached to the alpha-passenger domain, which may cause functional problems for the cargo in the case of enzymes or other proteins.

3.5.3. Characterization of Surface Displayed Proteins by Purified TEV Release Assay

In this thesis, our aim is to generate peptide release systems which can be precisely controlled by genetically produced TEV protease. To do that, we constructed GLP-1 and sfGLP-1 fused with alpha-passenger and beta-translocation domain of Ag43 autotransporter. Although the heat release and weak-bond disruption between alpha-passenger and beta-translocation domain shows dislocation of cargo protein with passenger domain, release of displayed proteins with TEV protease also critical for our design. To prove that, TEV release assay operated with using purified TEV protease. sfGFP and sfGLP1 displaying cells grown overnight in autoinduction medium at 30 ˚C, 200 rpm. After that, cells washed with 1xPBS (Phosphate Buffered Saline) for 2 times by centrifuging down at 3000 rpm for 10 minutes. Then, cells resuspended in 1x TEV buffer and 10 µg purified GST-TEV protein. After 16 hours of incubation at +4 ˚C in rotator, 250 µL cell sample taken and centrifuged down. Supernatant analyzed at M5 spectramax to detect released fluorescence levels (Figure 44).

From the results it can be seen that TEV protease can access its recognition site on the surface displayed proteins and can facilitate the release by cleaving the peptide backbone. In our design, TEV protease is not aimed to produce extracellularly, but with that assay, it is shown that biologically produced TEV could be the main element of our strategy that is designed to have controlled release of the surface displayed proteins. From the results it can also be seen that, although the release ratio for sfGFP and sfGLP1 obtained around 1-fold change, their maximum fluorescence is not same.

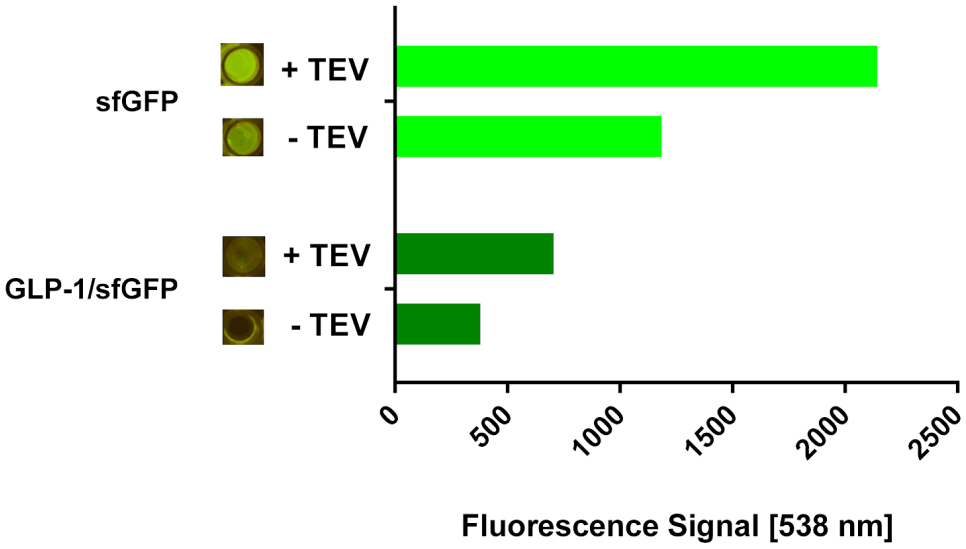

Figure 44: Supernatant fluorescence after TEV release assay. sfGFP displaying cells that carrying pET22B-T7-Ag43-sfGFP used as positive control. sfGLP1 displaying, pET22B-T7-Ag43-sfGFP carrying cells used as test group. Samples were divided into two groups as TEV uninduced (-) and TEV induced (+).

This is probably an indication of display efficiency for free sfGFP and GLP-1 tagged sfGFP protein. Although sfGFP is a fast folding mutant of fluorescent proteins, changes in the terminal regions can affect the folding and fluorescence efficiency [82].

3.5.4. Characterization of Surface Displayed Proteins by Genetically Produced TEV protease

In our strategy, we are aiming to build a response system that can sense extracellular stimulus and show its response by releasing target molecules. Experiments with TEV protease mediated release of surface displayed proteins including sfGLP1 can be released from the surface (Figure 45). As stated before, our strategy does not include addition of purified TEV protease to release the proteins, apart from this, we are aiming to produce TEV protease genetically as a control element for the release with an input molecule. To model that system, we co transformed pET22B-T7-Ag43-sfGLP1 carrying *E. coli* BL21(DE3) cells with pZA-tetO-Ag43-TEV plasmid (produced by Recep Erdem Ahan and kindly provided for this study, carrying Kanamycin resistance) which carries an inducible expression system that can be controlled with the addition of anhydrotetracycline (aTc). Genetic circuits that describe these modules illustrated in Figure 46. In that system, addition of aTc causes retardation of the repressing function of TetR transcriptional repressor, and this functional change starts the protein production from tetO promoter. In our case, this system can also be a suitable model for biosensor coupled release of the target proteins from the cell surface.

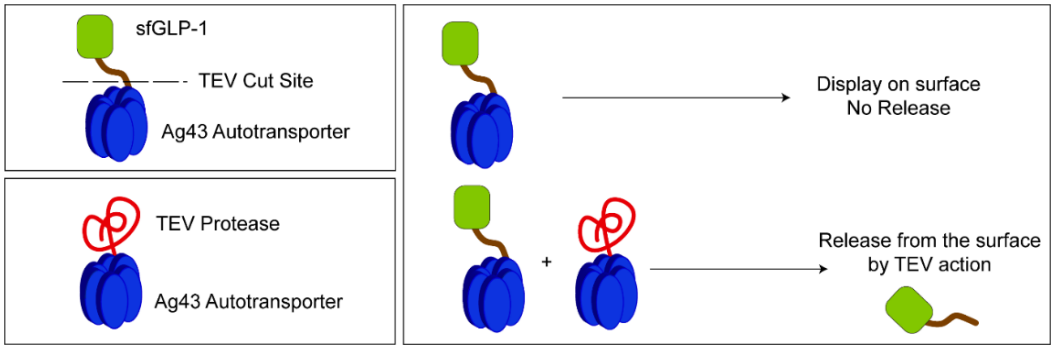

Figure 45: Illustration of overall mechanism to release sfGLP-1 from cell surface

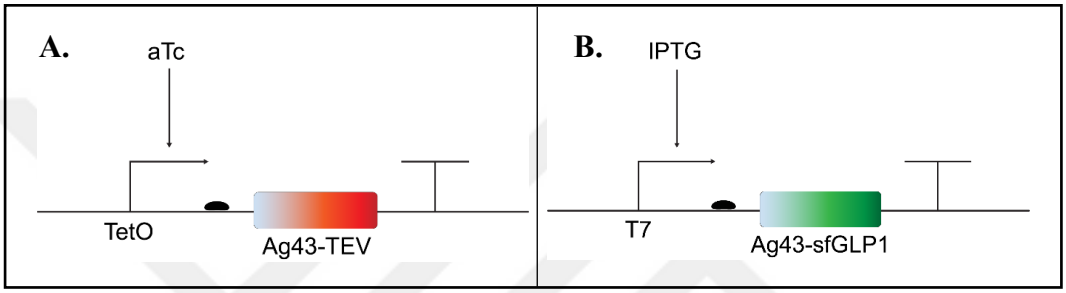

Figure 46: Co-transformed modules for genetically produced TEV protease release assay, **A)** aTc controlled Ag43-TEV expression circuit, **B)** IPTG controlled Ag43-sfGLP1 expression circuit

For testing the functionality of genetically produced TEV strategy, double plasmid carrying *E. coli* BL21(DE3) bacteria (which can produce both Ag43-TEV and Ag43-sfGLP1) and single plasmid carrying (which can only produce Ag43-sfGLP1) grown overnight in autoinduction at 200 rpm, 30 ˚C in LB medium to display proteins on cell surface. After that, cells transferred in 2XMOPS medium by centrifuging down cells at 3000 rpm for 10 minutes and washing the cells with 1xPBS for 2 times. After that, cells resuspended in 2XMOPS medium and each group divided into two subgroups as aTc (50 ng/µL) induced and uninduced. After 18h induction at 30 ˚C and 200 rpm shaker, 250 µL samples taken from the cells, samples centrifuged down at maximum speed for 2 minutes and fluorescence of supernatant measured by M5 spectramax (Figure 47).

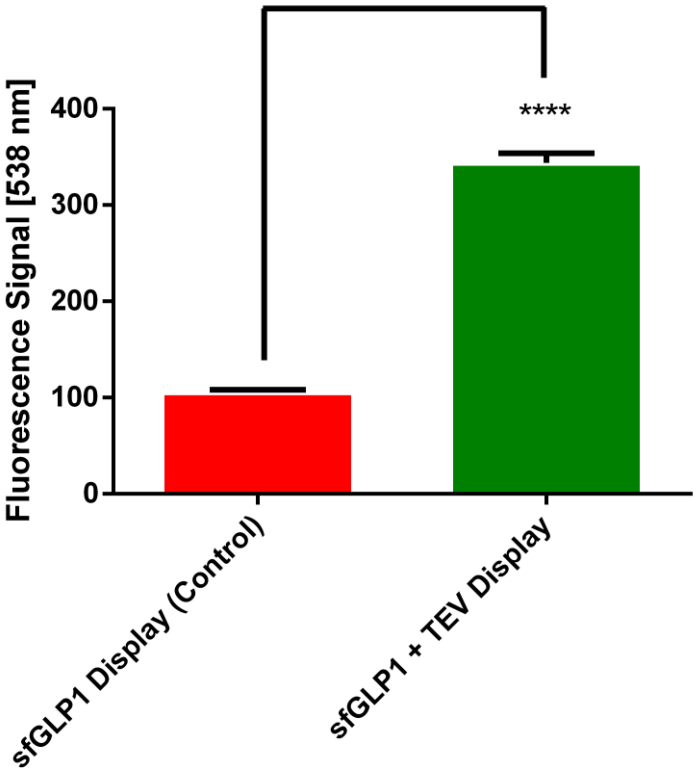

Figure 47: Genetically produced TEV release experiment for cells carrying Ag43-sfGFP or Ag43-sfGLP1 gene transformed with/without Ag43-TEV production plasmid. Statistical Analysis made for triplicates of samples with Student's T-Test (****: $p<0.0001$). Results minimized with wild type cell fluorescence.

In here, results are showing that genetically induced TEV protease could be displayed on the cell surface, can also protect its enzymatic activity to find its cognate sequence and can cleave peptide bond from that site to release surface displayed proteins. Overall, this model system strongly indicating that our system could be used to deliver surface displayed proteins to the environment if the production of Ag43-TEV could be coupled with a sensor mechanism as an output of the sensor. As also stated in our aim, we are later planning to design a glucose sensitive system which can control release of the surface displayed proteins by

changing glucose levels. Nearly 3-fold change in the supernatant fluorescence in that experiment shows that our system is a potential candidate for our future designs.

3.5.5. SDS-PAGE Analysis for the Surface Released Proteins

In order to detect and visualize the existence of sfGLP1 in heat released samples, we operated SDS-PAGE analysis as previously described method. Here, we are aimed to observe 52 kDa fragment of alpha-passenger domain and sfGLP-1 released from the surface (Figure 48).

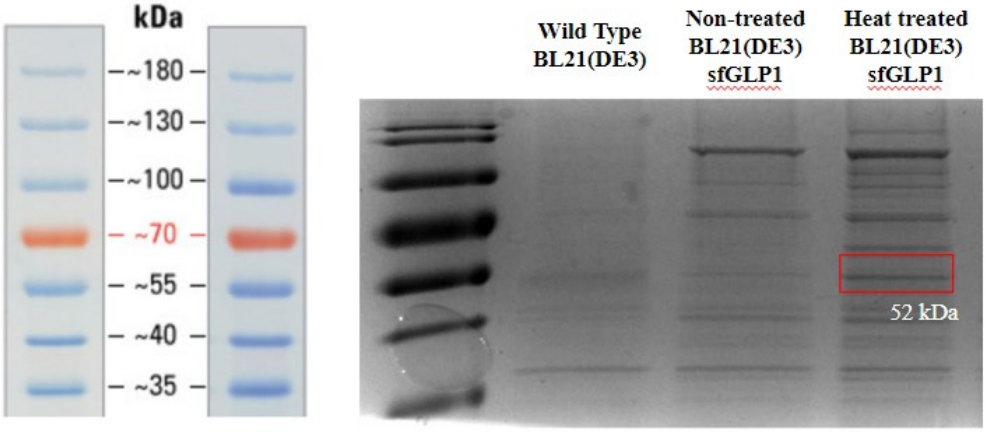

Figure 48: SDS-PAGE analysis with 12% SDS PAGE gel and Page Ruler (Thermo Scientific) protein ladder. 52 kDa overexpression band observed as expected near 55 kDa ladder band.

Here, we are also observing additional bands in the SDS PAGE gel in addition to predicted 52 kDa protein band. The reason behind this could be the burst of the cells during the procedures, or whole cell contamination during the experiments.

3.5.6. Mass Spectrometry (MS) Analyses

In order to analytically show the release of our target proteins from the surface, we operated MS analyses with the help of Dr. Ömür Çelikbıçak from Hacettepe University's HUNITEK analysis laboratories. Sample preparation and analyses operated by previously described methods and techniques. Results from the MS analyses for extracellular TEV release and genetically induced TEV release of sfGLP1 and GLP-1 obtained as illustrated below (Figure 49-56). Molecular weights for GLP-1 and sfGLP-1 calculated as 4778.59 Da and 32653.98 Da respectively. Note that for this experiment, GLP-1 is also produced with the same strategy that sfGLP1 release operated during two different TEV release strategies.

Experimental results above are showing that there is a strong evidence of released target protein/peptide to the supernatant by the TEV controlled release strategies. It should be stated that diverse bands in the results are also observed in SDS Analyses (Figure 11) operated during the release experiments. For the future of the experiments, toxicity or immunologic response to these bulk proteins might be investigated, but in the literature it is shown that *E. coli* Nissle 1917 strain is a safe probiotic strain which is naturally colonizes the human gut without causing immunologic effect. Images generated by Bruker Flex Analysis software. In the data, X-axis in the graph represents mass (since in m/z, z is generally considered as 1) and Y-axis in the graph represents intensity.

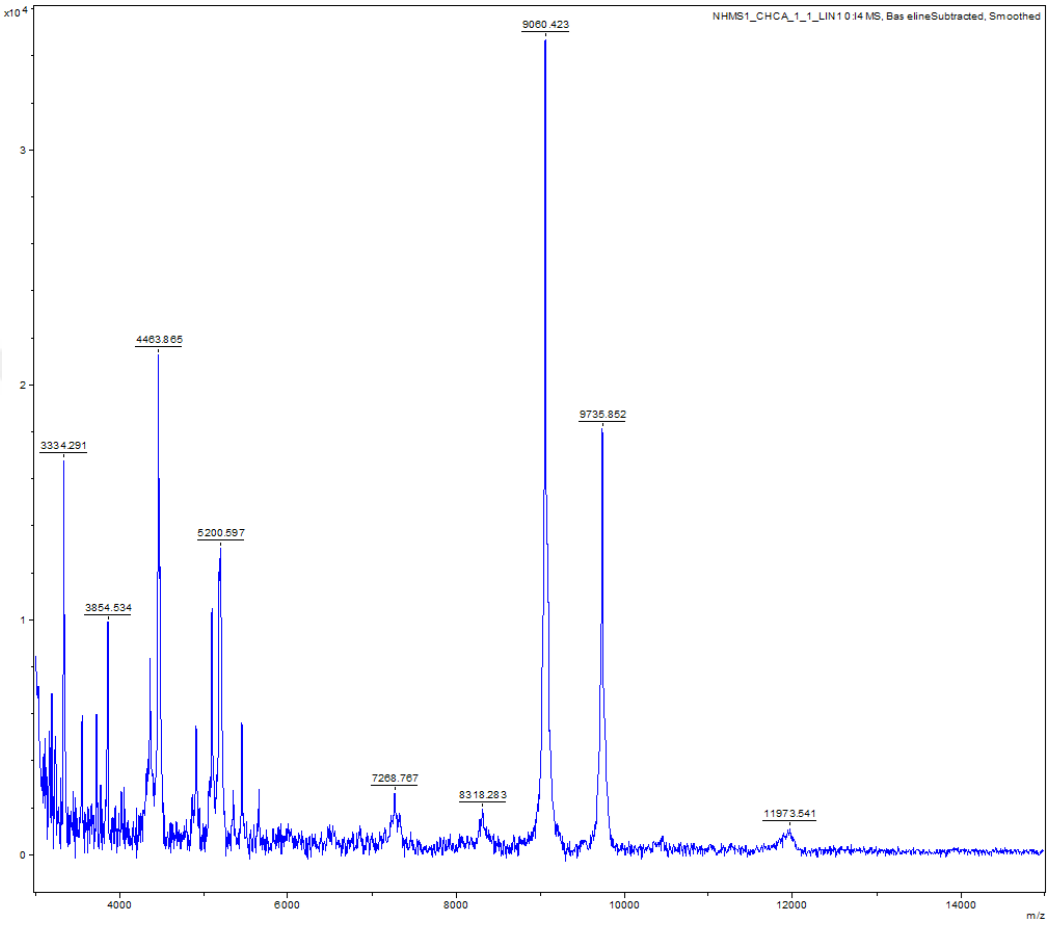

Figure 49: MS analysis results for wild type *E. coli* BL21(DE3) sample given as negative control for release experiment with purified TEV. Lower spectrum peaks (0-14 kDa) showing peaks for different molecular weight samples as expected. No trace detected for GLP-1.

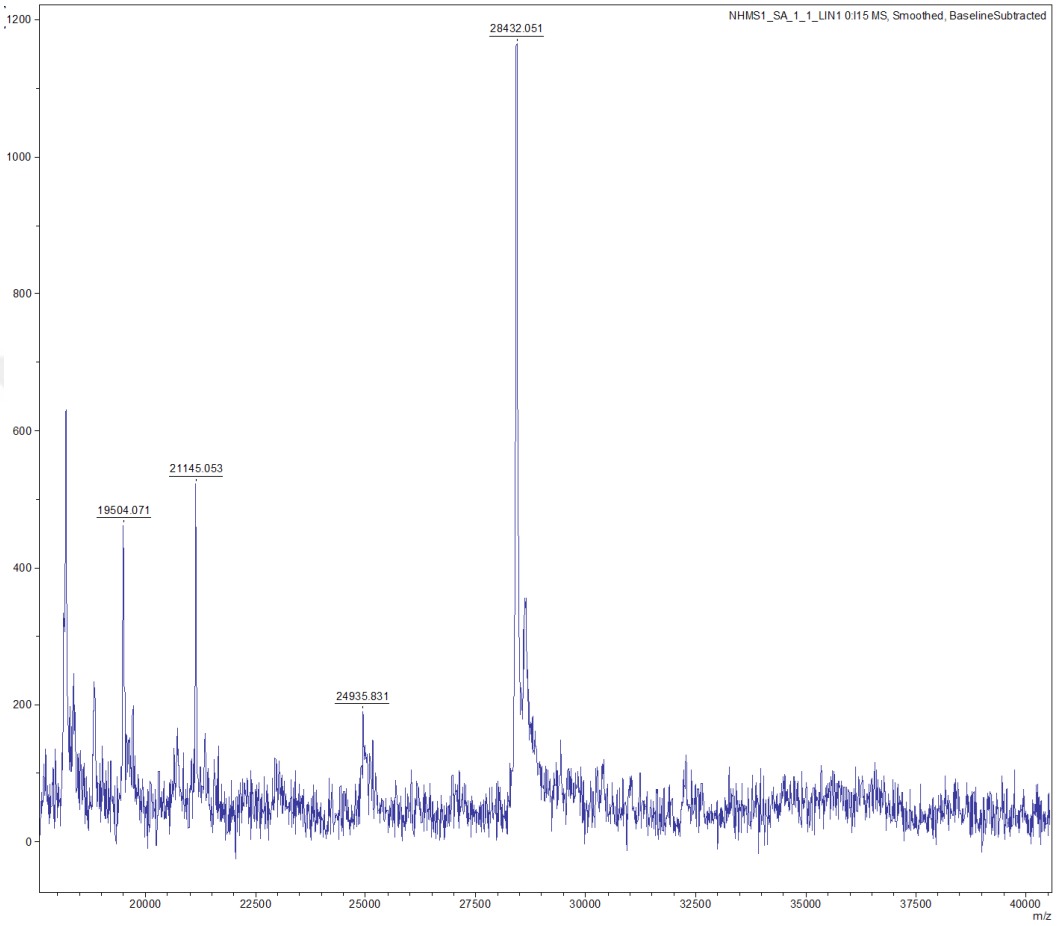

Figure 50: MS analysis results for wild type *E. coli* BL21(DE3) sample given as negative control for release experiment with purified TEV. Upper spectrum peaks (14-40 kDa) showing peaks for different molecular weight samples as expected. No trace detected for sfGLP-1.

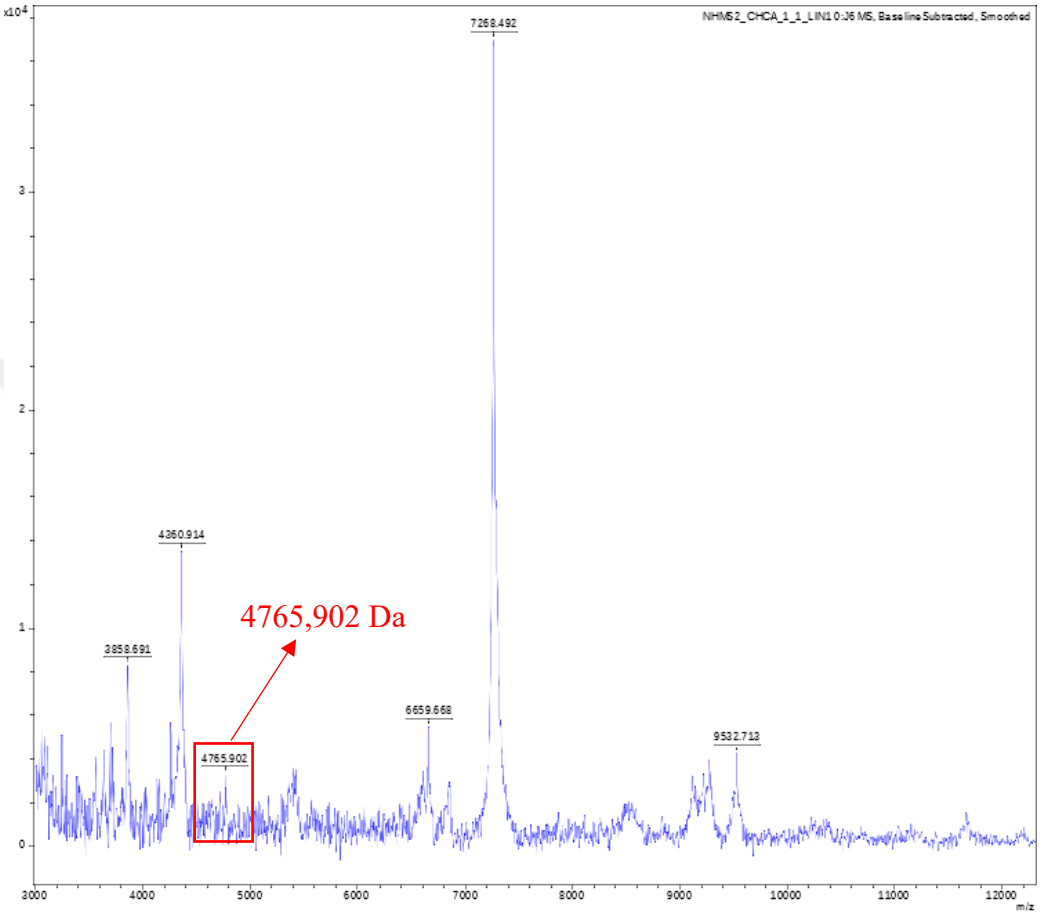

Figure 51: MS analysis results for *E. coli* BL21(DE3) - GLP-1 sample given for release experiment with purified TEV and expected GLP-1 in solution. Sample produced by extracellular TEV release of the GLP-1 from the surface. 4765.902 Da peak (squared in red) in the spectrum is interpreted as GLP-1 since it highly corresponds with expected molecular weight.

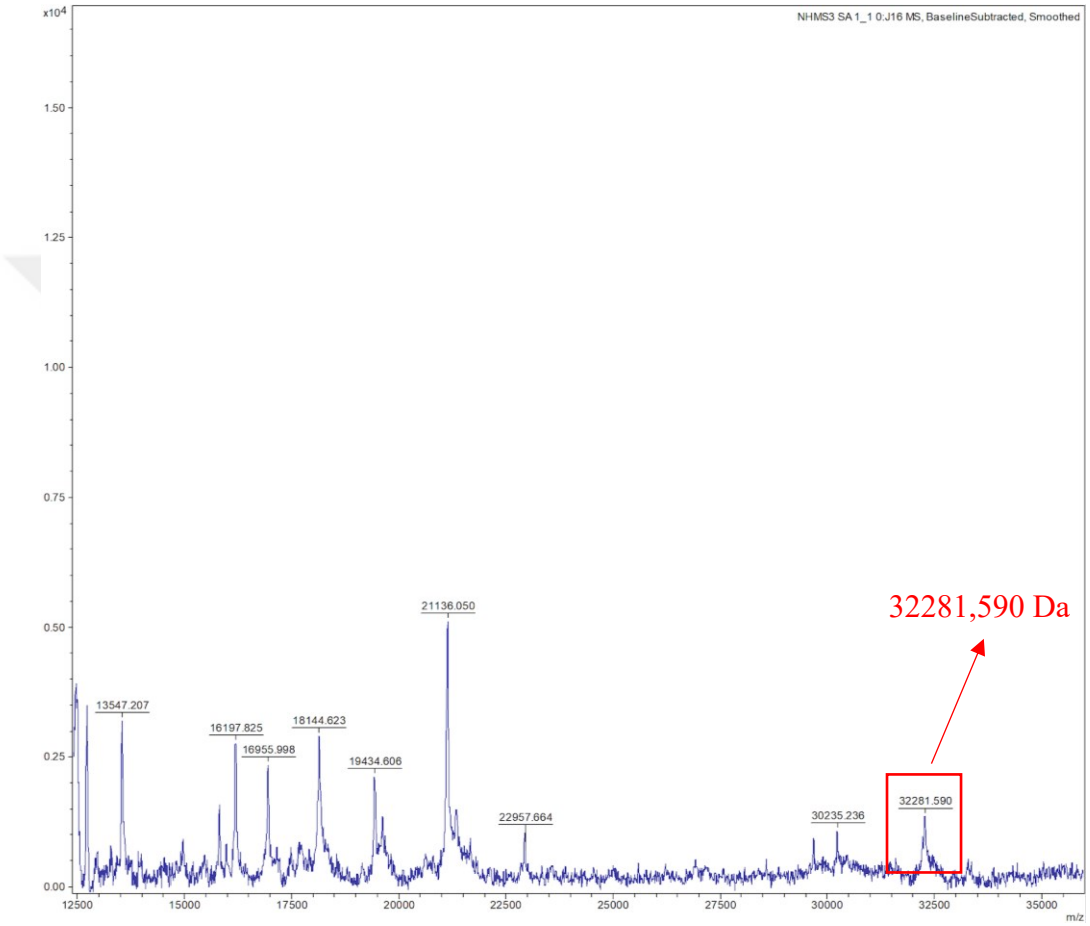

Figure 52: MS analysis results for *E. coli* BL21(DE3) - sfGLP-1 sample given for release experiment with purified TEV and expected sfGLP-1 in solution. Sample produced by extracellular TEV release of the sfGLP-1 from the surface. 32281.590 Da peak (squared in red) in the spectrum is interpreted as sfGLP-1 since it highly corresponds with expected molecular weight.

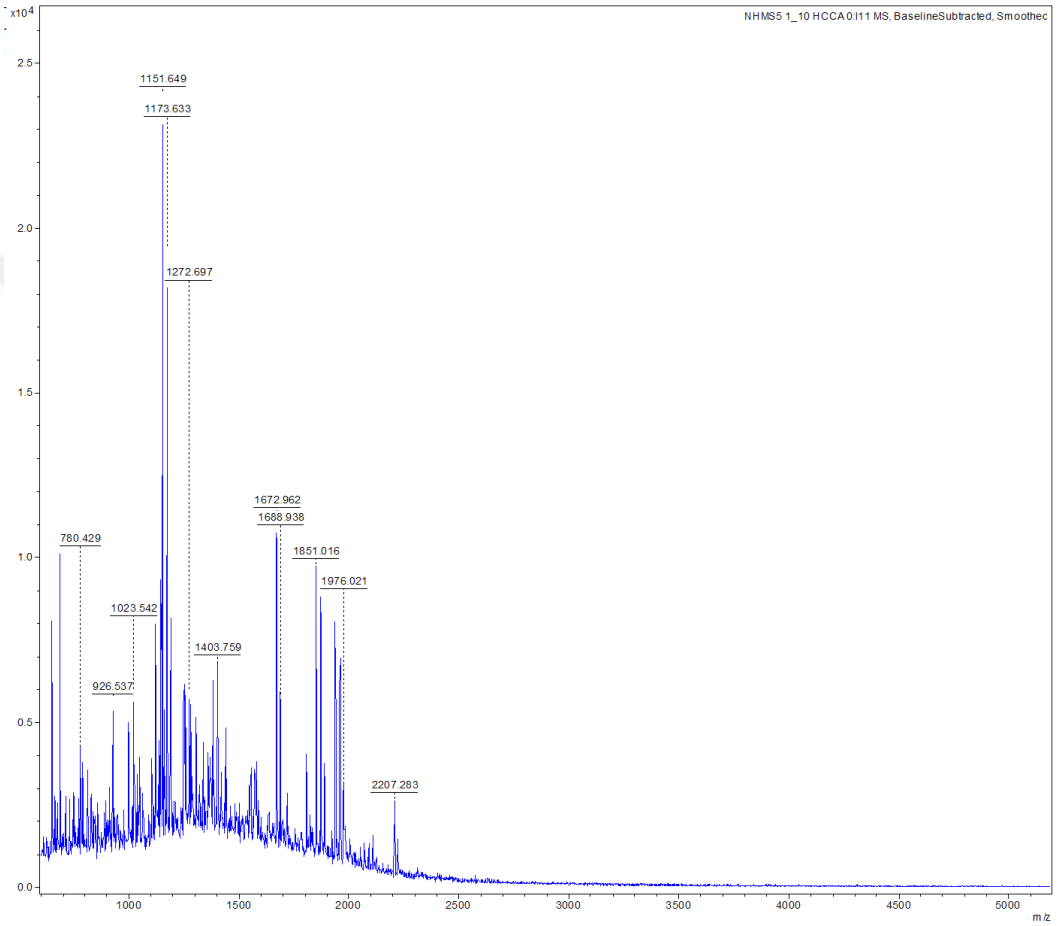

Figure 53: MS analysis results for wild type *E. coli* BL21(DE3) sample given as negative control for genetically produced TEV release experiment. Upper spectrum peaks showing peaks for different molecular weight samples as expected. No trace detected for sfGLP-1 or GLP-1.

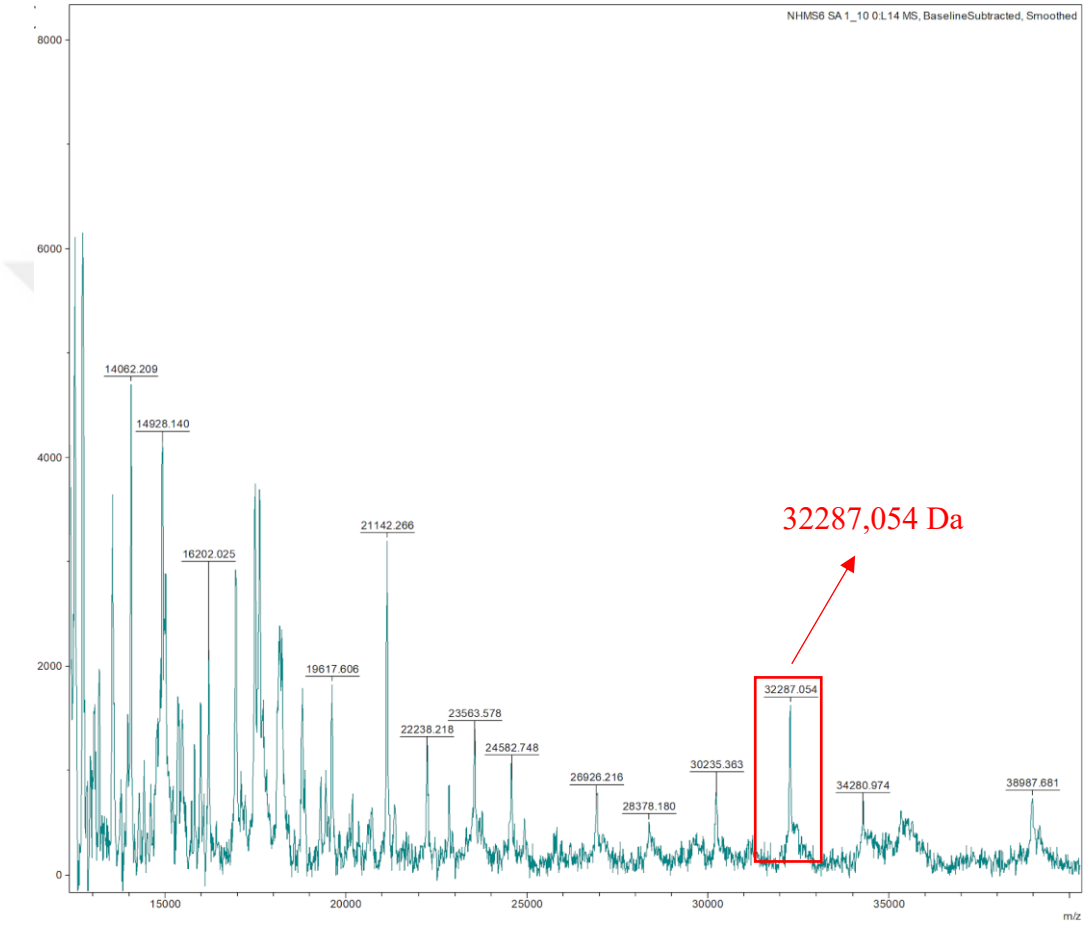

Figure 54: MS analysis results for *E. coli* BL21(DE3) - sfGLP-1 sample given for genetically produced TEV release experiment and expected sfGLP-1 in solution. Sample produced by genetically induced and surface displayed TEV release of the sfGLP-1 from the surface. 32287.054 Da peak (squared in red) in the spectrum is interpreted as sfGLP-1 since it highly corresponds with expected molecular weight.

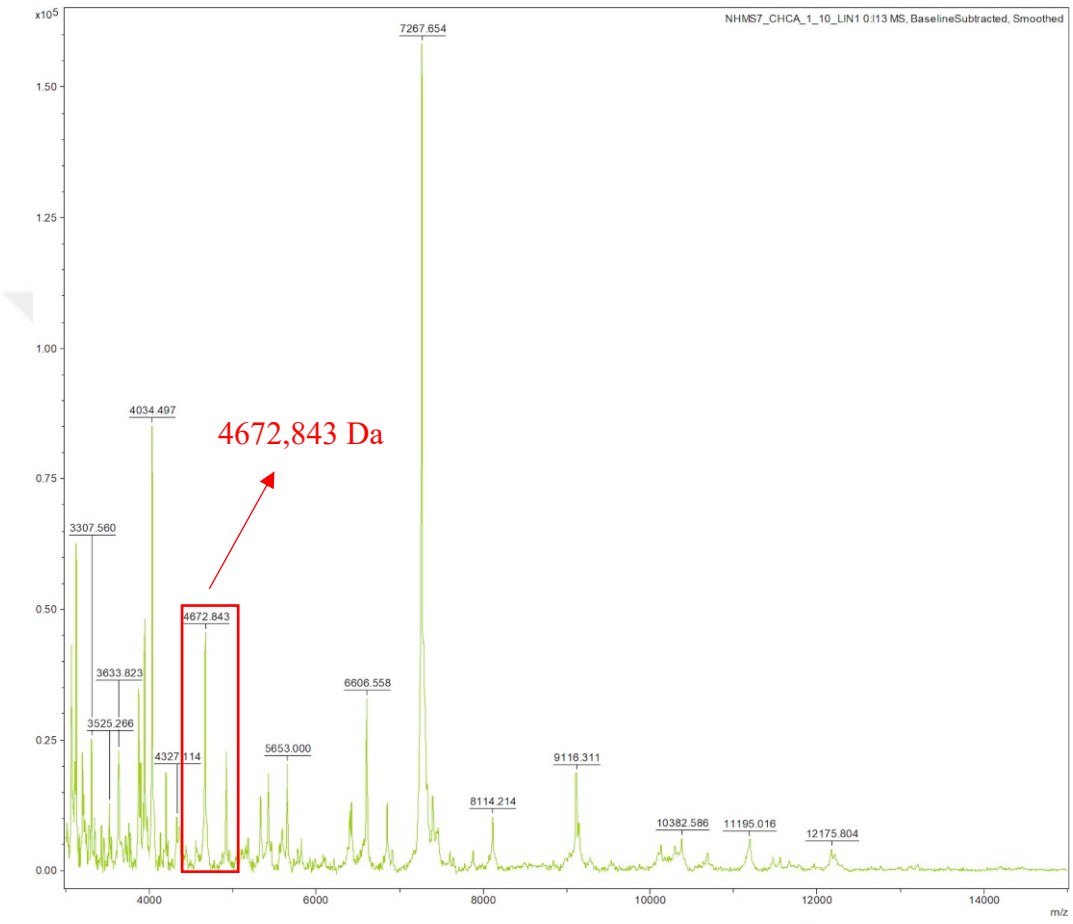

Figure 55: MS analysis results for *E. coli* BL21(DE3) - GLP-1 sample given for genetically produced TEV release experiment and expected GLP-1 in solution. Sample produced by genetically induced and surface displayed TEV release of the GLP-1 from the surface. 4672.843 Da peak (squared in red) in the spectrum is interpreted as GLP-1 since it highly corresponds with expected molecular weight.

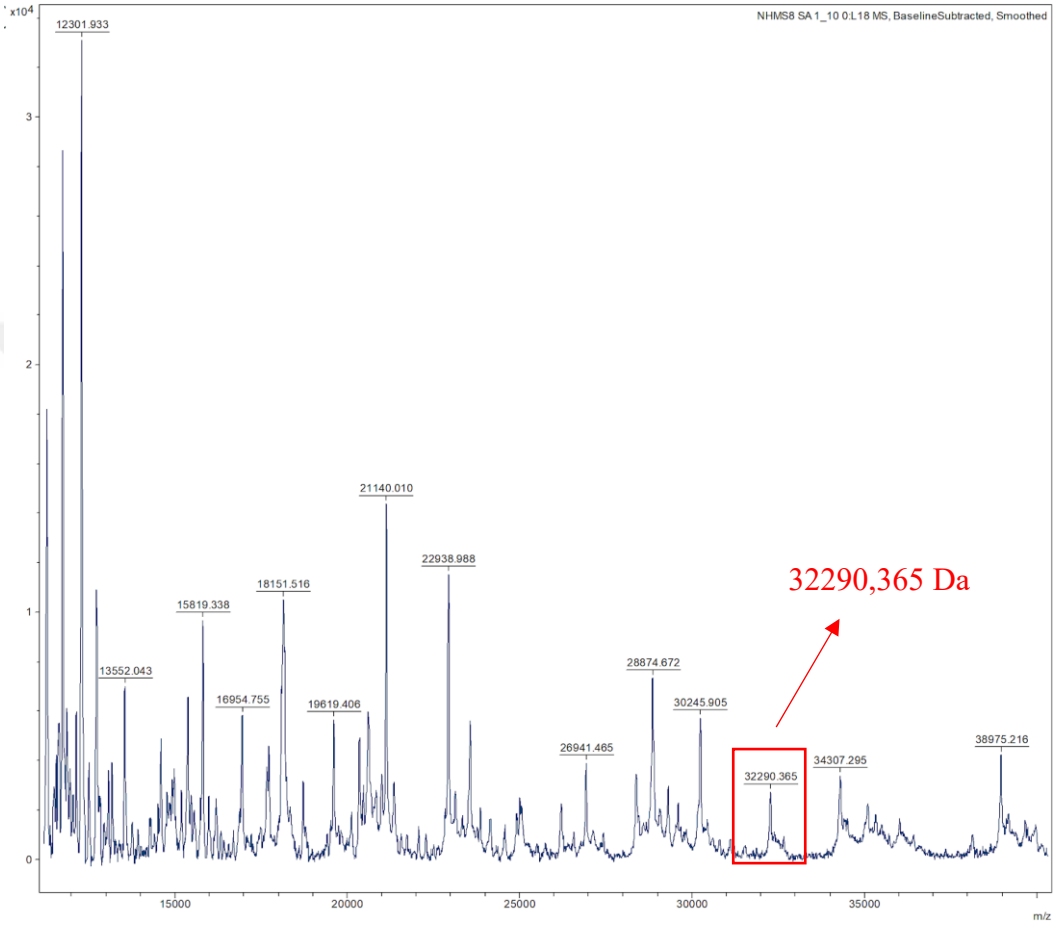

Figure 56: MS analysis results for *E. coli* BL21(DE3) - sfGLP-1 sample given for genetically produced TEV release experiment and expected sfGLP-1 in solution. Different from Figure 17, this sample generated by a longer genetic induction for Ag43-TEV display and sfGLP-1 release. Sample produced by genetically induced and surface displayed TEV release of the sfGLP-1 from the surface. 32290.365 Da peak (squared in red) in the spectrum is interpreted as sfGLP-1 since it highly corresponds with expected molecular weight.

3.5.7. Docking Studies for the Comparison of GLP-1 Analogues

After characterization and evaluation of the potential of TEV mediated release systems, we wanted to increase potential of our peptide release system by increasing the number of peptides in our repertoire. With that purpose, new GLP-1 analogues selected from the literature. Before cloning, selected peptide molecules characterized by peptide docking by using an online server, HPEPDOCK. In that server, possible structures for given peptide molecules calculated by MODPEP program and without long simulations, possible models for docking generated. After the docking analyses, structures investigated and visualized in PyMol molecular viewer (Figure 59). Binding energies for mGLP-1-His and human GLP-1(7-36) also obtained as shown below (Figure 57, 58);

Rank	1	2	3	4	5	6	7	8	9	10
Docking Score	-283.229	-278.311	-277.105	-274.813	-270.142	-258.948	-258.000	-256.699	-255.694	-253.008

Figure 57: Binding energies for best 10 models for the docking of human GLP-1(7-36) to human GLP1 receptor.

Rank	1	2	3	4	5	6	7	8	9	10
Docking Score	-280.809	-271.644	-267.458	-260.158	-255.454	-254.966	-254.775	-249.793	-248.904	-248.025

Figure 58: Binding energies for best 10 models for the docking of mGLP-1(7-36)-His to human GLP1 receptor.

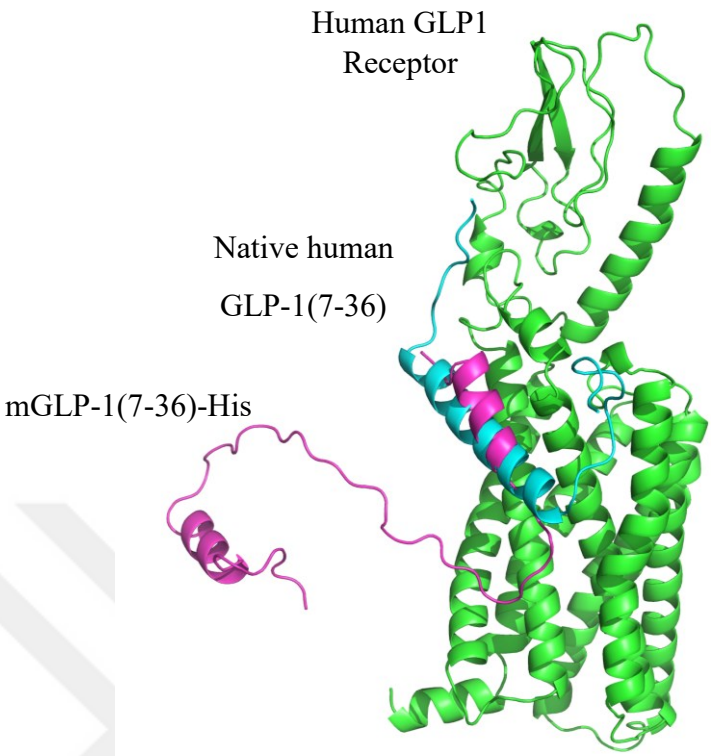

Figure 59: Docking results representing green (human GLP-1 receptor), purple (mGLP-1(7-36)-His) and blue (native human GLP-1(7-36)).

In the literature, binding site of the human GLP-1(7-36) hormone to the human GLP-1 receptor defined with a full length, peptide bound X-Ray crystal structure [83]. Here our docking results showing very strong correlation with this study, as the two of the candidate peptides calculated to bind alpha-helical regions between extracellular domain and periplasmic domain. It can be suggested that modifications on peptide structures for incorporation with peptide release systems may not be affecting binding capabilities of our candidate peptides. Besides, very low difference between binding energies of native and engineered structures of peptide molecules are showing that essential residues are neither affected by the modifications, nor changing the folding kinetics. Prior to in vitro activity studies, our docking results showing promising binding kinetics for designed peptides.

3.5.8. Construction of pET22B-T7 Plasmids for GLP-1 Analogues

After the docking studies, three GLP-1 analogues designed to enrich the peptide release repertoire in our study (Figure 60). These analogues named as mGLP1 (7-36)-His, which has a modified version of GLP-1 hormone for proteases, mGLP1(7-36)-PEN, which has mGLP1 fused with a cell penetrating peptide, and Exentin-4-PEN, which has an another GLP-1 analogue fused with cell penetrating peptide. These analogues ordered from IDT Company as gene fragments with Gibson assembly overlaps and assembled with plasmid backbone that is used to construct pET22B-T7-Ag43-GLP1 plasmid by using 1:8 backbone to insert ratio. After cloning, two colonies selected for each analogue and send to the Sanger sequencing (Appendix D3, 4, 5). With that, we will also be able to test different GLP-1 mutants for their ability to lower glucose levels in the future.

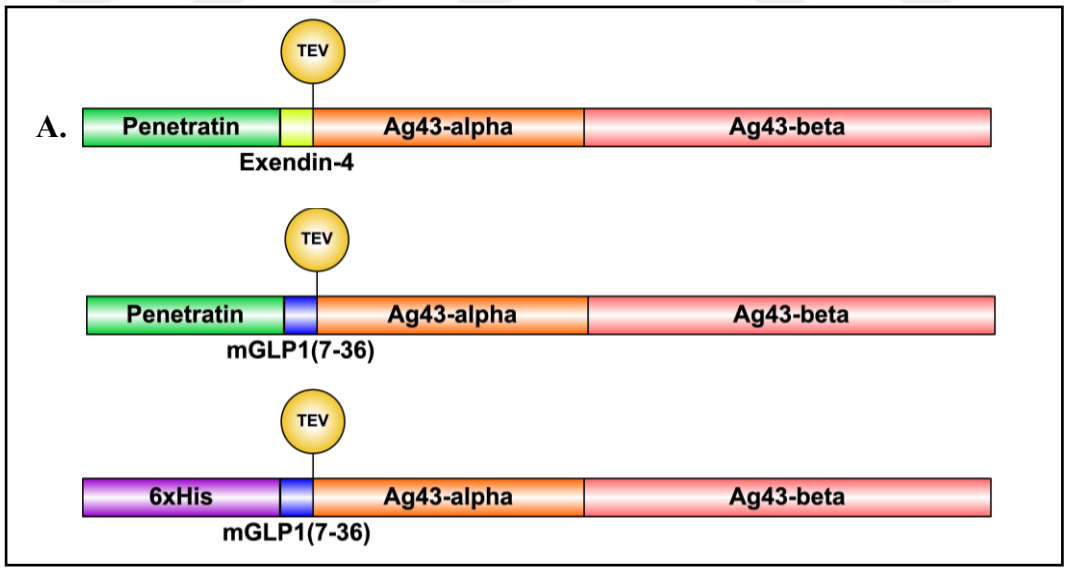

Figure 60: Illustration of GLP-1 analogues **A)** Exentin-4-PEN, **B)** mGLP1(7-36)-PEN, **C)** mGLP1 (7-36)-His

3.6. Design Strategies for Glucose Sensor Coupled sfGLP-1 release from *E. coli* Bacteria

As a final experiment to test our system, we designed two different constructs to control the release of sfGLP-1 from the surface of *E. coli* bacteria. This experiment designed to be a model for our main aim in this thesis, which is to build a biological system to detect glucose and respond by synthesizing therapeutic molecules with detection signal strength.

In order to do that, sfGLP-1 continuously displayed on cell surface by transferring its gene to the downstream region of a constitutive promoter, PROD, with SpxB enzyme to continuously express these two proteins. In a different plasmid, we cloned PerR continuously expressed from PROD promoter and Ag43-TEV from Ahp/Per hybrid promoter. With this design, it is aimed to display Ag43-TEV on the cell surface with correlated amount of glucose presented in the environment. Eventually, it is aimed to release Ag43-sfGLP1 to the environment by glucose controlled Ag43-TEV expression with illustrated strategies below (Figure 61).

During the experiments, cells grown in glycerol supplemented 2XMOPS medium at a certain cell number to provide continuous display of sfGLP1 to the surface. After that, glucose added to the medium with given concentrations to start Ag43-TEV display to the surface coupled by glucose sensor mechanism. At the end of the experiments, growth samples collected and supernatant fluorescence measured. Overall design and characterization strategy build to represent cell growth in living conditions and introduction of glucose to the environment.

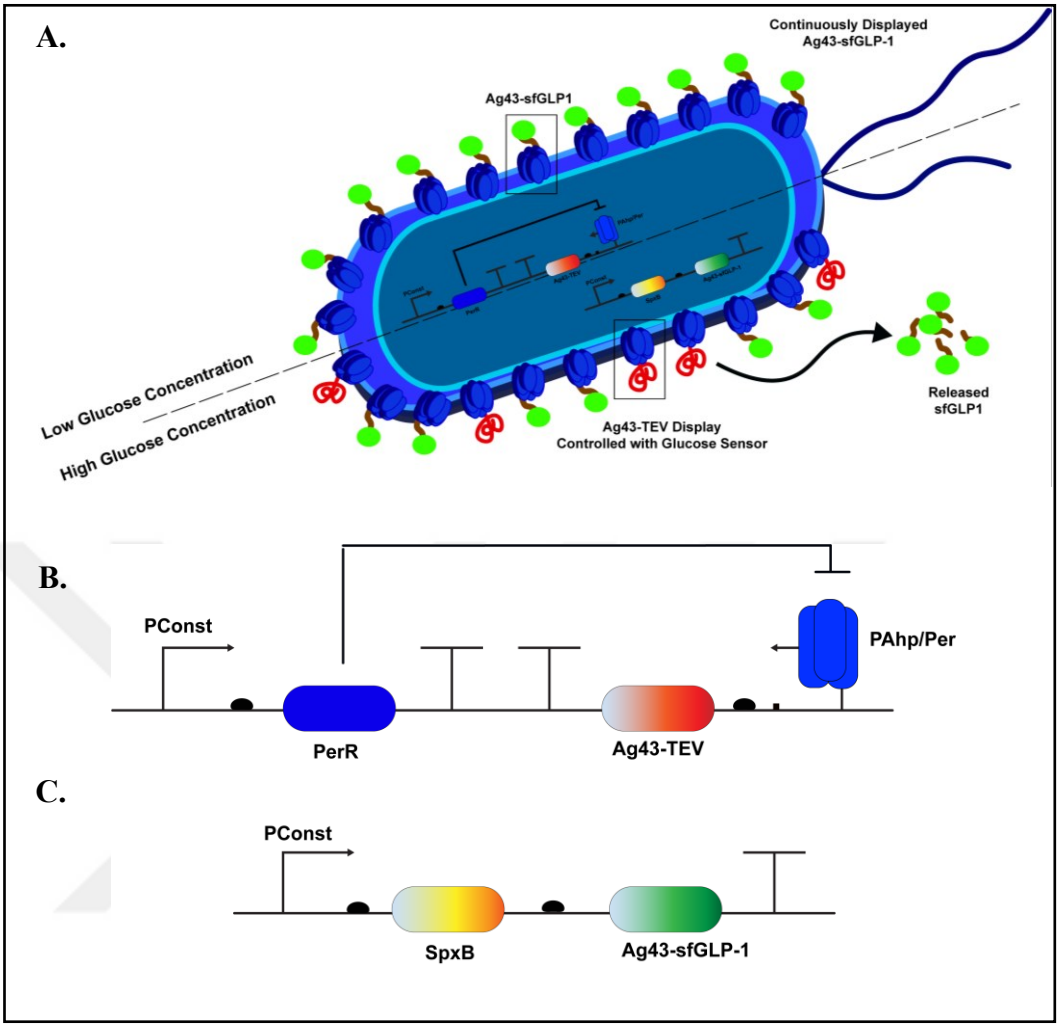

Figure 61: Illustration of glucose sensor coupled release strategy **A)** and genetic circuits for pZA-Ahp/Per-Ag43-TEV **B)** and pZS-PROD-SpxB-Ag43-sfGLP1 **C)**.

3.6.1 Cloning for pZS - SpxB - Ag43 - sfGLP1 and pZA - Ahp/Per - Ag43 - TEV plasmids

In order to construct pZA - PROD - PerR - Ahp/Per - Ag43 - TEV plasmid, previously built, PerR based hydrogen peroxide biosensor plasmid used as template to amplify 2.6 kb backbone with pZA-H2O2-R-Rev1 and pZA-V3-Rel-BB-For primers. Ag43-TEV insert (3369 bp) to generate that plasmid obtained from REA83 plasmid (previously built and kindly provided by Recep Erdem Ahan) with using pZA-V3-Rel-For and pZA-V3-Rel-Rev primers (Figure 62).

Two fragments joined together as previously described and Ag43-TEV gene characterized by colony PCR.

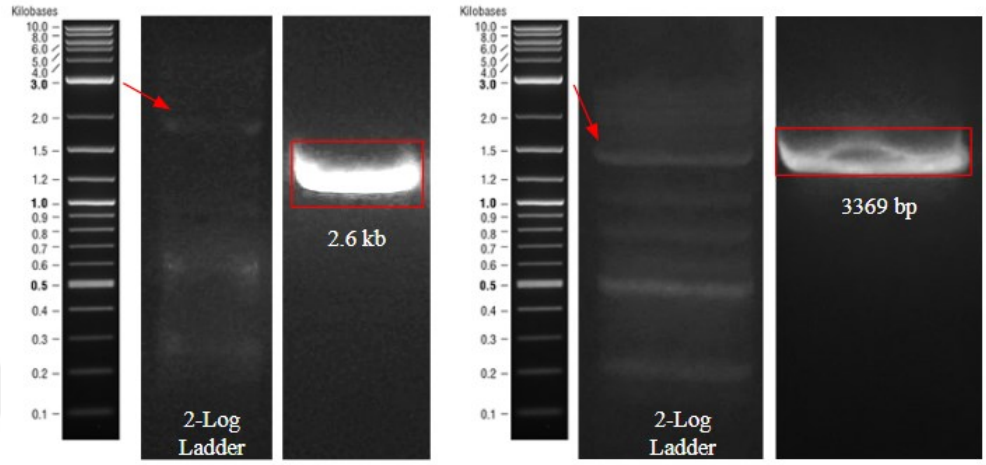

Figure 62: Agarose gel image for pZA - Ahp/Per - Ag43-TEV construct insert (right, 3369 bp) and backbone (right, 2.6 kb). 2-log (NEB) DNA ladder used for characterizations.

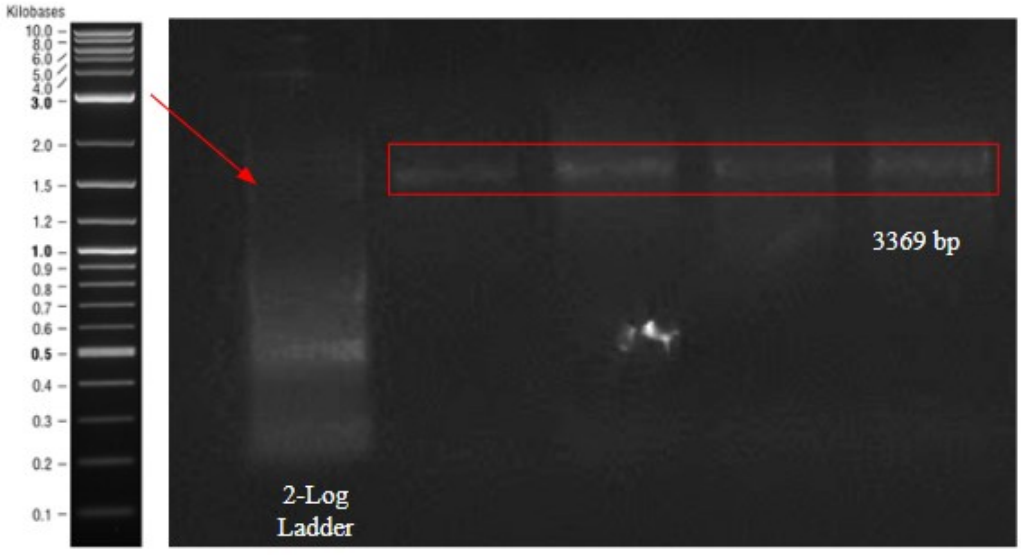

Figure 63: Agarose gel image for colony PCR to detect 3369 bp Ag43-TEV insert in for pZA - Ahp/Per - Ag43-TEV construct

For the construction of continuous expression of SpxB and continuous display of Ag43-sfGLP1, pZS-PROD-SpxB-Ag43-sfGLP1 plasmid built as previously described. In order to amplify backbone (3.7 kb), pZS-PROD plasmid previously built gold sensor plasmid amplified with REA97 and REA98 primers (Figure 64). After that, first insert SpxB gene amplified with pZS-PRODMC-Rev and SpxB-EF primers as 2004 bp amplicon (Figure 64) and Ag43-sfGLP1 gene amplified by using PELB-SpxBE-rev and Ag43-sfGLP1-pZS-For primers as 3474 bp amplicon (Figure 64). These three fragments joined together as previously described and characterized. sfGFP fluorescence also visually inspected for characterization.

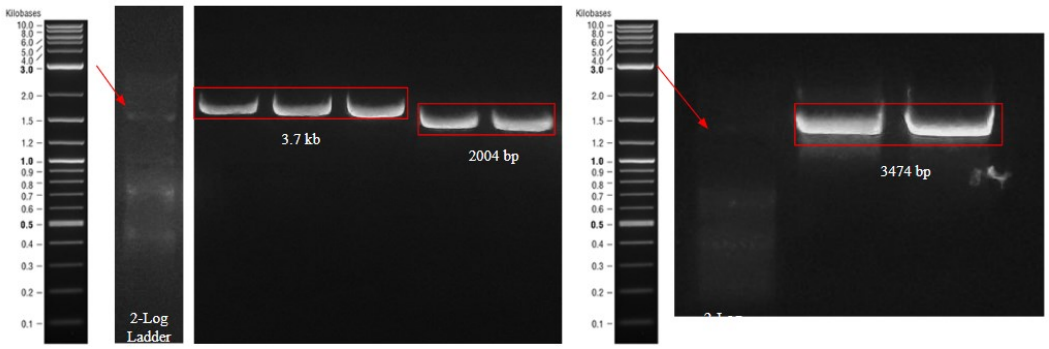

Figure 64: Agarose gel image for pZS-PROD-SpxB-Ag43-sfGLP1 construct. Backnone and first insert (left, 3.7 kb backbone, 2 kb insert) and second insert (right, 2.6 kb). 2-log (NEB) DNA ladder used for characterizations.

3.6.2 Characterization of Glucose Sensor Coupled Release System

In order to preliminarily test the release of sfGLP-1 from cell surface, we co-transformed pZS - PRD - SpxB - Ag43 - sfGLP1 and pZA - PROD - PerR - Ahp/Per - Ag43 - TEV plasmids into *E. coli* DH5α. In that experiment, we are aimed to continuously display sfGLP1 on *E. coli* surface, and by controlling the

expression of AG43-TEV via the glucose sensor, we wanted to adjust the release of the sfGLP1. SpxB and PerR also continuously expressed to build the system inside cell. During the experiment, cells grown in LB medium overnight at 37 ˚C, 200 rpm for overnight. After that cells passaged into fresh 2x MOPS (supplemented with 2% glycerol) medium with 1:100 dilution to grow until an OD600 value of 0.4-0.5. Then, cells induced with given amounts of glucose to test system response. Next, cells transferred in 30 ˚C, 200 rpm for overnight growth. Finally, fluorescence of cell supernatant measured as described before and following results obtained (Figure 65).

According to the results, it can be said that there is a significant change in fluorescence of the supernatant of growth media which is statistically significant. Although the signal ratio is very low, these results indicating that our system could be a good basis for optimizing glucose sensor mediated peptide release from the surface. In addition, it is known that glycerol, which is the primary carbon source during the experiments, can also be converted to the pyruvate by the *E. coli* metabolism. This is probably the main reason of high background fluorescence in low glucose growth conditions. To prevent this, experiment will repeated with alternative carbon sources such as acetate or succinate, which are not converted into pyruvate, yet supporting the growth.

Overall, whole-cell glucose biosensor coupled release strategy has a flexible and robust design which can be engineered more to optimize therapeutic strategies with the proposed system. Although physiological conditions are different inside the human body, we believe that our systems providing ideal basis modules to optimize complex operations.

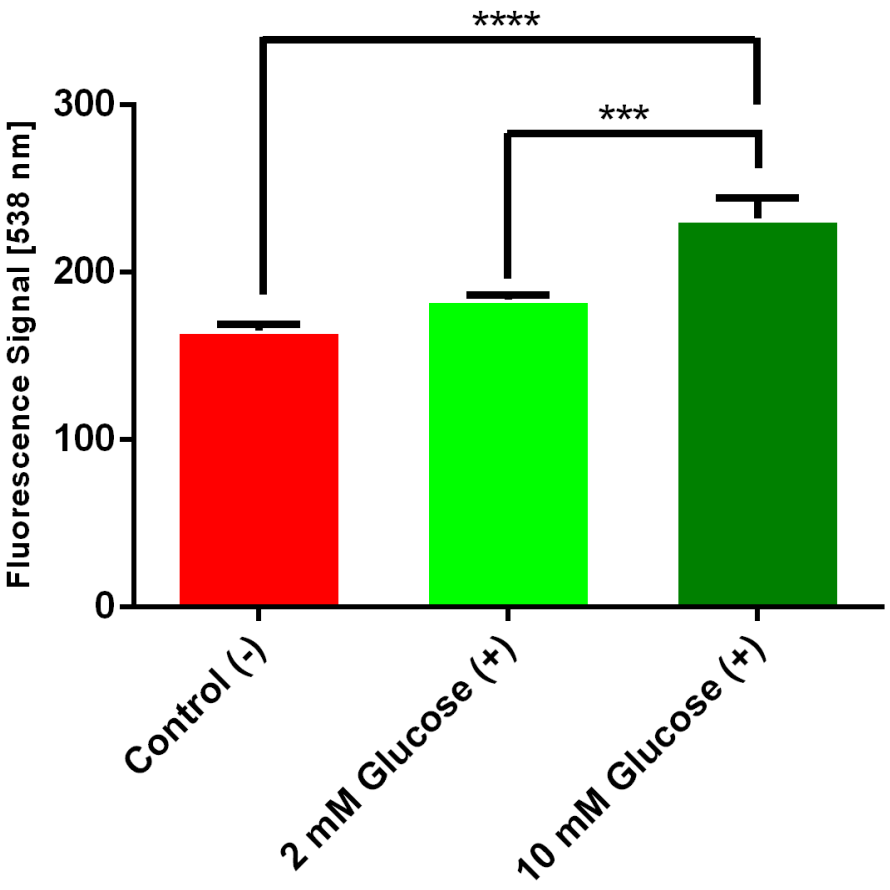

Figure 65: Glucose sensor controlled sfGLP-1 release characterized by measuring fluorescence at M5 Spectramax. Statistical analyses made by using triplicates of samples and by incorporating Tukey's Multiple Comparison Test (One Way ANOVA, ***: $p<0.001$, ****: $p<0.0001$).

CHAPTER 4

CONCLUSIONS

In conclusion, our prototype biological device can detect glucose levels and respond these glucose levels by releasing therapeutic molecules in a certain level. To achieve this, we engineered two different modules by also trying different strategies from the literature. Although they promise high specificity, two component systems having problems in physiological levels of glucose since the cell chassis also affected from the inducer. As an alternative strategy, GoX mediated glucose sensor design experiments showed us that hydrogen peroxide can be produced inside the cell but resistance mechanisms and internal generation of hydrogen peroxide could have negative effects on enzyme mediated designs on metabolite biosensors. Yet, SpxB mediated designs provided a better solution for our glucose sensor design by yielding sufficient levels of signal output. Apart from the sensor module, characterizations on release system resulted with positive and promising data about release characterization and future biological activity assays. Our heat release and extracellular TEV release experiments gave positive results as expected about the release of targeted molecules, and later MS analyses also confirmed our predictions. Besides, docking studies resulted with promising models that is giving valuable pre-visions about binding kinetics of our engineered peptides. Finally, preliminary experiments on incorporating release and sensing modules also yielded positive results and gave us insights about future characterizations. Overall, experiments on proposed strategy resulted with

promising outcomes for the design of the system. Development of such modules can also support research on different disease conditions, and could be an optimal basis for the development of theranostic biodevices for other biomedical applications.

BIBLIOGRAPHY

[1] Brune KD, Bayer TS. Engineering microbial consortia to enhance biomining and bioremediation. Front Microbiol. 2012;3.

[2] Manzoni R, Urrios A, Velazquez-Garcia S, de Nadal E, Posas F. Synthetic biology: insights into biological computation. Integr Biol-Uk. 2016;8:518-32.

[3] Riglar DT, Silver PA. Engineering bacteria for diagnostic and therapeutic applications. Nat Rev Microbiol. 2018;16:214-25.

[4] Pedrolli DB, Ribeiro NV, Squizato PN, de Jesus VN, Cozetto DA. Encineerinc Microolal Livinc Thera The Synthetic Bolocy Tooloox. Trends Biotechnol. 2019;37:100-15.

[5] Sedlmayer F, Aubel D, Fussenegger M. Synthetic gene circuits for the detection, elimination and prevention of disease. Nat Biomed Eng. 2018;2:399-415.

[6] Mathipa MG, Thantsha MS. Probiotic engineering: towards development of robust probiotic strains with enhanced functional properties and for targeted control of enteric pathogens. Gut Pathog. 2017;9.

[7] Way JC, Collins JJ, Keasling JD, Silver PA. Integrating Biological Redesign: Where Synthetic Biology Came From and Where It Needs to Go. Cell. 2014;157:151-61.

[8] Benner SA, Sismour AM. Synthetic biology. Nat Rev Genet. 2005;6:533-43.

[9] Canton B, Labno A, Endy D. Refinement and standardization of synthetic biological parts and devices. Nat Biotechnol. 2008;26:787-93.

[10] Steidler L, Neirynck S, Huyghebaert N, Snoeck V, Vermeire A, Goddeeris B, et al. Biological containment of genetically modified Lactococcus lactis for intestinal delivery of human interleukin 10. Nat Biotechnol. 2003;21:785-9.

[11] Ahmed A, Rushworth JV, Hirst NA, Millner PA. Biosensors for Whole-Cell Bacterial Detection. Clin Microbiol Rev. 2014;27:631-46.

[12] Wright O, Stan GB, Ellis T. Building-in biosafety for synthetic biology. Microbiol-Sgm. 2013;159:1221-35.

[13] Farzadfard F, Lu TK. Emerging applications for DNA writers and molecular recorders. Science. 2018;361:870-5.

[14] Esvelt KM, Wang HH. Genome-scale engineering for systems and synthetic biology. Mol Syst Biol. 2013;9.

[15] Claesen J, Fischbach MA. Synthetic Microbes As Drug Delivery Systems. Acs Synth Biol. 2015;4:358-64.

[16] Sanders ME. Probiotics: Considerations for human health. Nutr Rev. 2003;61:91-9.

[17] Backhed F, Fraser CM, Ringel Y, Sanders ME, Sartor RB, Sherman PM, et al. Defining a Healthy Human Gut Microbiome: Current Concepts, Future Directions, and Clinical Applications. Cell Host Microbe. 2012;12:611-22.

[18] Klaenhammer TR, Kleerebezem M, Kopp MV, Rescigno M. The impact of probiotics and prebiotics on the immune system. Nat Rev Immunol. 2012;12:728-34.

[19] Bezkorovainy A. Probiotics: determinants of survival and growth in the gut. Am J Clin Nutr. 2001;73:399s-405s.

[20] He L, Yang HJ, Tang JL, Liu ZD, Chen YY, Lu BH, et al. Intestinal probiotics E. coli Nissle 1917 as a targeted vehicle for delivery of p53 and Tum-5 to solid tumors for cancer therapy. J Biol Eng. 2019;13.

[21] Kurtz CB, Millet YA, Puurunen MK, Perreault M, Charbonneau MR, Isabella VM, et al. An engineered E-coli Nissle improves hyperammonemia and survival in mice and shows dose-dependent exposure in healthy humans. Sci Transl Med. 2019;11.

[22] Chua KJ, Kwok WC, Aggarwal N, Sun T, Chang MW. Designer probiotics for the prevention and treatment of human diseases. Curr Opin Chem Biol. 2017;40:8-16.

[23] Swofford CA, Van Dessel N, Forbes NS. Quorum-sensing Salmonella selectively trigger protein expression within tumors. Cancer Res. 2015;75.

[24] Yang GL, Jiang YL, Yang WT, Du F, Yao YB, Shi CW, et al. Effective treatment of hypertension by recombinant Lactobacillus plantarum expressing angiotensin converting enzyme inhibitory peptide. Microb Cell Fact. 2015;14.

[25] Geldart K, Borrero J, Kaznessis YN. Chloride-Inducible Expression Vector for Delivery of Antimicrobial Peptides Targeting Antibiotic-Resistant Enterococcus faecium. Appl Environ Microb. 2015;81:3889-97.

[26] Wei C, Xun AY, Wei XX, Yao J, Wang JY, Shi RY, et al. Bifidobacteria Expressing Tumstatin Protein for Antitumor Therapy in Tumor-Bearing Mice. Technol Cancer Res T. 2016;15:498-508.

[27] Grozdanov L, Raasch C, Schulze E, Sonnenborn U, Gottschalk G, Hacker J, et al. Analysis of the genome structure of the nonpathogenic probiotic Escherichia coli strain Nissle 1917. J Bacteriol. 2004;186:5432-41.

[28] Duan FP, March JC. Engineered bacterial communication prevents Vibrio cholerae virulence in an infant mouse model. P Natl Acad Sci USA. 2010;107:11260-4.

[29] Hwang IY, Koh E, Wong A, March JC, Bentley WE, Lee YS, et al. Engineered probiotic Escherichia coli can eliminate and prevent Pseudomonas aeruginosa gut infection in animal models. Nat Commun. 2017;8.

[30] Ou BM, Yang Y, Tham WL, Chen L, Guo JT, Zhu GQ. Genetic engineering of probiotic Escherichia coli Nissle 1917 for clinical application. Appl Microbiol Biot. 2016;100:8693-9.

[31] Olokoba AB, Bojuwoye EJ, Olokoba LB, Braimoh KT, Inikori AK. Gallstone Disease and Type-2 Diabetes Mellitus-the Link. Jcpsp-J Coll Physici. 2007;17:594-7.

[32] Atkinson MA, Eisenbarth GS. Type 1 diabetes: new perspectives on disease pathogenesis and treatment. Lancet. 2001;358:221-9.

[33] Lee MK, Kwon HS. The Number of Metabolic Syndrome Components and Incidence Rates of Type 2 Diabetes-A Korean National Sample Cohort Study. Diabetes. 2018;67.

[34] O'Rahilly S, Barroso I, Wareham NJ. Genetic factors in type 2 diabetes: The end of the beginning? Science. 2005;307:370-3.

[35] Kahn SE. The relative contributions of insulin resistance and beta-cell dysfunction to the pathophysiology of Type 2 diabetes. Diabetologia. 2003;46:3-19.

[36] Qin JJ, Li YR, Cai ZM, Li SH, Zhu JF, Zhang F, et al. A metagenome-wide association study of gut microbiota in type 2 diabetes. Nature. 2012;490:55-60.

[37] Hanefeld M, Koehler C, Gallo S, Benke I, Ott P. Impact of the individual components of the metabolic syndrome and their different combinations on the prevalence of atherosclerotic vascular disease in type 2 diabetes: the Diabetes in Germany (DIG) study. Cardiovasc Diabetol. 2007;6.

[38] Imperatore G, Liese AD, Boyle JP, Liu LL, Thompson TJ, Mayer-Davis EJ, et al. Projections of Type 1 and Type 2 Diabetes Burden in the U. S. Population Aged < 20 Years Through 2050 Dynamic modeling of incidence, mortality, and population growth. Diabetes Care. 2012;35:2515-20.

[39] Bowker SL, Majumdar SR, Veugelers P, Johnson JA. Increased cancer-related mortality for patients with type 2 diabetes who use sulforrylureas or insulin. Diabetes Care. 2006;29:254-8.

[40] Chamberlain JJ, Rhinehart AS, Shaefer CF, Neuman A. Diagnosis and Management of Diabetes: Synopsis of the 2016 American Diabetes Association Standards of Medical Care in Diabetes. Ann Intern Med. 2016;164:542-+.

[41] Drab SR. Incretin-Based Therapies for Type 2 Diabetes Mellitus: Current Status and Future Prospects. Pharmacotherapy. 2010;30:609-24.

[42] Duan FF, Liu JH, March JC. Engineered Commensal Bacteria Reprogram Intestinal Cells Into Glucose-Responsive Insulin-Secreting Cells for the Treatment of Diabetes. Diabetes. 2015;64:1794-803.

[43] Zeng Z, Yu R, Zuo FL, Zhang B, Peng DJ, Ma HQ, et al. Heterologous Expression and Delivery of Biologically Active Exendin-4 by Lactobacillus paracasei L14. Plos One. 2016;11.

[44] Drucker DJ, Sherman SI, Gorelick FS, Bergenstal RM, Sherwin RS, Buse JB. Incretin-based therapies for the treatment of type 2 diabetes: evaluation of the risks and benefits. Diabetes Care. 2010;33:428-33.

[45] Khalil AS, Collins JJ. Synthetic biology: applications come of age. Nat Rev Genet. 2010;11:367-79.

[46] Blount BA, Weenink T, Vasylechko S, Ellis T. Rational Diversification of a Promoter Providing Fine-Tuned Expression and Orthogonal Regulation for Synthetic Biology. Plos One. 2012;7.

[47] Daunert S, Barrett G, Feliciano JS, Shetty RS, Shrestha S, Smith-Spencer W. Genetically engineered whale-cell sensing systems: Coupling biological recognition with reporter genes. Chem Rev. 2000;100:2705-38.

[48] West AH, Stock AM. Histidine kinases and response regulator proteins in two-component signaling systems. Trends Biochem Sci. 2001;26:369-76.

[49] Mitrophanov AY, Groisman EA. Signal integration in bacterial two-component regulatory systems. Gene Dev. 2008;22:2601-11.

[50] Levskaya A, Chevalier AA, Tabor JJ, Simpson ZB, Lavery LA, Levy M, et al. Engineering Escherichia coli to see light - These smart bacteria 'photograph' a light pattern as a high-definition chemical image. Nature. 2005;438:441-2.

[51] Dietrich JA, Shis DL, Alikhani A, Keasling JD. Transcription Factor-Based Screens and Synthetic Selections for Microbial Small-Molecule Biosynthesis. Acs Synth Biol. 2013;2:47-58.

[52] Baumgartner JW, Kim C, Brissette RE, Inouye M, Park C, Hazelbauer GL. Transmembrane Signaling by a Hybrid Protein - Communication from the

Domain of Chemoreceptor Trg That Recognizes Sugar-Binding Proteins to the Kinase/Phosphatase Domain of Osmosensor Envz. J Bacteriol. 1994;176:1157-63.

[53] Panteli JT, Forbes NS. Engineered Bacteria Detect Spatial Profiles in Glucose Concentration Within Solid Tumor Cell Masses. Biotechnol Bioeng. 2016;113:2474-84.

[54] Andrianantoandro E, Basu S, Karig DK, Weiss R. Synthetic biology: new engineering rules for an emerging discipline. Mol Syst Biol. 2006;2.

[55] Libis V, Delepine B, Faulon JL. Expanding Biosensing Abilities through Computer-Aided Design of Metabolic Pathways. Acs Synth Biol. 2016;5:1076-85.

[56] Harms H, Wells MC, van der Meer JR. Whole-cell living biosensors - are they ready for environmental application? Appl Microbiol Biot. 2006;70:273-80.

[57] Wang BJ, Barahona M, Buck M. A modular cell-based biosensor using engineered genetic logic circuits to detect and integrate multiple environmental signals. Biosens Bioelectron. 2013;40:368-76.

[58] Ouzounis CA, Coulson RMR, Enright AJ, Kunin V, Pereira-Leal JB. Classification schemes for protein structure and function. Nat Rev Genet. 2003;4:508-19.

[59] Vaughan TJ, Osbourn JK, Tempest PR. Human antibodies by design. Nat Biotechnol. 1998;16:535-9.

[60] Wiedenmann J, Oswald F, Nienhaus GU. Fluorescent Proteins for Live Cell Imaging: Opportunities, Limitations, and Challenges. Iubmb Life. 2009;61:1029-42.

[61] Rothbauer U, Zolghadr K, Muyldermans S, Schepers A, Cardoso MC, Leonhardt H. A versatile nanotrap for biochemical and functional studies with fluorescent fusion proteins. Mol Cell Proteomics. 2008;7:282-9.

[62] Papanikou E, Karamanou S, Economou A. Bacterial protein secretion through the translocase nanomachine. Nat Rev Microbiol. 2007;5:839-51.

[63] Mergulhao FJM, Summers DK, Monteiro GA. Recombinant protein secretion in Escherichia coli. Biotechnol Adv. 2005;23:177-202.

[64] Zhang GJ, Brokx S, Weiner JH. Extracellular accumulation of recombinant proteins fused to the carrier protein YebF in Escherichia coli. Nat Biotechnol. 2006;24:100-4.

[65] Kjaergaard K, Hasman H, Schembri MA, Klemm P. Antigen 43-mediated autotransporter display, a versatile bacterial cell surface presentation system. J Bacteriol. 2002;184:4197-204.

[66] Ahan RE, Kirpat BM, Saltepe B, Seker UOS. A Self-Actuated Cellular Protein Delivery Machine. Acs Synth Biol. 2019;8:686-96.

[67] Sices HJ, Kristie TM. A genetic screen for the isolation and characterization of site-specific proteases. P Natl Acad Sci USA. 1998;95:2828-33.

[68] Song Y, Li P, Du Y. Overexpression of TrxA::BjMAT2 (Thioredoxin::Metallothionein type 2 from Brassica Juncea) fusion protein in Escherichia coli and in vitro cleavage by TEV protease. Adv Mater Res-Switz. 2011;183-185:947-+.

[69] Polayes DA, Goldstein A, Hughes AJ, Johnston SA, Dougherty WG. Efficient Release of Proteins and Peptides from Fusion Proteins by Tev Protease, Recombinant. Faseb J. 1994;8:A1373-A.

[70] Kapust RB, Waugh DS. Controlled intracellular processing of fusion proteins by TEV protease. Protein Expres Purif. 2000;19:312-8.

[71] Guex N, Peitsch MC. SWISS-MODEL and the Swiss-PdbViewer: An environment for comparative protein modeling. Electrophoresis. 1997;18:2714-23.

[72] Zhang Y. I-TASSER server for protein 3D structure prediction. Bmc Bioinformatics. 2008;9.

[73] Trott O, Olson AJ. Software News and Update AutoDock Vina: Improving the Speed and Accuracy of Docking with a New Scoring Function, Efficient Optimization, and Multithreading. J Comput Chem. 2010;31:455-61.

[74] Grosdidier A, Zoete V, Michielin O. SwissDock, a protein-small molecule docking web service based on EADock DSS. Nucleic Acids Res. 2011;39:W270-W7.

[75] Zhou P, Jin BW, Li H, Huang SY. HPEPDOCK: a web server for blind peptide-protein docking based on a hierarchical algorithm. Nucleic Acids Res. 2018;46:W443-W50.

[76] Blum-Oehler G, Oswald S, Eiteljorge K, Sonnenborn U, Schulze J, Kruis W, et al. Development of strain-specific PCR reactions for the detection of the probiotic Escherichia coli strain Nissle 1917 in fecal samples. Res Microbiol. 2003;154:59-66.

[77] Fox BG, Blommel PG. Autoinduction of protein expression. Curr Protoc Protein Sci. 2009;Chapter 5:Unit 5 23.

[78] Neidhardt FC, Bloch PL, Smith DF. Culture medium for enterobacteria. J Bacteriol. 1974;119:736-47.

[79] Schmid SR, Sheth RU, Wu A, Tabor JJ. Refactoring and Optimization of Light-Switchable Escherichia coli Two-Component Systems. Acs Synth Biol. 2014;3:820-31.

[80] Moreau PL. Diversion of the metabolic flux from pyruvate dehydrogenase to pyruvate oxidase decreases oxidative stress during glucose metabolism in nongrowing Escherichia coli cells incubated under aerobic, phosphate starvation conditions. J Bacteriol. 2004;186:7364-8.

[81] Kjaergaard K, Hasman H, Schembri MA, Klemm P. Antigen 43-mediated autotransporter display, a versatile bacterial cell surface presentation system. J Bacteriol. 2002;184:4197-204.

[82] Zhang Z, Tang R, Zhu D, Wang W, Yi L, Ma L. Non-peptide guided auto-secretion of recombinant proteins by super-folder green fluorescent protein in Escherichia coli. Sci Rep. 2017;7:6990.

[83] Jazayeri A, Rappas M, Brown AJH, Kean J, Errey JC, Robertson NJ, et al. Crystal structure of the GLP-1 receptor bound to a peptide agonist. Nature. 2017;546:254-8.

APPENDIX A

DNA sequences used in this study

Table A1: DNA sequences of genes and genetic elements used in this study

Gene / Element	Sequence
T7 Terminator	CAAAAAACCCCTCAAGACCCGTTTAGAGGCCCCAAG GGGTTATGCTAG
Ag43 Beta Translocation Domain	GAAGGTCACATTCAGTGTGGCCTGACCGTTATACCC TTCAGCGCTGCTGCCGCTGACGCTGTGGGCATAACC GGCCTGAACGCCCAGGGTGATATTTTCCCGGACACG GGCTTCCAGTCCGGCCTGCAGGTCCAGTGATGTGCC ATTCTGTGAGGGAGAGAACGTCATCCCGCTGCCTGC AGTGGAAGTCCCCACACGCATATCTCCCCGGGAGCT GAAGGTGCGGATAACAGAAGGCTGTACCCACCAGTT CACCGGTAATTCACTCACACTGTGTTTTGCACTGTCA CGCAGGGGGGCACGGGATGAGGTGCCTTCGCCAAA GGTCATATCGTTGTGGCTGCCCAGACGGAAACCGGC ACGCACATGTTGTGCACTGCCATGCCCGAACTTCAC ATAACCGGCGTTGTCCTTACCGTCATCCAGGGAAAG TCCCTGCCAGGTATACTGCAGTTGTGGCTCCAGCATC AGGTTGTCAGTGATACTGAAGGGCAGACCGGTTTCC AGTGAGCCCAGCCAGCCCCAGCCCCGGGCGCGGAA GTCGTTATTGTCCGATGACGCTTTCATGCTGTGGCGG GTTCCCTGTGCCACAATGTCAGCCCACAGGCCGGAG GACGTGTGTACCAGATTCAGGTATCCGCCCAGGCTG CCGGCATCATCCCGGACCGTGCCGGCACGGGAGCCG TCATCATCCTTAACATCAACGGAAGAATGGCCAGCA GCACCATATACCCCCGCGGTCACAGACATACCGGCA ACCTCTGTTCTCATCAGGTCACCCTCCAGACGGACG AATCCATAGCTGCCGCTGCTTTCCGGCGTGGCCCCA CGGGCAATACCGCCATTGTTATCGTGACCGAGATGA CCGCCCTGAATGCTGAGACGGACGCTGTTGTTTTCA CCATTTACACCGGTCTGATGGCTGCGGGAGCCTGCC ACAATCCGGTCATAGTCCATTGCCTGTGTCAGCATG GAGGCATACAGGGGGACTTCTGCACGATAAGCATTT TCACTGCGCAGATACCAGCTCTCATCACTGTCCCGGT TGAGGGAGTAGTTAAAGGCACCGGCCTGCAGCCTGT TCCCCTGGACAAAGGCCCCTTCCTCCGTGGTGGCAC

	CGTTAATGGCTTCCACCACCTGAATACCCTTACCGCT GGTCGCCAGCCCCGACGCACTGTTGCCGGCGTTCAC CAGGTTCAGGATGGTTTTTCCGGTTGCCCTGCCGCCG TCAATGACCAGTCTGTCAGCATTGTTCTGTGCCATAT CCGGGCGTACACGCAGGCTGATGGTGCCATTCTGTC CGTTCAGGTTTTTCACTTTCAGGGTTGCCGGTACGAA CTTCCCTGTGCGGGTGGAGGTGAAATGAATCTGTCC GGCATGGCTGAGGTCATCCACCACCGACTGCACCGT GGCGTTATCGGGGATATTCCAGGTGGCACCGGAGGC GAGAGTGACATTCGTGGG
Ag43 Alpha Subunit	CGCACAACCATCAATAAAAACGGTCGCCAGATTGTG AGAGCTGAAGGAACGGCAAATACCACTGTGGTTTAT GCCGGCGGCGACCAGACTGTACATGGTCACGCACTG GATACCACGCTGAATGGGGGATACCAGTATGTGCAC AACGGCGGTACAGCGTCTGACACTGTTGTGAACAGT GACGGCTGGCAGATTGTCAAAAACGGGGGTGTGGCC GGGAATACCACCGTTAATCAGAAGGGCAGACTGCA GGTGGACGCCGGTGGTACAGCCACGAATGTCACCCT GAAGCAGGGCGGCGCACTGGTTACCAGTACGGCTGC AACCGTTACCGGCATAAACCGCCTGGGAGCATTCTC TGTTGTGGAGGGTAAAGCTGATAATGTCGTACTGGA AAATGGCGGACGCCTGGATGTGCTGACCGGACACAC AGCCACTAATACCCGCGTGGATGATGGCGGAACGCT GGATGTCCGCAACGGTGGCACCGCCACCACCGTATC CATGGGAAATGGCGGTGTACTGCTGGCCGATTCCGG TGCCGCTGTCAGTGGTACCCGGAGCGACGGAAAGGC ATTCAGTATCGGAGGCGGTCAGGCGGATGCCCTGAT GCTGGAAAAAGGCAGTTCATTCACGCTGAACGCCGG TGATACGGCCACGGATACCACGGTAAATGGCGGACT GTTCACCGCCAGGGGCGGCACACTGGCGGGCACCAC CACGCTGAATAACGGCGCCATACTTACCCTTTCCGG GAAGACGGTGAACAACGATACCCTGACCATCCGTGA AGGCGATGCACTCCTGCAGGGAGGCTCTCTCACCGG TAACGGCAGCGTGGAAAAATCAGGAAGTGGCACAC TCACTGTCAGCAACACCACACTCACCCAGAAAGCCG TCAACCTGAATGAAGGCACGCTGACGCTGAACGACA GTACCGTCACCACGGATGTCATTGCTCAGCGCGGTA CAGCCCTGAAGCTGACCGGCAGCACTGTGCTGAACG GTGCCATTGAC
TEV Recognition Site	GAAAACCTGTACTTTCAGGGC
GLP-1 (7-36) *E. Coli* Optimized	CATGCGGAAGGCACCTTTACCAGCGATGTGAGCAGC TATCTGGAAGGCCAGGCGGCGAAAGAATTTATTGCG TGGCTGGTGAAAGGCCGC

PELB Signal Sequence	ATGAAATACCTGCTGCCGACCGCTGCTGCTGGTCTG CTGCTCCTCGCTGCCCAGCCGGCGATGGCC
T7 Promoter	TAATACGACTCACTATAGG
sfGFP	ATGCGTAAAGGCGAAGAGCTGTTCACTGGTGTCGTC CCTATTCTGGTGGAACTGGATGGTGATGTCAACGGT CATAAGTTTTCCGTGCGTGGCGAGGGTGAAGGTGAC GCAACTAATGGTAAACTGACGCTGAAGTTCATCTGT ACTACTGGTAAACTGCCGGTACCTTGGCCGACTCTG GTAACGACGCTGACTTATGGTGTTCAGTGCTTTGCTC GTTATCCGGACCATATGAAGCAGCATGACTTCTTCA AGTCCGCCATGCCGGAAGGCTATGTGCAGGAACGCA CGATTTCCTTTAAGGATGACGGCACGTACAAAACGC GTGCGGAAGTGAAATTTGAAGGCGATACCCTGGTAA ACCGCATTGAGCTGAAAGGCATTGACTTTAAAGAAG ACGGCAATATCCTGGGCCATAAGCTGGAATACAATT TTAACAGCCACAATGTTTACATCACCGCCGATAAAC AAAAAAATGGCATTAAAGCGAATTTTAAAATTCGCC ACAACGTGGAGGATGGCAGCGTGCAGCTGGCTGATC ACTACCAGCAAAACACTCCAATCGGTGATGGTCCTG TTCTGCTGCCAGACAATCACTATCTGAGCACGCAAA GCGTTCTGTCTAAAGATCCGAACGAGAAACGCGATC ATATGGTTCTGCTGGAGTTCGTAACCGCAGCGGGCA TCACGCATGGTATGGATGAACTGTACAAA
Modified GLP-1 (7-36) *E. coli* optimized	CATGGCGAAGGCACCTTTACCAGCGATGTGAGCAGC TATCTGGAAGGCCAGGCGGCGCAGGAATTTATTGCG TGGCTGGTGGACGGCTGTCGC
PENETRATIN *E. coli* optimized	CGTCAGATTAAAATTTGGTTTCAGAATCGTCGTATG AAATGGAAAAAA
EXENTIN-4 *E. coli* optimized	CATGGCGAAGGCACCTTTACCAGCGATCTGAGCAAA CAGATGGAAGAAGAAGCGGTGCGCCTGTTTATTGAA TGGCTGAAAAACGGCGGCCCGAGCAGCGGCGCGCC GCCGCCGAGC
PROD Promoter	CACAGCTAACACCACGTCGTCCCTATCTGCTGCCCTA GGTCTATGAGTGGTTGCTGGATAACTTTACGGGCAT GCATAAGGCTCGTATAATATATTCAGGGAGACCACA ACGGTTTCCCTCTACAAATAATTTTGTTTAACTTT
Ribosome Binding Site, HucR	AAGGAG
OxyR Gene	ATGAATATTCGTGATCTTGAGTACCTGGTGGCATTG GCTGAACACCGCCATTTTCGGCGTGCGGCAGATTCC

	TGCCACGTTAGCCAGCCGACGCTTAGCGGGCAAATT CGTAAGCTGGAAGATGAGCTGGGCGTGATGTTGCTG GAGCGGACCAGCCGTAAAGTGTTGTTCACCCAGGCG GGAATGCTGCTGGTGGATCAGGCGCGTACCGTGCTG CGTGAGGTGAAAGTCCTTAAAGAGATGGCAAGCCA GCAGGGCGAGACGATGTCCGGACCGCTGCACATTGG TTTGATTCCCACAGTTGGACCGTACCTGCTACCGCAT ATTATCCCTATGCTGCACCAGACCTTTCCAAAGCTGG AAATGTATCTGCATGAAGCACAGACCCACCAGTTAC TGGCGCAACTGGACAGCGGCAAACTCGATTGCGTGA TCCTCGCGCTGGTGAAAGAGAGCGAAGCATTCATTG AAGTGCCGTTGTTTGATGAGCCAATGTTGCTGGCTAT CTATGAAGATCACCCGTGGGCGAACCGCGAATGCGT ACCGATGGCCGATCTGGCAGGGGAAAAACTGCTGAT GCTGGAAGATGGTCACTGTTTGCGCGATCAGGCAAT GGGTTTCTGTTTTGAAGCCGGGGCGGATGAAGATAC ACACTTCCGCGCGACCAGCCTGGAAACTCTGCGCAA CATGGTGGCGGCAGGTAGCGGGATCACTTTACTGCC AGCGCTGGCTGTGCCGCCGGAGCGCAAACGCGATGG GGTTGTTTATCTGCCGTGCATTAAGCCGGAACCACG CCGCACTATTGGCCTGGTTTATCGTCCTGGCTCACCG CTGCGCAGCCGCTATGAGCAGCTGGCAGAGGCCATC CGCGCAAGAATGGATGGCCATTTCGATAAAGTTTTA AAACAGGCGGTTTAA
rrnb_T1 Transcriptional Terminator	CAAATAAAACGAAAGGCTCAGTCGAAAGACTGGGC CTTTCGTTTTATCTGTTGTTTGTCGGTGAACGCTCTCC TGAGTAGGACAAAT
Ribosome Binding Site (RBS30)	CTAGAGATTAAAGAGGAGAAATACTAGATG
AhpCp1 Promoter	TACGAAGGTTGTAAGGTAAAACTTATCGATTTGATA ATGGAAACGCATTAGCCGAATCGGCAAAAATTGGTT ACCTTACATCTCATCGAAAACACGGAGGAAGTATAG
Trg Periplasmic Domain	ATGAATACAACTCCCTCACAGCGATTAGGTTTTTTGC ATCACATCAGGTTGGTTCCGTTATTTGCCTGCATTCT AGGCGGTATCTTAGTTCTATTCGCATTAAGTTCAGCC CTGGCTGGCTATTTCCTCTGGCAGGCCGATCGCGATC AGCGTGATGTTACTGCGGAGATTGAGATTCGGACCG GGTTAGCGAACAGTTCAGATTTTTTGCGTTCAGCCCG GATCAATATGATTCAGGCCGGGGCTGCGAGTCGTAT TGCGGAAATGGAAGCAATGAAGCGAAATATTGCGC AAGCCGAATCGGAGATTAAACAGTCGCAGCAAGGTT ATCGTGCTTATCAGAATCGACCGGTGAAAACACCTG CTGATGAAGCCCTCGACACTGAATTAAATCAACGCT

	TTCAGGCTTATATCACGGGTATGCAACCTATGTTGA AATATGCCAAAAATGGCATGTTTGAAGCGATTATCA ATCATGAAAGTGAGCAGATCCGACCGCTGGATAATG CTTATACCGATATTTTGAACAAAGCCGTTAAGATAC GTAGCACCAGAGCCAACCAACTGGCGGAACTGGCCC ATCAGCGCACCCGCCTGGGTGGGATGTTCATGATTG GCGCGTTTGTGCTTGCCCTGGTCATGACGCTGATAAC ATTTATGGTGCTACGTCGGATCGTCATTCGTCCACTG CAACATGCCGCACAACGGATTGAAAAAATCGCCAGT GGCGATCTGACGATGAATGATGAACCGGCGGGTCGT AATGAAATCGGTCGCTTAAGTCGTCATTTACAG
PerR from *Bacillus Subtillis*	ATGGCTGCACATGAACTAAAAGAAGCCTTAGAAACG TTGAAGGAAACCGGAGTTCGCATTACTCCTCAACGT CATGCGATTCTGGAATATCTCGTTAACTCTATGGCTC ATCCAACAGCGGACGATATATATAAAGCTCTGGAAG GGAAATTTCCTAACATGAGCGTAGCGACGGTATATA ACAATTTGCGTGTGTTCCGGGAATCAGGTTTGGTAA AAGAGCTCACATACGGTGATGCTTCCAGCAGATTCG ATTTTGTCACATCCGATCACTATCACGCGATTTGCGA AAACTGCGGTAAAATTGTGGACTTCCACTACCCGGG CCTTGATGAAGTGGAGCAGCTCGCTGCCCACGTCAC GGGCTTCAAGGTAAGCCACCACCGTTTAGAAATTTA CGGCGTCTGCCAAGAGTGTTCGAAAAAAGAAAATCA TTAA
B1002 Transcriptional Terminator	CGCAAAAAACCCCGCTTCGGCGGGGTTTTTTCGC
Ahp/Per Hybrid Promoter	TACGAAGGTTGTAAGGTAAAACTTATCGATTTGATA ATGGAAACGCATTAGCCGTTATAATTATTATAAGTT ACCTTACATCTCATCGAAAACACGGAGGAAGTATAG
TEV Protease	GGTGAGAGCCTGTTTAAGGGTCCTCGCGATTACAAC CCGATCAGCAGTACCATCTGCCACCTGACCAACGAG AGTGATGGCCATACCACCAGCCTGTATGGCATCGGC TTCGGCCCGTTTATCATCACCAACAAACACCTGTTTC GCCGCAACAATGGCACCCTGCTGGTGCAGAGCCTGC ATGGCGTGTTCAAAGTGAAGAACACCACCACCCTGC AGCAGCACCTGATCGATGGCCGCGACATGATTATCA TCCGCATGCCGAAAGACTTCCCGCCGTTTCCGCAGA AACTGAAATTCCGCGAACCGCAGCGCGAAGAACGC ATTTGTCTGGTGACCACCAATTTTCAGACCAAAAGC ATGAGCAGCATGGTGAGCGATACCAGTTGCACCTTT CCGAGCAGCGATGGCATCTTCTGGAAACACTGGATT CAAACCAAAGATGGCCAGTGTGGCAGCCCGCTGGTG AGTACCCGCGATGGCTTTATCGTGGGCATTCATAGT

	GCCAGTAATTTTACCAACACCAATAATTACTTTACCA GCGTGCCGAAGAACTTCATGGAACTGCTGACCAACC AGGAAGCACAGCAGTGGGTGAGCGGTTGGCGCCTG AATGCAGATAGCGTGCTGTGGGGCGGCCATAAAGTG TTCATGGTGAAACCGGAAGAACCGTTCCAGCCGGTG AAAGAAGCCACCCAGCTGATGAAT
SpxB Gene	ATGACTCAAGGGAAAATTACTGCATCGGCAGCAATG CTTAACGTATTGAAAACATGGGGCGTAGATACAATC TACGGTATCCCATCAGGAACACTCAGCTCATTGATG GACGCTTTGGCTGAAGACAAAGATATCCGCTTCTTA CAAGTTCGCCACGAAGAGACAGGTGCTCTTGCAGCG GTTATGCAAGCTAAATTCGGCGGCTCAATCGGGGTT GCAGTTGGTTCAGGTGGTCCAGGTGCGACTCACTTG ATTAACGGTGTTTACGATGCAGCTATGGATGACACT CCATTCCTAGCGATCCTTGGATCACGTCCAGTTAACG AATTGAACATGGATGCTTTCCAAGAGCTTAACCAAA ACCCAATGTACAACGGTATCGCTGTTTACAACAAAC GTGTAGCTTACGCTGAGCAATTGCCAAAAGTAATTG ACGAAGCCTGCCGTGCTGCAATTTCTAAAAAAGGTC CAGCTGTTGTTGAAATTCCAGTAAACTTCGGTTTCCA AGAAATCGACGAAAACTCATACTACGGTTCAGGTTC ATACGAACGCTCATTCATCGCTCCTGCTTTGAACGA AGTTGAAATCGACAAAGCTGTTGAAATCTTGAACAA TGCTGAACGCCCAGTTATCTATGCTGGATTTGGTGGT GTTAAAGCTGGTGAAGTGATTACTGAATTGTCACGT AAAATCAAAGCACCAATCATCACAACTGGTAAAAAC TTTGAAGCTTTCGAATGGAACTATGAAGGTTTGACA GGTTCTGCTTACCGTGTTGGTTGGAAACCAGCCAAC GAAGTGGTCTTTGAAGCAGACACAGTTCTTTTCCTTG GTTCAAACTTCGCATTTGCTGAAGTTTACGAAGCATT CAAGAACACTGAAAAATTCATACAAGTCGATATCGA CCCTTACAAACTTGGTAAACGTCATGCCCTTGACGCT TCAATCCTTGGTGATGCTGGTCAAGCAGCTAAAGCT ATCCTTGACAAAGTAAACCCAGTTGAATCAACTCCA TGGTGGCGTGCAAACGTTAAGAACAACCAAAACTGG CGTGATTACATGAACAAACTCGAAGGTAAAACTGAG GGTGAATTGCAATTGTATCAAGTTTACAATGCAATC AACAAACATGCTGATCAAGACGCTATCTACTCAATC GACGTAGGTAACACTACTCAAACATCTACTCGTCAC CTTCACATGACACCTAAGAATATGTGGCGTACATCT CCGCTCTTTGCGACAATGGGTATTGCCCTTCCTGGTG GTATCGCTGCTAAGAAAGACAATCCAGATCGCCAAG TATGGAACATCATGGGTGATGGAGCATTCAACATGT GCTACCCAGACGTTATCACAAACGTTCAATACGACC TTCCAGTTATCAACCTTGTCTTCTCAAATGCTGAGTA CGGCTTCATCAAGAACAAATACGAAGATACAAACA AACACTTGTTTGGTGTAGACTTCACAAACGCTGACT

	ACGCTAAAATTGCGGAAGCTCAAGGAGCTGTTGGAT TCACAGTTGACCGTATCGAAGACATCGATGCAGTTG TTGCAGAAGCTGTTAAATTGAACAAAGAAGGTAAAA CTGTTGTCATCGATGCTCGCATCACTCAACACCGTCC ACTTCCAGTAGAAGTACTTGAATTGGATCCAAAACT TCACTCAGAAGAAGCTATCAAAGCCTTCAAGGAAAA ATACGAAGCAGAAGAACTCGTACCATTCCGTCTCTT CTTGGAAGAAGAAGGATTGCAATCACGCGCAATTAA ATAATAA

APPENDIX B

List of primers used in this thesis

Table B1: PCR Primers used in this thesis

#	Primer Name	Sequence 5'-3'
1	Ag43-GLP1-FOR1	AGGCCAGGCGGCGAAAGAATTTATTGCGTG GCTGGTGAAAGGCCGCGAAAACCTGTACTTT CAGGGCG
2	Ag43-GLP1-FOR2	AGGCACCTTTACCAGCGATGTGAGCAGCTAT CTGGAAGGCCAGGCGGCGAAAGAATTTATT GCGT
3	Ag43-GLP1-FOR3	GTTTTTATTGATGGTTGTGCGCTTAAGGCTGC CACCGCCCTGAAAGTACAGGTTTTCGCGGCC TTTCACCAG
4	GLP1-Lig-For	CTGCTCCTCGCTGCCCAGCCGGCGATGGCCA TGGGCCATGCGGAAGGCACCTTTACCAGCGA TGT
5	GLP1-Lig-Rev	GCCCAGCCGGCGATGGCCATGGgcactagtatgggc catgcggaaggc
6	sfGLP1-F	GGTAAAGGTGCCTTCCGCATGGCCCATACCT TTGTACAGTTCATCCATACCATGCGTG
7	sfGLP1-R	TGCCCAGCCGGCGATGGCCATGGGCACTAGT ATGCGTAAAGGCGAAGAGCTGT
8	NH1	TGCGAACCTTTGGGAGTACAAACAGAATTCA TGAATACAACTCCCTCA
9	NH5-NW	CTGTAAATGACGACTTAAGCGACC
10	NH4-NW	GGGTCGTAATGAAATCGGTCGCTTAAGTCGT CATTTACAGCATATGGCGGCTGGTGTT

11	NH6	GAATTCTGTTTGTACTCCCAAAGG
12	GOX-PET22B-FOR	ATAACAATTCCCCTCTAGAATTAAAGAGGAG AAAGGTACCATGAAATACCTGCTGCCGA
13	GOX-PET22B-REV	TAGCAGCCGGATCTCAGTGGTGGTGGTGGTG GTGCTCGAGTTATTACCCACGAGGGACTAAC
14	Oxy6	CTGAGCCTTTCGTTTTATTTGATGCCACGCGT TCACTAGTTTAAACCGCCTGTTTTAAAACT
15	Oxy7	CCTCTACAAATAATTTTGTTTAACTTTAAGGA GGGATCCAATGAATATTCGTGATCTTGAGTA C
16	AhpCp1-1	GGTTACCTTACATCTCATCGAAAACACGGAG GAAGTATAGTCTAGAATTAACTTTAAGCTAG AGATTAA
17	AhpCp1-2	CTTATCGATTTGATAATGGAAACGCATTAGC CGAATCGGCAAAAATTGGTTACCTTACATCT CATCGA
18	AhpCp1-3	ATCAGCCCACTGACGCGGAATTCTACGAAGG TTGTAAGGTAAAACTTATCGATTTGATAATG GAAACG
19	NH-ECNKO	TCAGCAAAAAACCCCTCAAGAC
20	pZA-H2O2-S3-For	ACTAGTGAACGCGTGGCATCAAATAAAACG AA
21	pZA-H2O2-S3-Rev	TGGATCCCTCCTTAAAGTTAAACAAAA
22	PerR-For	CCTCTACAAATAATTTTGTTTAACTTTAAGGA GGGATCCAATGGCTGCACATGAACTAAAAG AAGCC
23	PerR-Rev	CGTTTTATTTGATGCCACGCGTTCACTAGTTT ATTAATGATTTTCTTTTTTCGAACACTCTTGG CA
24	pZA-H2O2-R-Rev1	CGCAAAAAACCCCGCTTCGGCGGGGTTTTTT CGCCTCGAGATTTGTCCTACTCAGGAGAGCG TTCAC

25	pZA-H2O2-BB-F	CGATAAGTTTTACCTTACAACCTTCGTAGAA TTCCCGCCGCCCTAGACCTAGGGGATATATT CCG
26	pZA-H2O2-R-For1	GCGAAAAAACCCCGCCGAAGCGGGGTTTTTT GCGTCATCATTTGTACAGTTCATCCATACCAT GCGTG
27	AhpCp1-PerR-R1	GATAATGGAAACGCATTAGCCGTTATAATTA TTATAAGTTACCTTACATCTCATCGAAAAC
28	AhpCp1-PerR-R2	GAATTCTACGAAGGTTGTAAGGTAAAACTTA TCGATTTGATAATGGAAACGCATTAGCCGTT
29	pZA-H2O2-Insert-R	GCGAGGAAGCGGAATATATCCCCTAGGTCTA GGGCGGCGGGAATTCTACGAAGGTTGTAAG GT
30	SpxB-For	TACAAATAATTTTGTTTAACTTTAAGGAGGG ATCCATGACTCAAGGGAAAATTACTGCATCG G
31	SpxB-Rev	TTCTTTTAGTTCATGTGCAGCCATTGGATCCC TCCTTAAGCTTTTATTATTTAATTGCGCGTGA TTGC
32	SpxB-M2-BB-For	CTATACTTCCTCCGTGTTTTCGATGAGATG
33	SpxB-M2-BB-Rev	ATGCGTAAAGGCGAAGAGCTG
34	REA97	GACGTCGGAATTGCCAGCTG
35	REA98	AAGCTTGGATCCCTGCAG
36	pZS-PRODMC-Rev	AGGGCTTCCCAACCTTACCAGAGGGCGCCCC AGCTGGCAATTCCGACGTCCACAGCTAACAC CACGTC
37	SpxB-EF	TGGATCCCTCCTTAAGCTTTTATTATTTAATT
38	PELB-SpxBE-rev	TTAAATAATAAAAGCTTAAGGAGGGATCCA ATGAAATACCTGCTGCCGACCG
39	Ag43-sfGLP1-pZS-	GGGCCCTGAGGCCTGCAGGGATCCAAGCTTT TATCAGAAGGTCACATTCAGTGTGGC

	For	
40	pZA-V3-Rel-BB- For	CTAGTATTTCTCCTCTTTAATCTCTAGCTTAA AGTTAA
41	pZA-V3-Rel-For	AAAAACCCCGCCGAAGCGGGGTTTTTTGCGT CATCAGAAGGTCACATTCAGTGTGGCC
42	pZA-V3-Rel-Rev	TTTAAGCTAGAGATTAAAGAGGAGAAATACT AGATGAAATACCTGCTGCCGACCG

APPENDIX C

Plasmid maps used in this study

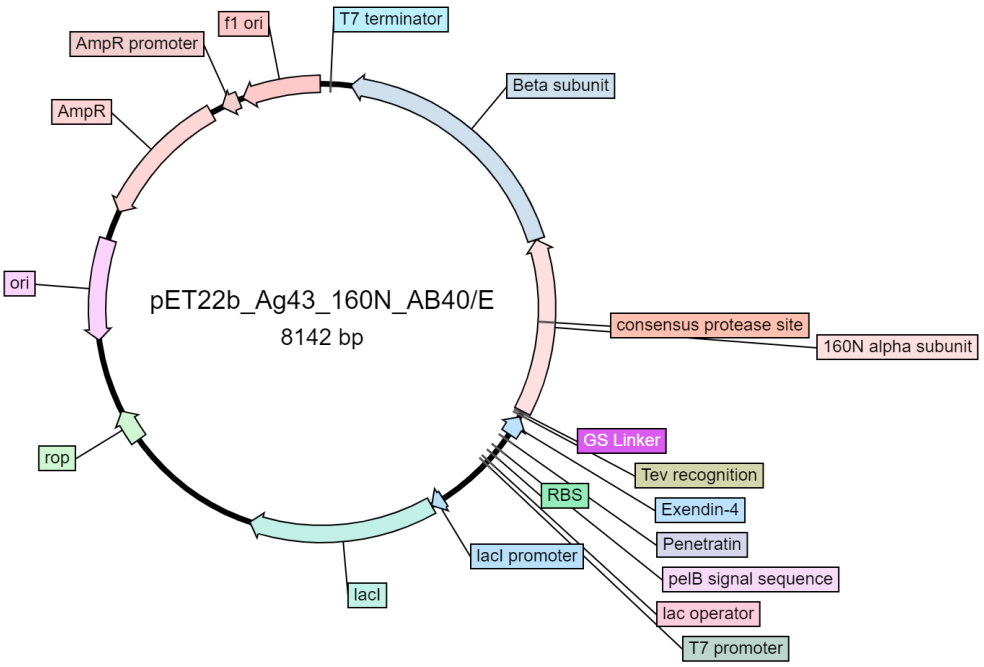

Figure C1: Map of PET22b – T7 - Ag43 – Exentin – 4 – PEN plasmid

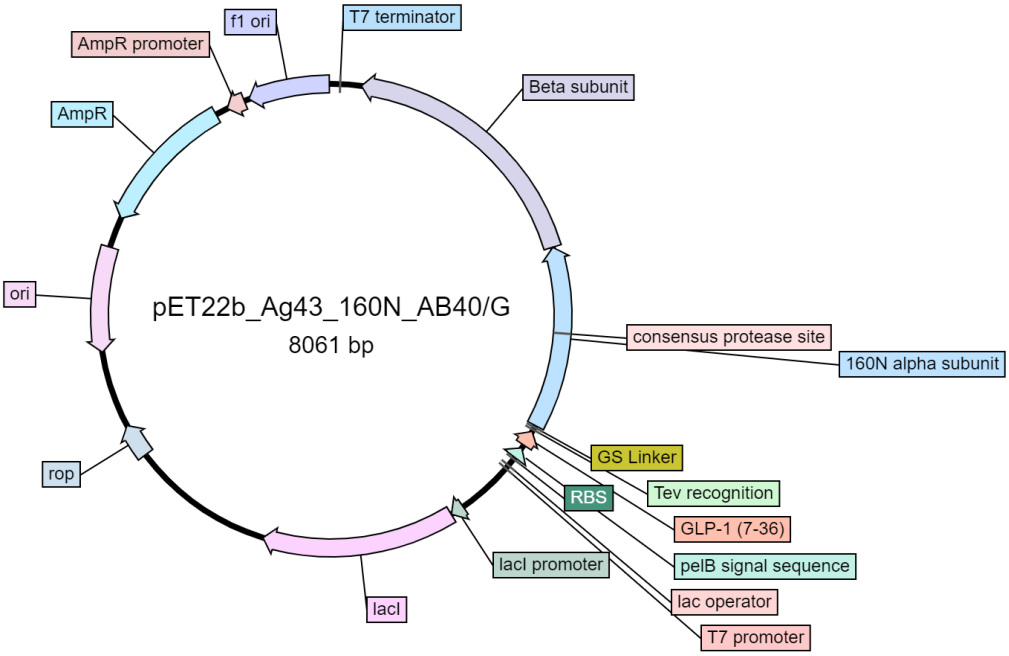

Figure C2: Map of PET22b – T7 - Ag43 – GLP-1 (7-36) plasmid

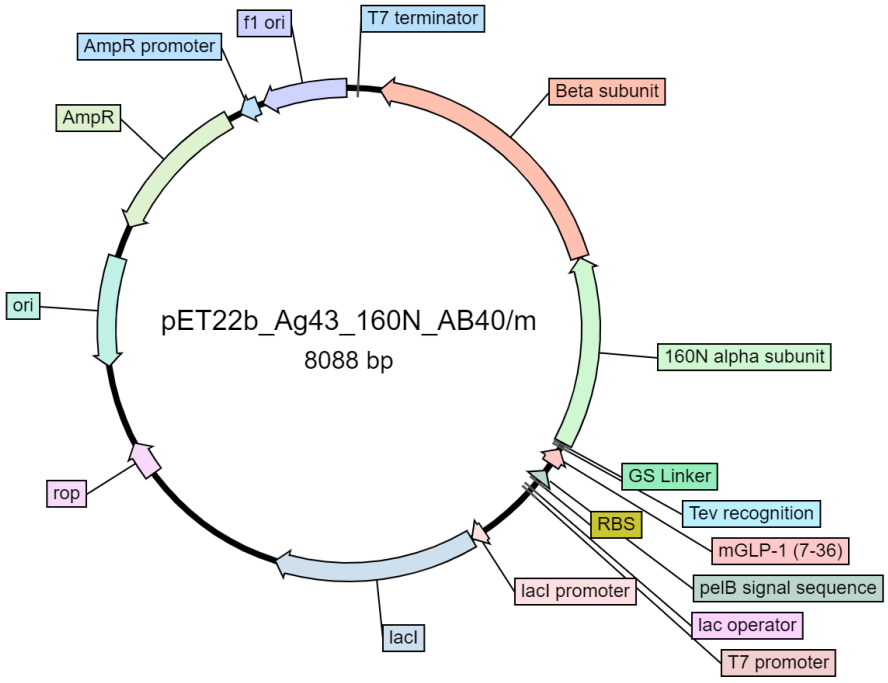

Figure C3: Map of PET22b – T7 - Ag43 – mGLP-1 (7-36) plasmid

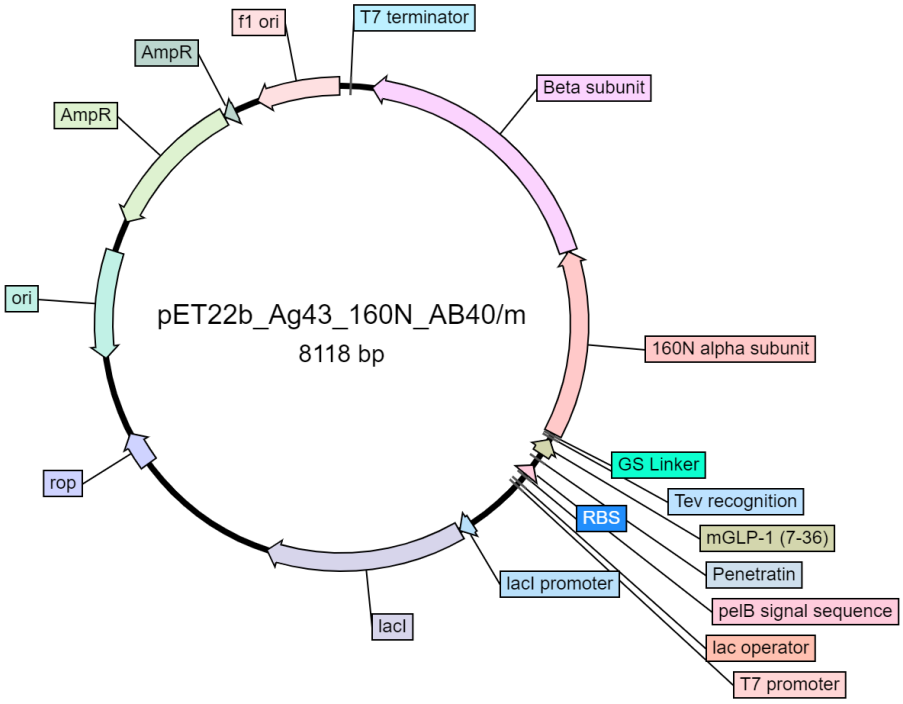

Figure C4: Map of PET22b – T7 - Ag43 – mGLP-1 (7-36) – PEN plasmid

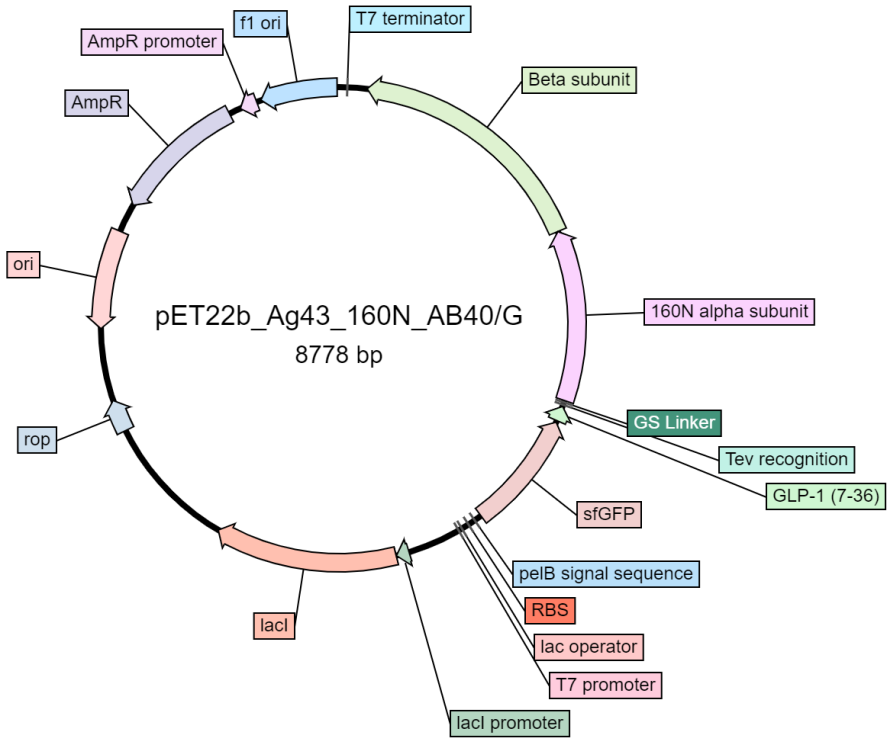

Figure C5: Map of PET22b – T7 - Ag43 – sfGLP-1 (7-36) plasmid

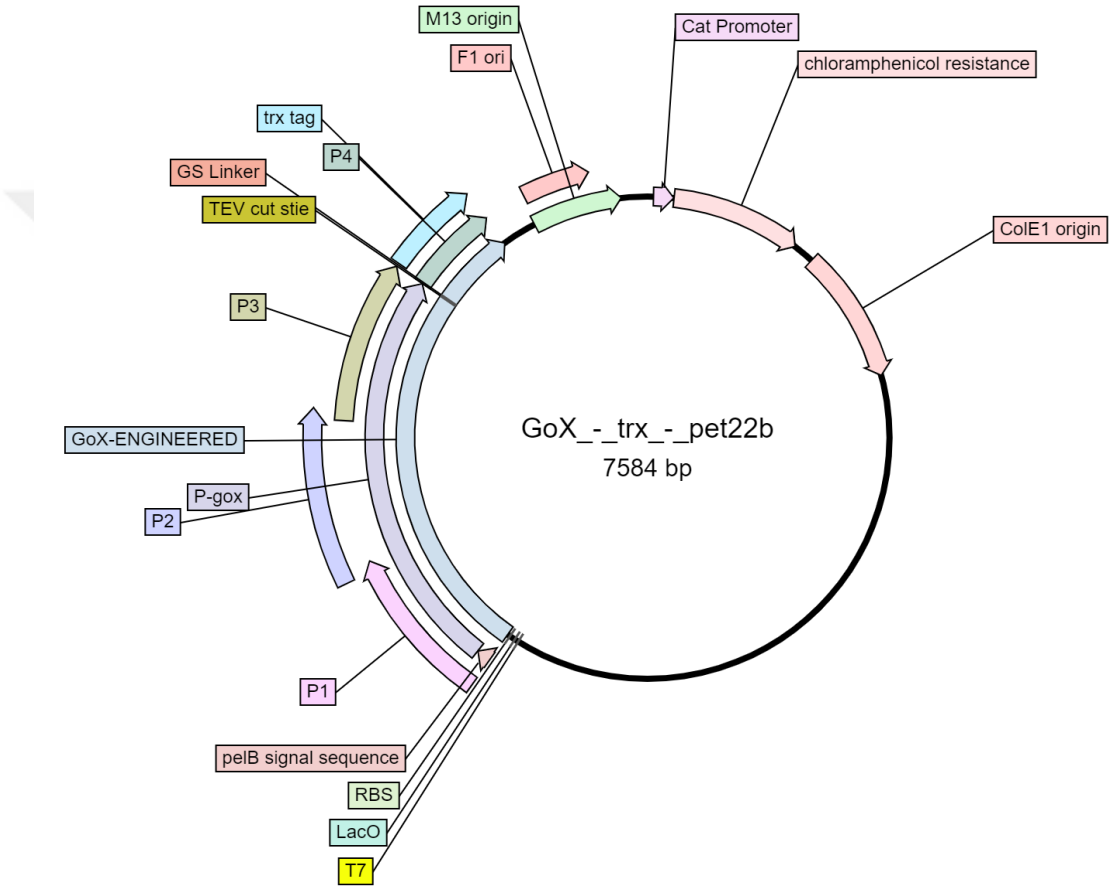

Figure C6: Map of PET22b – T7 – GoX - Trx plasmid

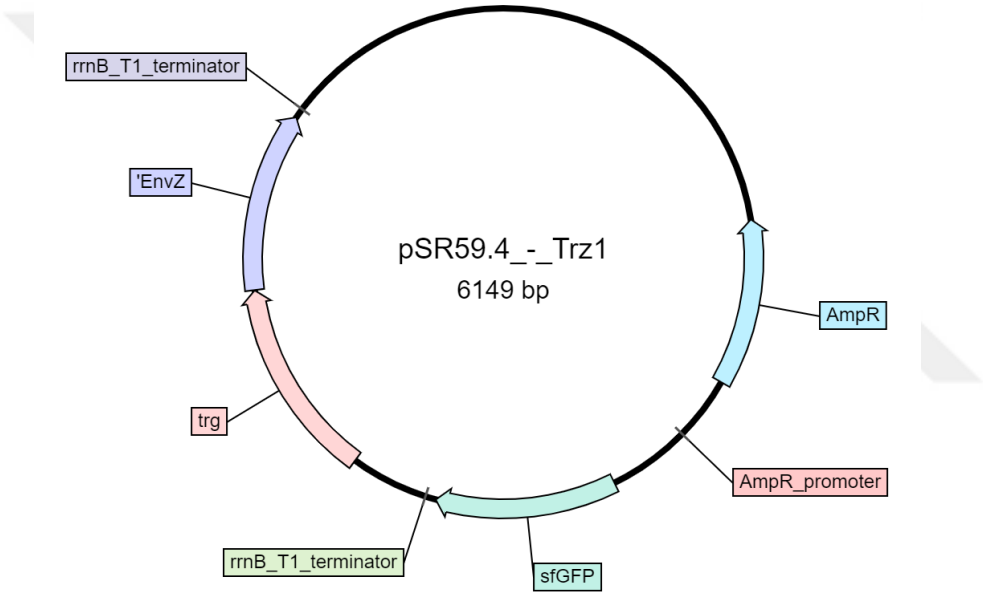

Figure C7: Map of PSR59.5-Trz1 plasmid

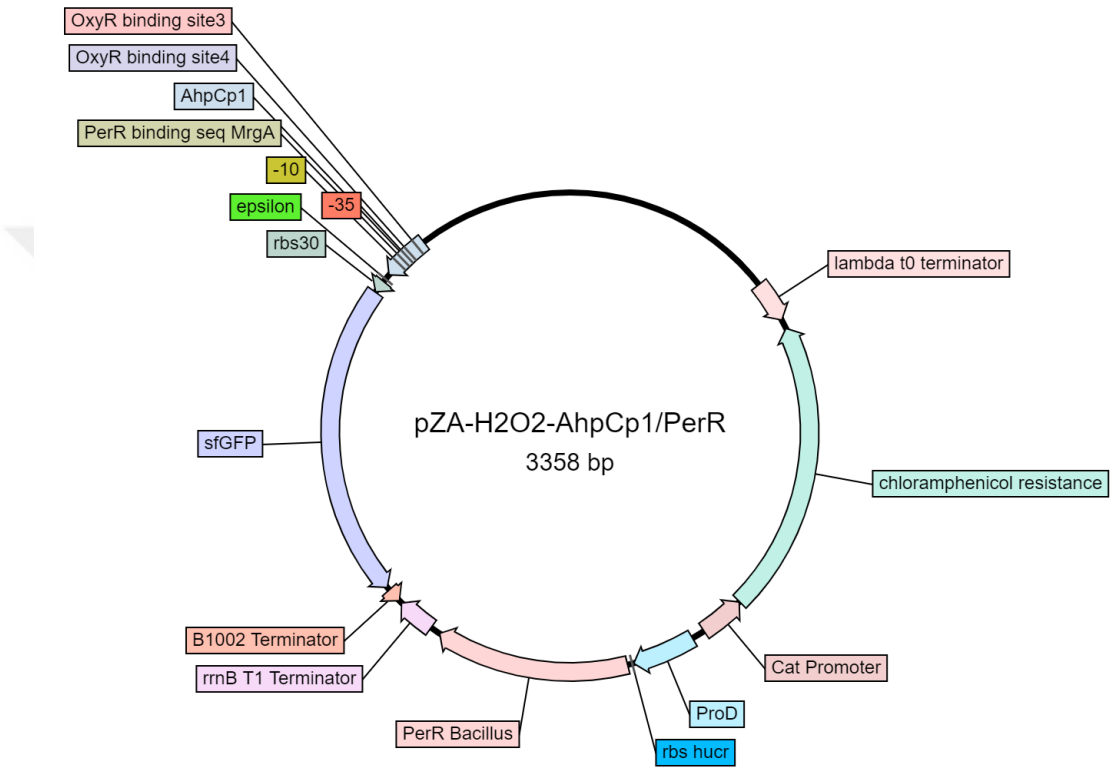

Figure C8: Map of PZA-PROD-PerR-Ahp/Per-SFGFP plasmid

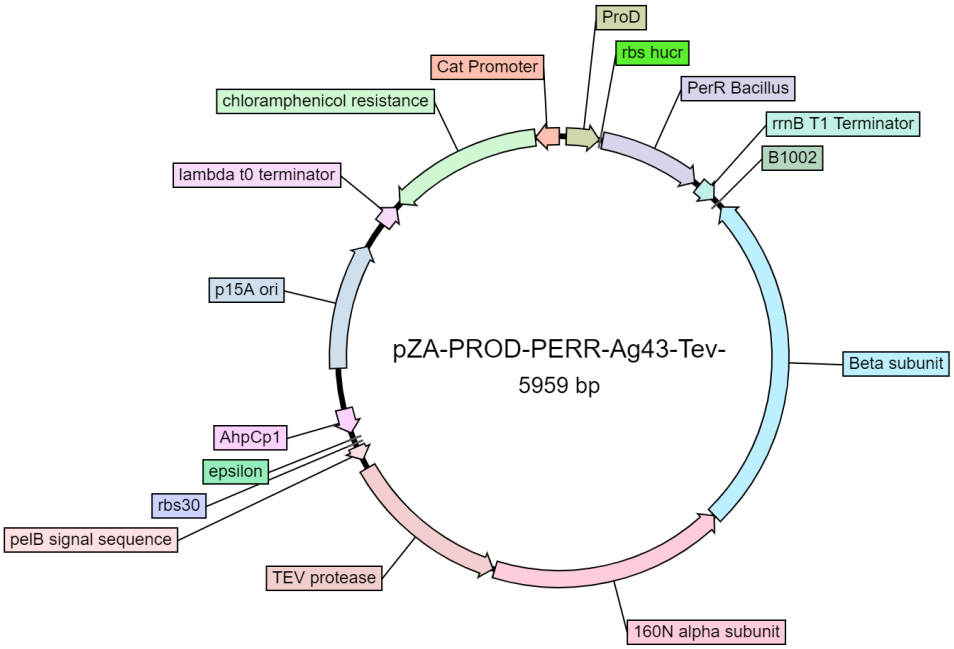

Figure C9: Map of PZA-PROD-PERR-AHP/PER-AG43-TEV plasmid

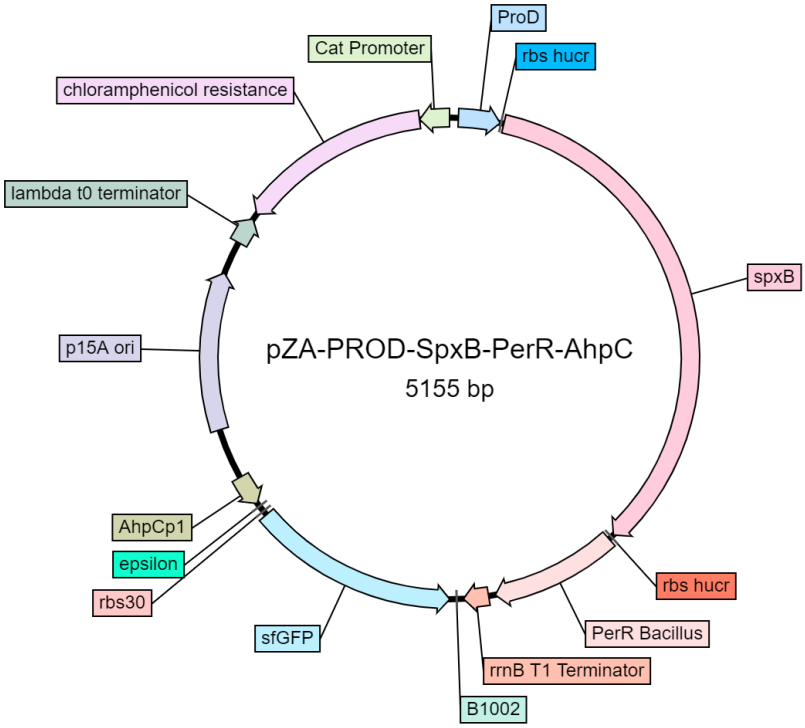

Figure C10: Map PZA-PROD-SPXB-PERR-AHP/PER-SFGFP plasmid

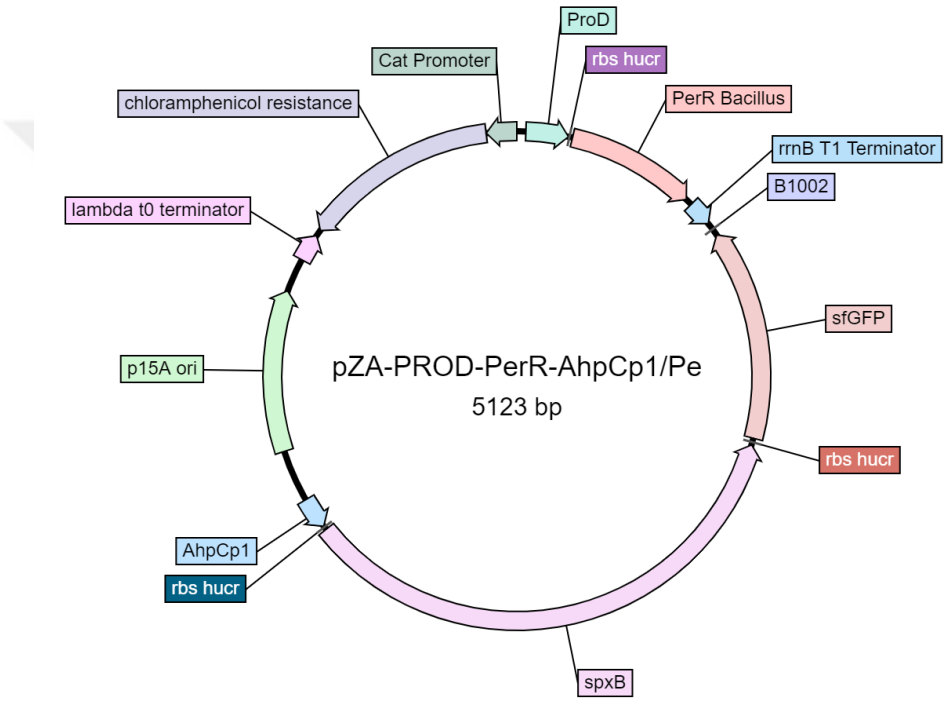

Figure C11: Map of PZA-PROD-PERR-AHP/PER-SPXB-SFGFP plasmid

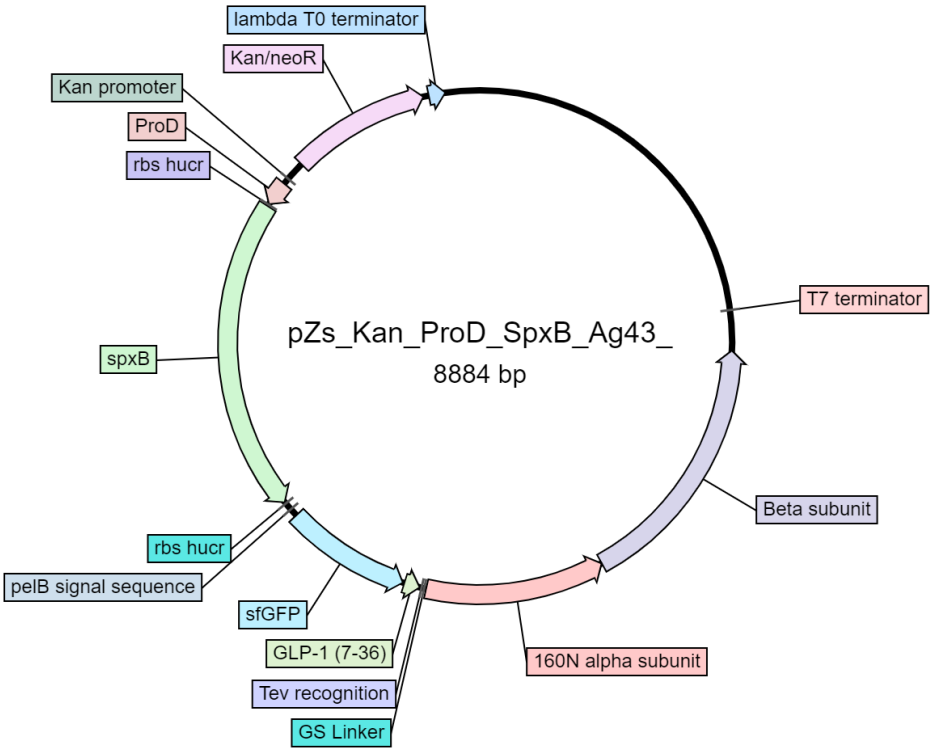

Figure C12: Map of PZS-PROD-SPXB-AG43-SFGLP1 plasmid

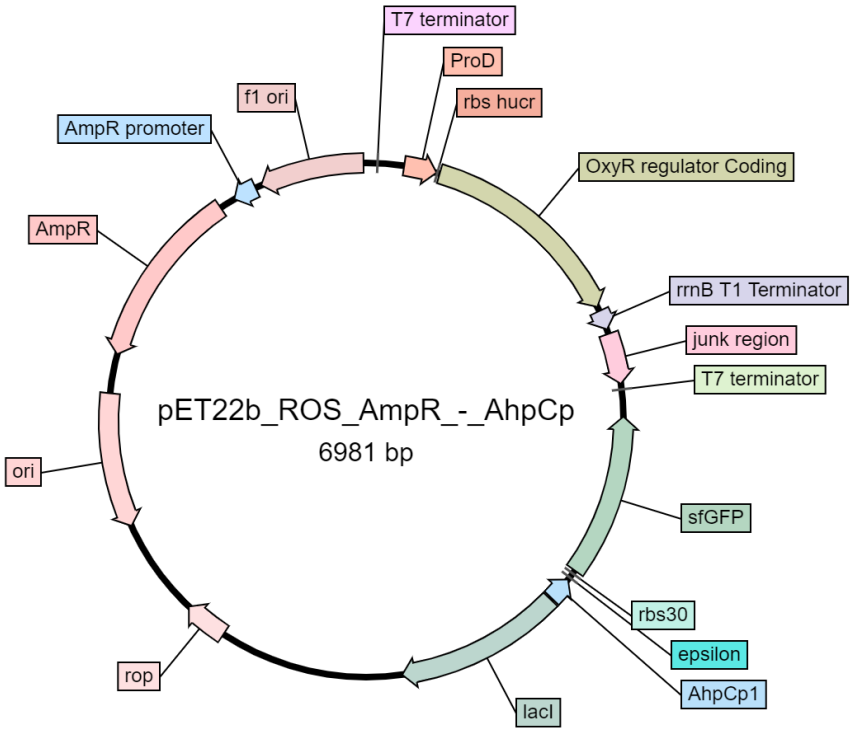

Figure C13: Map of PET22B-PROD-OXYR-AHPCP1-SFGFP plasmid

APPENDIX D

Sanger sequencing results for the plasmids used in this thesis.

Note that template sequences squared in red, and sequencing results squared in blue in all of the alignment figures. Mismatches investigated from trace file and verified from the signal.

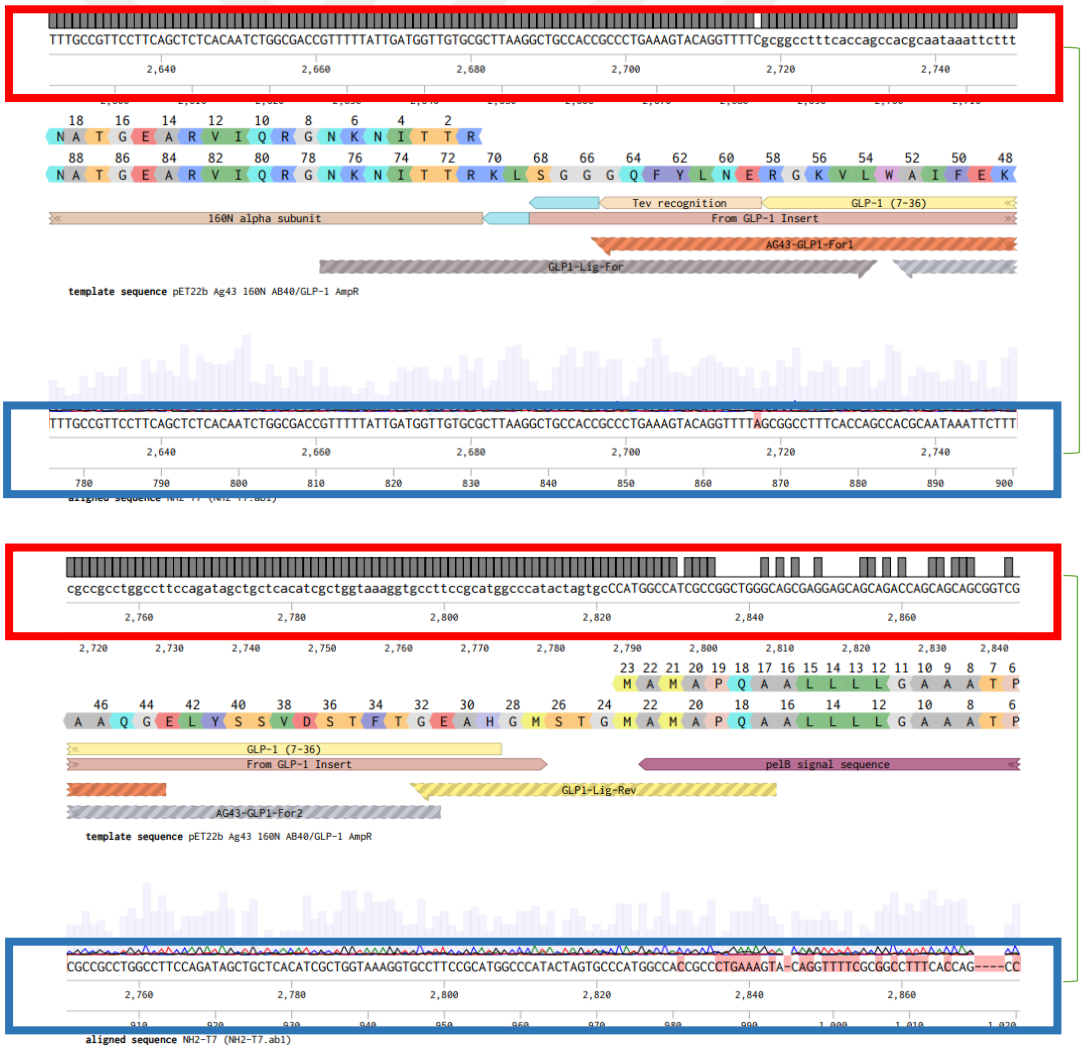

Figure D1: Sequencing result alignment of GLP-1 (7-36) generated by Benchling.


160N alpha subunit
Tev recognition
From GLP-1 Insert
AG43-GLP1-For1
GLP1-Lig-For
template sequence pET22b Ag43 160N AB40/GLP-1-sfGFP AmpR
aligned sequence NH1-t7 (1) (NH1-t7 (1).ab1)
From GLP-1 Insert
GLP-1 (7-36)
sfGFP
AG43-GLP1-For1
sfGLP1-F
AG43-GLP1-For2
template sequence pET22b Ag43 160N AB40/GLP-1-sfGFP AmpR
aligned sequence NH1-t7 (1) (NH1-t7 (1).ab1)
sfGFP
template sequence pET22b Ag43 160N AB40/GLP-1-sfGFP AmpR
aligned sequence NH1-t7 (1) (NH1-t7 (1).ab1)
sfGFP
template sequence pET22b Ag43 160N AB40/GLP-1-sfGFP AmpR
aligned sequence NH1-t7 (1) (NH1-t7 (1).ab1)

Figure D2: Sequencing result allignment of sfGLP-1 generated by Benchling.

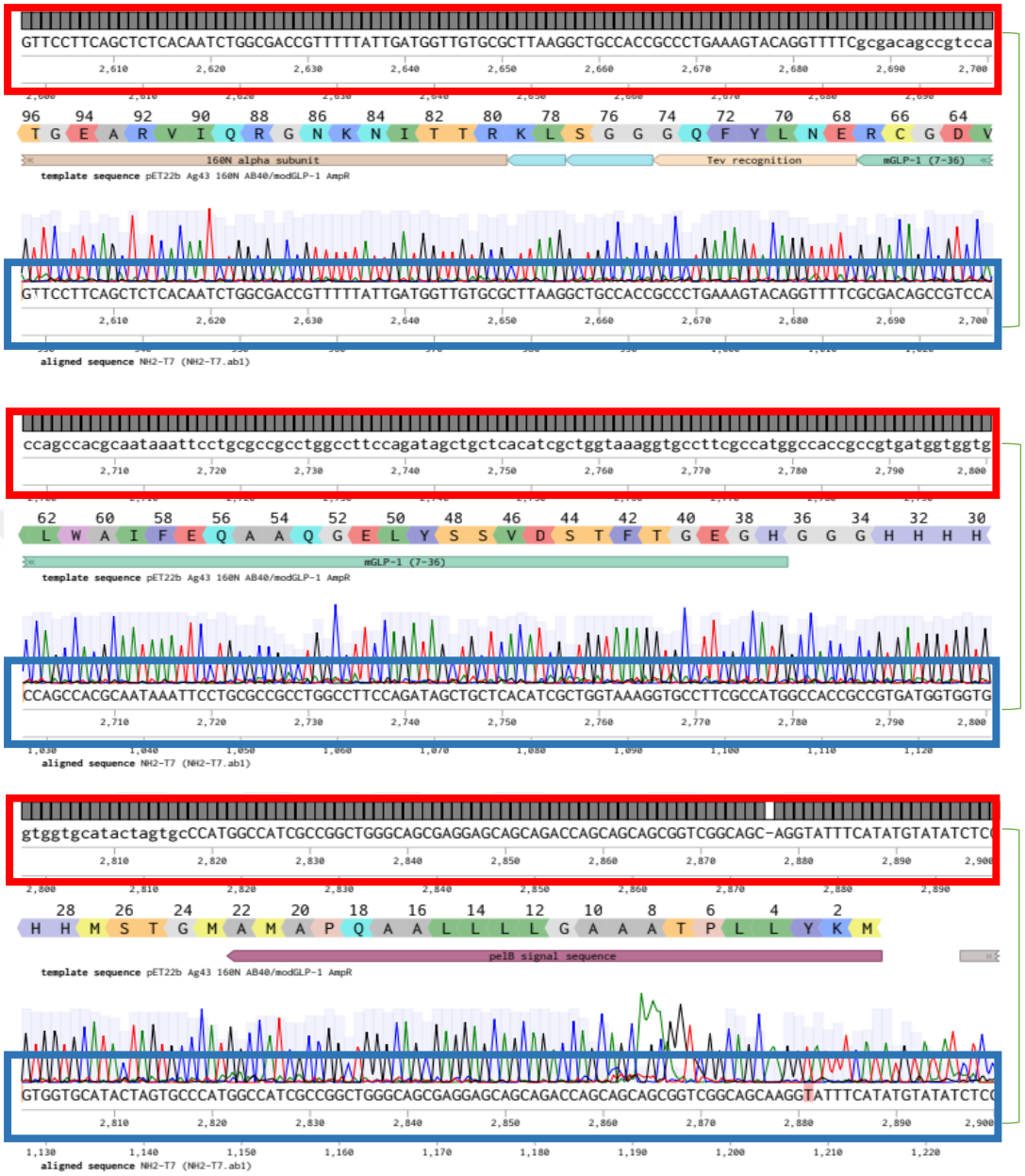

Figure D3: Sequencing result allignment of mGLP-1 (7-36) generated by Benchling.

Figure D4: Sequencing result alignment of Exentin-4-PEN generated by Benchling

Figure D5: Sequencing result alignment of mGLP-1 – PEN generated by Benchling


TCATACCAGATTTAGCTGGTGACGAACGTGAGCTTTTTTAAGAATACACGCTTACAAATTGTTGCGAACCTTTGGGAGTACAAACAGAATTCatgaatac
3,610 3,620 3,630 3,640 3,650 3,660 3,670 3,680 3,690 3,700
M N T
trg
NH6.4
NH1
template sequence pSR59.4 - PCR - seq - his
TNNTACCNGANTTAGCTGGTGACGAACGTGAGCTTTTTTAAGAATACACGCTTACAAATTGTTGCGAACCTTTGGGAGTACAAACAGAATTCATGAATAC
aligned sequence 20-TS-FOR3-NH (20-TS-FOR3-NH.ab1)
aactccctcacagcgattaggttttttgcatcacatcaggttggttccgttatttgcctgcattctaggcggtatcttagttctattcgcattaagttca
4 6 8 10 12 14 16 18 20 22 24 26 28 30 32 34 36
T P S Q R L G F L H H I R L V P L F A C I L G G I L V L F A L S S
trg
NH1
template sequence pSR59.4 - PCR - seq - his
AACTCCCTCACAGCGATTAGGTTTTTTGCATCACATCAGGTTGGTTCCGTTATTTGCCTGCATTCTAGGCGGTATCTTAGTTCTATTCGCATTAAGTTCA
aligned sequence 20-TS-FOR3-NH (20-TS-FOR3-NH.ab1)
gccctggctggctatttcctctggcaggccgatcgcgatcagcgtgatgttactgcggagattgagattcggaccgggttagcgaacagttcagattttt
38 40 42 44 46 48 50 52 54 56 58 60 62 64 66 68
A L A G Y F L W Q A D R D Q R D V T A E I E I R T G L A N S S D F
trg
template sequence pSR59.4 - PCR - seq - his
GCCCTGGCTGGCTATTTCCTCTGGCAGGCCGATCGCGATCAGCGTGATGTTACTGCGGAGATTGAGATTCGGACCGGGTTAGCGAACAGTTCAGATTTTT
aligned sequence 20-TS-FOR3-NH (20-TS-FOR3-NH.ab1)

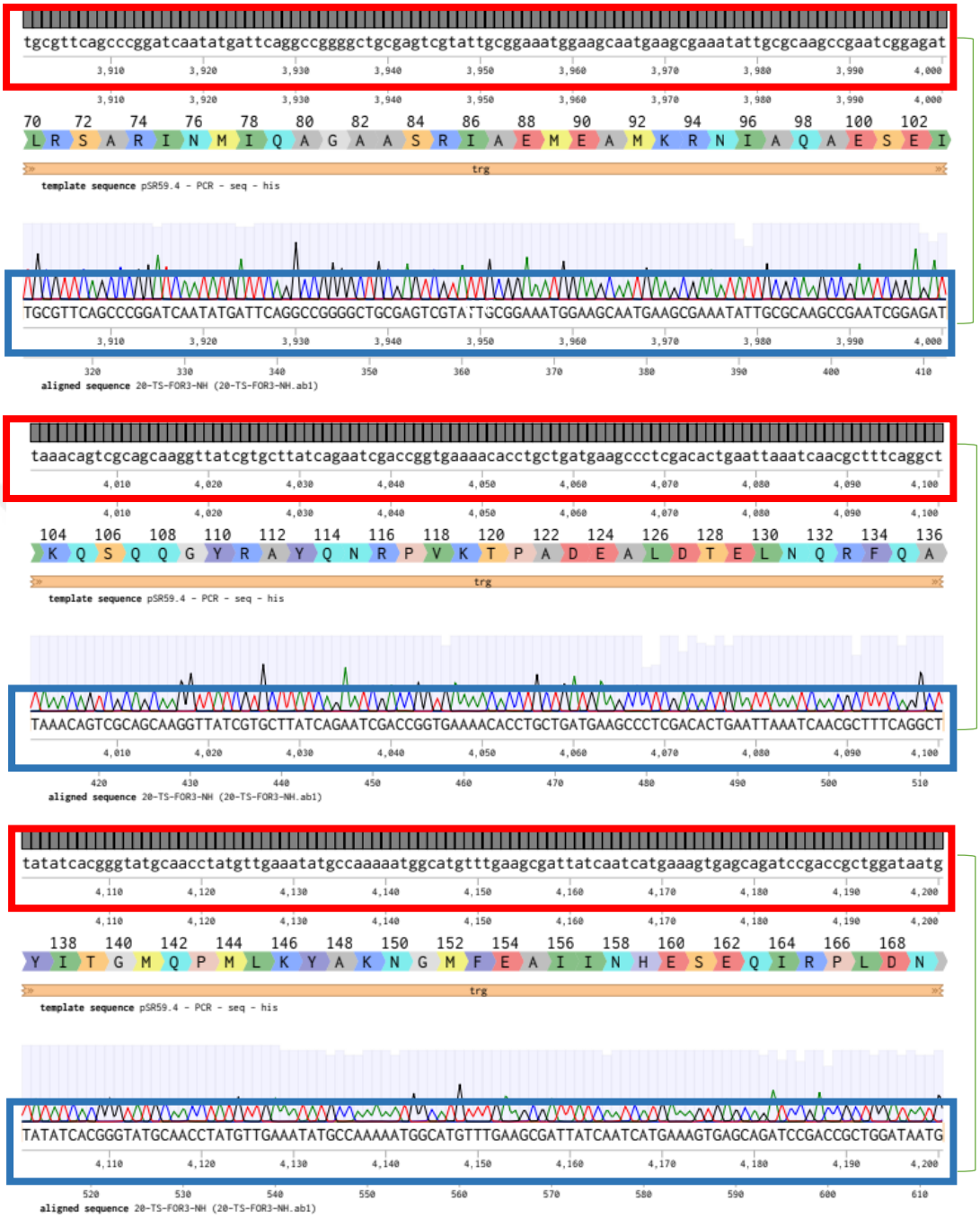
tgcgttcagcccggatcaatatgattcaggccggggctgcgagtcgtattgcggaaatggaagcaatgaagcgaaatattgcgcaagccgaatcggagat
3,910 3,920 3,930 3,940 3,950 3,960 3,970 3,980 3,990 4,000
70 72 74 76 78 80 82 84 86 88 90 92 94 96 98 100 102
L R S A R I N M I Q A G A A S R I A E M E A M K R N I A Q A E S E I
trg
template sequence pSR59.4 - PCR - seq - his
TGCGTTCAGCCCGGATCAATATGATTCAGGCCGGGGCTGCGAGTCGTATTGCGGAAATGGAAGCAATGAAGCGAAATATTGCGCAAGCCGAATCGGAGAT
320 330 340 350 360 370 380 390 400 410
aligned sequence 20-TS-FOR3-NH (20-TS-FOR3-NH.ab1)
taaacagtcgcagcaaggttatcgtgcttatcagaatcgaccggtgaaaacacctgctgatgaagccctcgacactgaattaaatcaacgctttcaggct
4,010 4,020 4,030 4,040 4,050 4,060 4,070 4,080 4,090 4,100
104 106 108 110 112 114 116 118 120 122 124 126 128 130 132 134 136
K Q S Q Q G Y R A Y Q N R P V K T P A D E A L D T E L N Q R F Q A
trg
template sequence pSR59.4 - PCR - seq - his
TAAACAGTCGCAGCAAGGTTATCGTGCTTATCAGAATCGACCGGTGAAAACACCTGCTGATGAAGCCCTCGACACTGAATTAAATCAACGCTTTCAGGCT
420 430 440 450 460 470 480 490 500 510
aligned sequence 20-TS-FOR3-NH (20-TS-FOR3-NH.ab1)
tatatcacgggtatgcaacctatgttgaaatatgccaaaaatggcatgtttgaagcgattatcaatcatgaaagtgagcagatccgaccgctggataatg
4,110 4,120 4,130 4,140 4,150 4,160 4,170 4,180 4,190 4,200
138 140 142 144 146 148 150 152 154 156 158 160 162 164 166 168
Y I T G M Q P M L K Y A K N G M F E A I I N H E S E Q I R P L D N
trg
template sequence pSR59.4 - PCR - seq - his
TATATCACGGGTATGCAACCTATGTTGAAATATGCCAAAAATGGCATGTTTGAAGCGATTATCAATCATGAAAGTGAGCAGATCCGACCGCTGGATAATG
520 530 540 550 560 570 580 590 600 610
aligned sequence 20-TS-FOR3-NH (20-TS-FOR3-NH.ab1)

Figure D6: Sequencing result alignment of Trg generated by Benchling

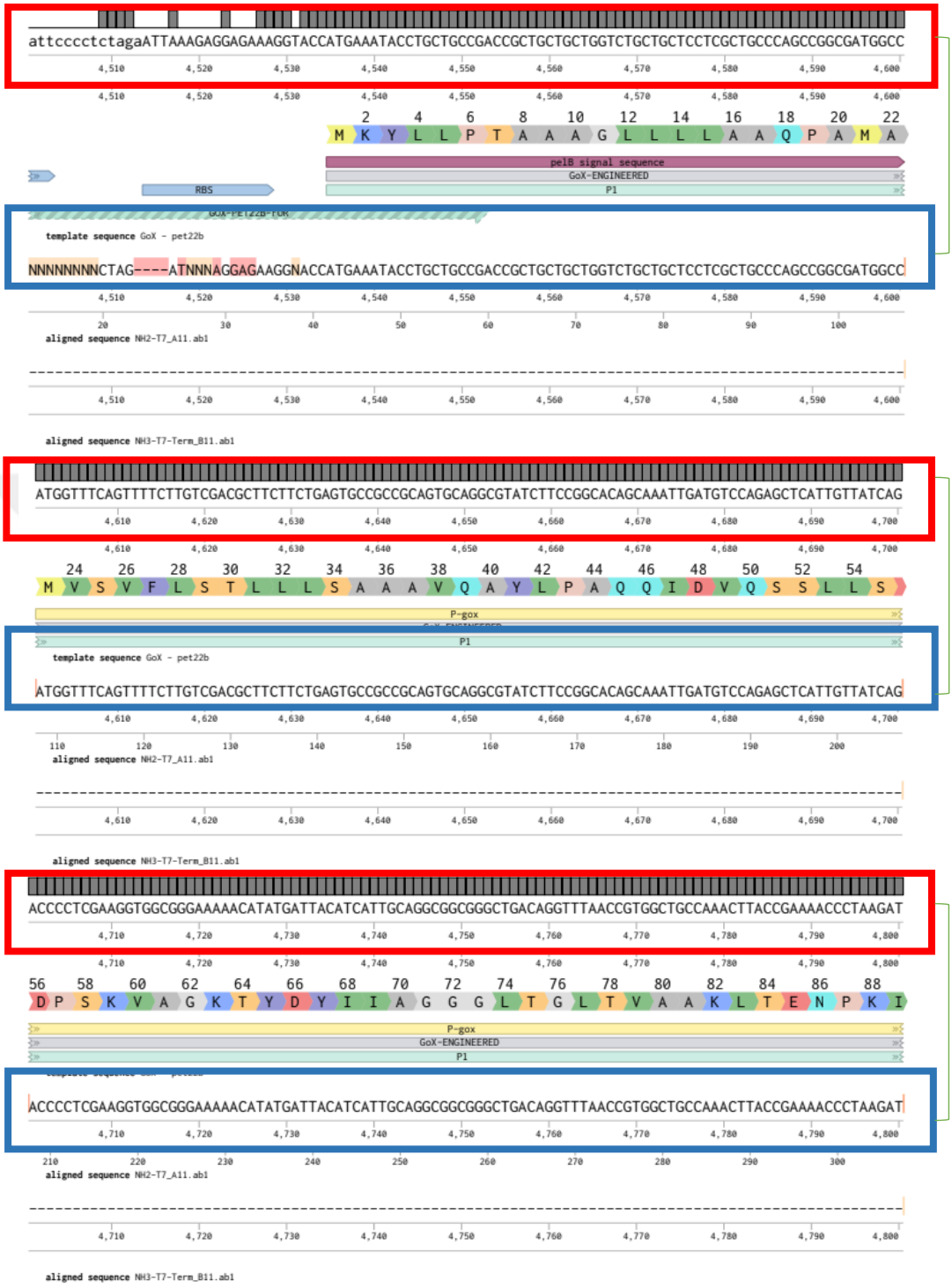
attcccctctagaATTAAAGAGGAGAAAGGTACCATGAAATACCTGCTGCCGACCGCTGCTGCTGGTCTGCTGCTCCTCGCTGCCCAGCCGGCGATGGCC
M K Y L L P T A A A G L L L L A A Q P A M A
pelB signal sequence
GoX-ENGINEERED
P1
RBS
template sequence GoX - pet22b
NNNNNNNNCTAG----ATNNNAGGAGAAGGNACCATGAAATACCTGCTGCCGACCGCTGCTGCTGGTCTGCTGCTCCTCGCTGCCCAGCCGGCGATGGCC
aligned sequence NH2-T7_A11.ab1
aligned sequence NH3-T7-Term_B11.ab1
ATGGTTTCAGTTTTCTTGTCGACGCTTCTTCTGAGTGCCGCCGCAGTGCAGGCGTATCTTCCGGCACAGCAAATTGATGTCCAGAGCTCATTGTTATCAG
M V S V F L S T L L L S A A A V Q A Y L P A Q Q I D V Q S S L L S
P-gox
P1
template sequence GoX - pet22b
ATGGTTTCAGTTTTCTTGTCGACGCTTCTTCTGAGTGCCGCCGCAGTGCAGGCGTATCTTCCGGCACAGCAAATTGATGTCCAGAGCTCATTGTTATCAG
aligned sequence NH2-T7_A11.ab1
aligned sequence NH3-T7-Term_B11.ab1
ACCCCTCGAAGGTGGCGGGAAAAACATATGATTACATCATTGCAGGCGGCGGGCTGACAGGTTTAACCGTGGCTGCCAAACTTACCGAAAACCCTAAGAT
D P S K V A G K T Y D Y I I A G G G L T G L T V A A K L T E N P K I
P-gox
GoX-ENGINEERED
P1
ACCCCTCGAAGGTGGCGGGAAAAACATATGATTACATCATTGCAGGCGGCGGGCTGACAGGTTTAACCGTGGCTGCCAAACTTACCGAAAACCCTAAGAT
aligned sequence NH2-T7_A11.ab1
aligned sequence NH3-T7-Term_B11.ab1

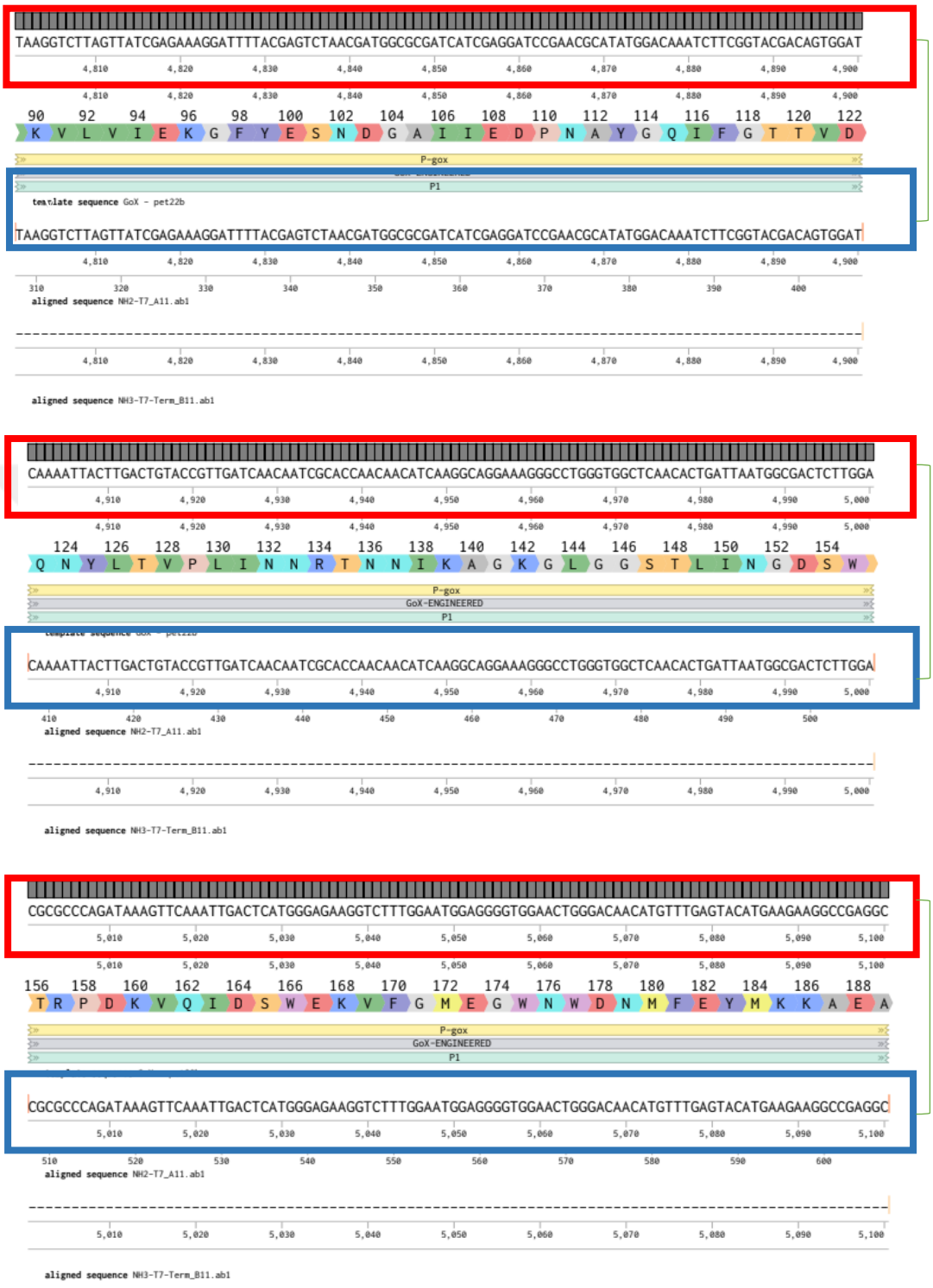
TAAGGTCTTAGTTATCGAGAAAGGATTTTACGAGTCTAACGATGGCGCGATCATCGAGGATCCGAACGCATATGGACAAATCTTCGGTACGACAGTGGAT
90 92 94 96 98 100 102 104 106 108 110 112 114 116 118 120 122
K V L V I E K G F Y E S N D G A I I E D P N A Y G Q I F G T T V D
P-gox
P1
template sequence GoX - pet22b
TAAGGTCTTAGTTATCGAGAAAGGATTTTACGAGTCTAACGATGGCGCGATCATCGAGGATCCGAACGCATATGGACAAATCTTCGGTACGACAGTGGAT
aligned sequence NH2-T7_A11.ab1
aligned sequence NH3-T7-Term_B11.ab1
CAAAATTACTTGACTGTACCGTTGATCAACAATCGCACCAACAACATCAAGGCAGGAAAGGGCCTGGGTGGCTCAACACTGATTAATGGCGACTCTTGGA
124 126 128 130 132 134 136 138 140 142 144 146 148 150 152 154
Q N Y L T V P L I N N R T N N I K A G K G L G G S T L I N G D S W
P-gox
GoX-ENGINEERED
P1
CAAAATTACTTGACTGTACCGTTGATCAACAATCGCACCAACAACATCAAGGCAGGAAAGGGCCTGGGTGGCTCAACACTGATTAATGGCGACTCTTGGA
aligned sequence NH2-T7_A11.ab1
aligned sequence NH3-T7-Term_B11.ab1
CGCGCCCAGATAAAGTTCAAATTGACTCATGGGAGAAGGTCTTTGGAATGGAGGGGTGGAACTGGGACAACATGTTTGAGTACATGAAGAAGGCCGAGGC
156 158 160 162 164 166 168 170 172 174 176 178 180 182 184 186 188
T R P D K V Q I D S W E K V F G M E G W N W D N M F E Y M K K A E A
P-gox
GoX-ENGINEERED
P1
CGCGCCCAGATAAAGTTCAAATTGACTCATGGGAGAAGGTCTTTGGAATGGAGGGGTGGAACTGGGACAACATGTTTGAGTACATGAAGAAGGCCGAGGC
aligned sequence NH2-T7_A11.ab1
aligned sequence NH3-T7-Term_B11.ab1

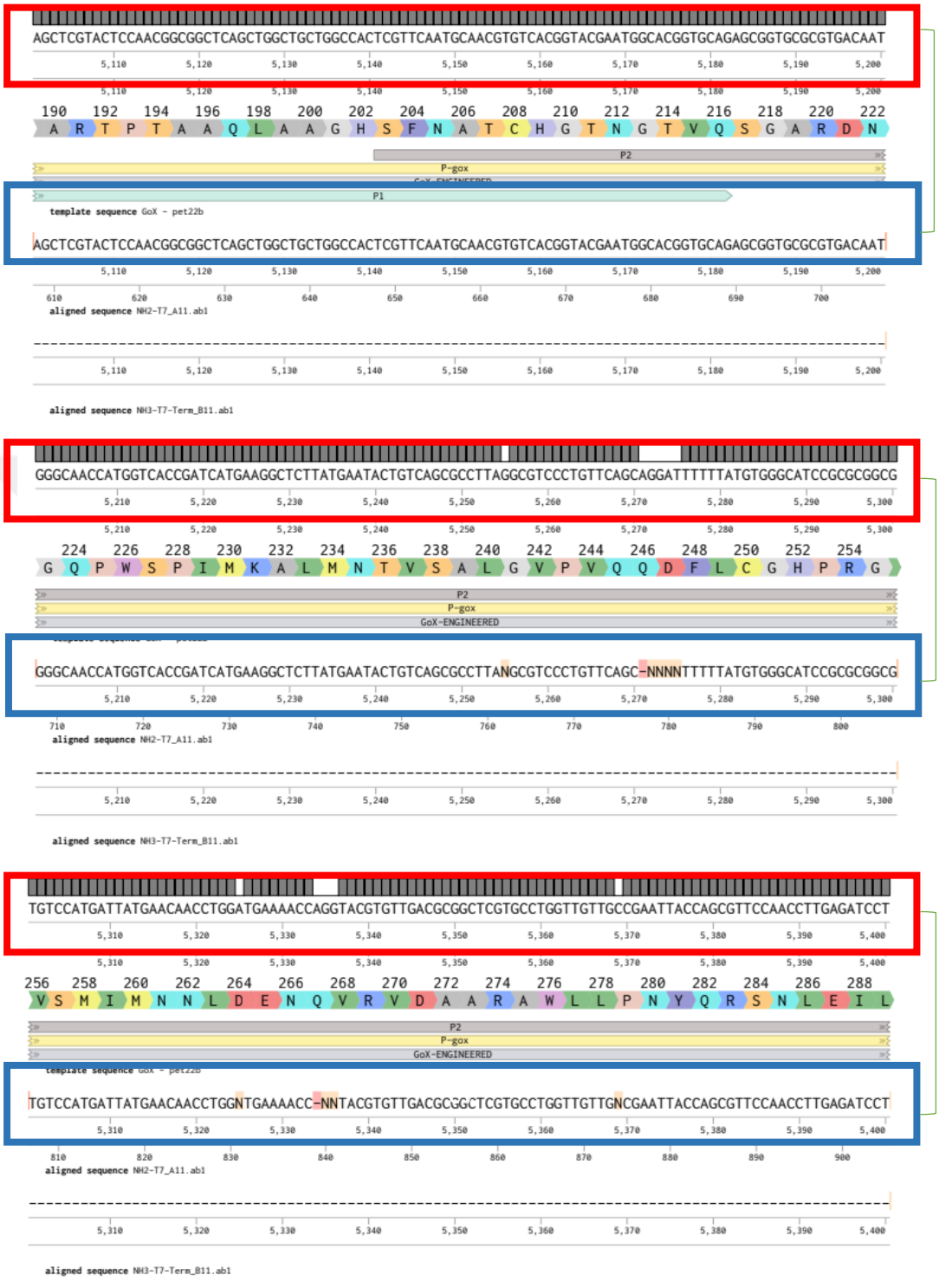
AGCTCGTACTCCAACGGCGGCTCAGCTGGCTGCTGGCCACTCGTTCAATGCAACGTGTCACGGTACGAATGGCACGGTGCAGAGCGGTGCGCGTGACAAT
5,110 5,120 5,130 5,140 5,150 5,160 5,170 5,180 5,190 5,200
190 192 194 196 198 200 202 204 206 208 210 212 214 216 218 220 222
A R T P T A A Q L A A G H S F N A T C H G T N G T V Q S G A R D N
P2
P-gox
P1
template sequence GoX - pet22b
AGCTCGTACTCCAACGGCGGCTCAGCTGGCTGCTGGCCACTCGTTCAATGCAACGTGTCACGGTACGAATGGCACGGTGCAGAGCGGTGCGCGTGACAAT
5,110 5,120 5,130 5,140 5,150 5,160 5,170 5,180 5,190 5,200
610 620 630 640 650 660 670 680 690 700
aligned sequence NH2-T7_A11.ab1
5,110 5,120 5,130 5,140 5,150 5,160 5,170 5,180 5,190 5,200
aligned sequence NH3-T7-Term_B11.ab1
GGGCAACCATGGTCACCGATCATGAAGGCTCTTATGAATACTGTCAGCGCCTTAGGCGTCCCTGTTCAGCAGGATTTTTTATGTGGGCATCCGCGCGGCG
5,210 5,220 5,230 5,240 5,250 5,260 5,270 5,280 5,290 5,300
224 226 228 230 232 234 236 238 240 242 244 246 248 250 252 254
G Q P W S P I M K A L M N T V S A L G V P V Q Q D F L C G H P R G
P2
P-gox
GoX-ENGINEERED
GGGCAACCATGGTCACCGATCATGAAGGCTCTTATGAATACTGTCAGCGCCTTANGCGTCCCTGTTCAGC-NNNNTTTTTATGTGGGCATCCGCGCGGCG
5,210 5,220 5,230 5,240 5,250 5,260 5,270 5,280 5,290 5,300
710 720 730 740 750 760 770 780 790 800
aligned sequence NH2-T7_A11.ab1
5,210 5,220 5,230 5,240 5,250 5,260 5,270 5,280 5,290 5,300
aligned sequence NH3-T7-Term_B11.ab1
TGTCCATGATTATGAACAACCTGGATGAAAACCAGGTACGTGTTGACGCGGCTCGTGCCTGGTTGTTGCCGAATTACCAGCGTTCCAACCTTGAGATCCT
5,310 5,320 5,330 5,340 5,350 5,360 5,370 5,380 5,390 5,400
256 258 260 262 264 266 268 270 272 274 276 278 280 282 284 286 288
V S M I M N N L D E N Q V R V D A A R A W L L P N Y Q R S N L E I L
P2
P-gox
GoX-ENGINEERED
template sequence GoX - pet22b
TGTCCATGATTATGAACAACCTGGNTGAAAACC-NNTACGTGTTGACGCGGCTCGTGCCTGGTTGTTGNCGAATTACCAGCGTTCCAACCTTGAGATCCT
5,310 5,320 5,330 5,340 5,350 5,360 5,370 5,380 5,390 5,400
810 820 830 840 850 860 870 880 890 900
aligned sequence NH2-T7_A11.ab1
5,310 5,320 5,330 5,340 5,350 5,360 5,370 5,380 5,390 5,400
aligned sequence NH3-T7-Term_B11.ab1


GGGTCAGGCCGTCTTCTTCGCTAACTTCACCGAAACATTCGGCGATTACGCTCCGCAGGCACGCGACTTGTTAAACACCAAGCTTGACCAGTGGGCTGAA
5,710 5,720 5,730 5,740 5,750 5,760 5,770 5,780 5,790 5,800
390 392 394 396 398 400 402 404 406 408 410 412 414 416 418 420 422
G Q A V F F A N F T E T F G D Y A P Q A R D L L N T K L D Q W A E
P2
P-gox
GoX-ENGINEERED
P3
template sequence GoX - pet22b
aligned sequence NH2-T7_A11.ab1
GGGTCAGGCCGTCTTCTTCGCTAACTTCACCGAAACATTCGGCGATTACGNTCCGCAGGCACGCGACTTGTTAAACACCAAGCTTGACCAGTGGGCTGAA
70 80 90 100 110 120 130 140 150 160
aligned sequence NH3-T7-Term_B11.ab1
GAGACTGTTGCCCGCGGCGGATTCCACAACGTTACCGCCTTAAAGGTACAATATGAAAACTACCGTAATTGGCTGTTAGACGAAGACGTTGCCTTTGCAG
5,810 5,820 5,830 5,840 5,850 5,860 5,870 5,880 5,890 5,900
424 426 428 430 432 434 436 438 440 442 444 446 448 450 452 454
E T V A R G G F H N V T A L K V Q Y E N Y R N W L L D E D V A F A
P-gox
GoX-ENGINEERED
P3
template sequence GoX - pet22b
aligned sequence NH2-T7_A11.ab1
GAGACTGTTGCCCGCGGCGGATTCCACAACGTTACCGCCTTAAAGGTACAATATGAAAACTACCGTAATTGGCTGTTAGACGAAGACGTTGCCTTTGCAG
170 180 190 200 210 220 230 240 250 260
aligned sequence NH3-T7-Term_B11.ab1
AACTTTTCATGGATACAGAGGGGAAGATCAATTTTGATCTTTGGGACCTTATTCCGTTCACTCGTGGTAGCGTCCATATCCTGTCGAGCGATCCCTATTT
5,910 5,920 5,930 5,940 5,950 5,960 5,970 5,980 5,990 6,000
456 458 460 462 464 466 468 470 472 474 476 478 480 482 484 486 488
E L F M D T E G K I N F D L W D L I P F T R G S V H I L S S D P Y L
P-gox
GoX-ENGINEERED
P3
template sequence GoX - pet22b
aligned sequence NH2-T7_A11.ab1
AACTTTTCATGGATACAGAGGGGAAGATCAATTTTGATCTTTGGGACCTTATTCCGTTCACTCGTGGTAGCGTCCATATCCTGTCGAGCGATCCCTATTT
270 280 290 300 310 320 330 340 350 360
aligned sequence NH3-T7-Term_B11.ab1


GTGGCAATTTGCCAACGATCCTAAATTTTTCCTTAACGAGTTTGATTTGCTTGGCCAGGCAGCTGCTTCAAAACTTGCTCGCGACTTGACGTCACAAGGT
6,010 6,020 6,030 6,040 6,050 6,060 6,070 6,080 6,090 6,100
490 492 494 496 498 500 502 504 506 508 510 512 514 516 518 520 522
W Q F A N D P K F F L N E F D L L G Q A A A S K L A R D L T S Q G
P-gox
GoX-ENGINEERED
P3
template sequence GoX - pet22b
aligned sequence NH2-T7_A11.ab1
GTGGCAATTTGCCAACGATCCTAAATTTTTCCTTAACGAGTTTGATTTGCTTGGCCAGGCAGCTGCTTCAAAACTTGCTCGCGACTTGACGTCACAAGGT
370 380 390 400 410 420 430 440 450 460
aligned sequence NH3-T7-Term_B11.ab1
GCCATGAAAGAGTACTTCGCGGGCGAAACGTTGCCTGGTTATAACCTTGTCCAGAACGCAACGCTTTCCCAGTGGTCGGACTATGTCTTGCAAAACTTCC
6,110 6,120 6,130 6,140 6,150 6,160 6,170 6,180 6,190 6,200
524 526 528 530 532 534 536 538 540 542 544 546 548 550 552 554
A M K E Y F A G E T L P G Y N L V Q N A T L S Q W S D Y V L Q N F
P-gox
GoX-ENGINEERED
P3
template sequence GoX - pet22b
aligned sequence NH2-T7_A11.ab1
GCCATGAAAGAGTACTTCGCGGGCGAAACGTTGCCTGGTTATAACCTTGTCCAGAACGCAACGCTTTCCCAGTGGTCGGACTATGTCTTGCAAAACTTCC
470 480 490 500 510 520 530 540 550 560
aligned sequence NH3-T7-Term_B11.ab1
GCCCAAACTGGCATGCCGTTTCCAGTTGTAGTATGATGTCTCGTGAGTTGGGCGGTGTGGTGGACGCAACCGCGAAGGTTTATGGCACGCAAGGACTGCG
6,210 6,220 6,230 6,240 6,250 6,260 6,270 6,280 6,290 6,300
556 558 560 562 564 566 568 570 572 574 576 578 580 582 584 586 588
R P N W H A V S S C S M M S R E L G G V V D A T A K V Y G T Q G L R
P-gox
GoX-ENGINEERED
P3
template sequence GoX - pet22b
aligned sequence NH2-T7_A11.ab1
GCCCAAACTGGCATGCCGTTTCCAGTTGTAGTATGATGTCTCGTGAGTTGGGCGGTGTGGTGGACGCAACCGCGAAGGTTTATGGCACGCAAGGACTGCG
570 580 590 600 610 620 630 640 650 660
aligned sequence NH3-T7-Term_B11.ab1

Figure D7: Sequencing result alignment of GoX generated by Benchling.

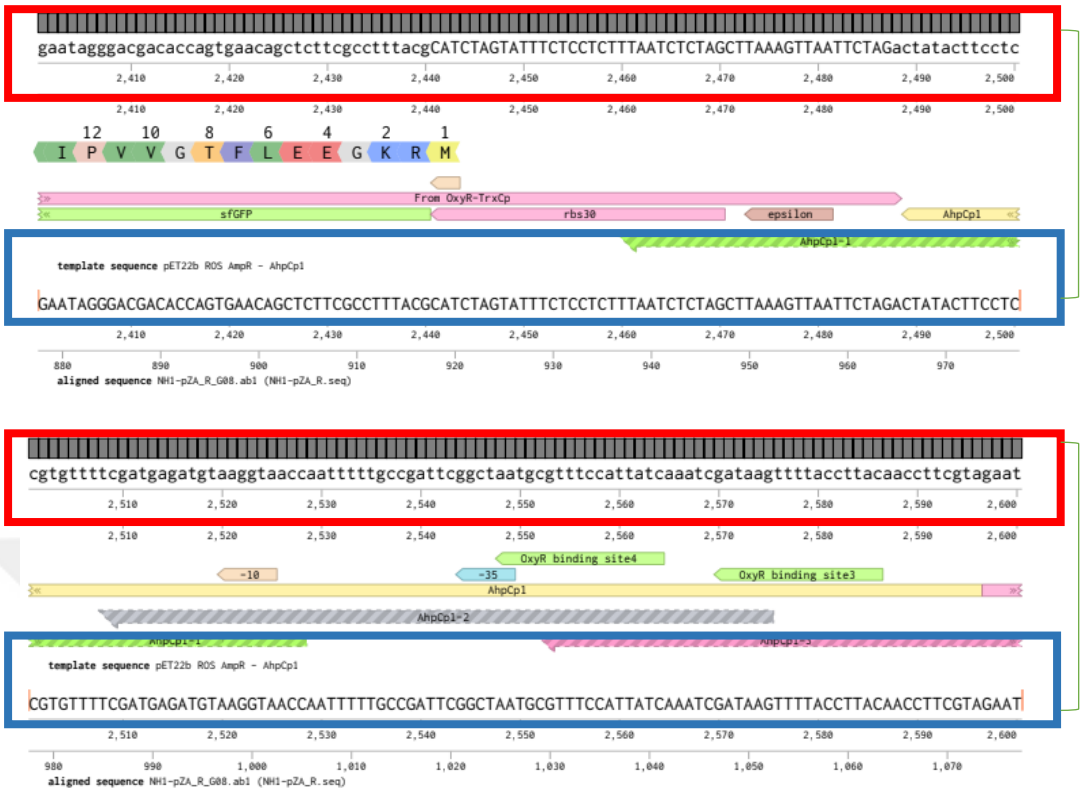

Figure D8: Sequence alignment of AhpCp1 promoter generated by Benchling.


actttAAGGAGggatccAatggctgcacatgaactaaaagaagccttagaaacgttgaaggaaaccggagttcgcattactcctcaacgtcatgcgattc
M A A H E L K E A L E T L K E T G V R I T P Q R H A I
PerR Bacillus
pZA-H2O2-S3-Rev
PerR-For
template sequence pZA-H2O2-AhpCp1/PerR
ACTTTAAGGAGGGATCCAATGGCTGCACATGAACTAAAAGAAGCCTTAGAAACGTTGAAGGAAACCGGAGTTCGCATTACTCCTCAACGTCATGCGATTC
aligned sequence NH1-rec-seq-rev (NH1-rec-seq-rev.ab1)
tggaatatctcgttaactctatggctcatccaacagcggacgatatatataaagctctggaagggaaatttcctaacatgagcgtagcgacggtatataa
L E Y L V N S M A H P T A D D I Y K A L E G K F P N M S V A T V Y N
PerR Bacillus
template sequence pZA-H2O2-AhpCp1/PerR
TGGAATATCTCGTTAACTCTATGGCTCATCCAACAGCGGACGATATATATAAAGCTCTGGAAGGGAAATTTCCTAACATGAGCGTAGCGACGGTATATAA
aligned sequence NH1-rec-seq-rev (NH1-rec-seq-rev.ab1)
caatttgcgtgtgttccgggaatcaggtttggtaaaagagctcacatacggtgatgcttccagcagattcgattttgtcacatccgatcactatcacgcg
N L R V F R E S G L V K E L T Y G D A S S R F D F V T S D H Y H A
PerR Bacillus
template sequence pZA-H2O2-AhpCp1/PerR
CAATTTGCGTGTGTTCCGGGAATCAGGTTTGGTAAAAGAGCTCACATACGGTGATGCTTCCAGCAGATTCGATTTTGTCACATCCGATCACTATCACGCG
aligned sequence NH1-rec-seq-rev (NH1-rec-seq-rev.ab1)

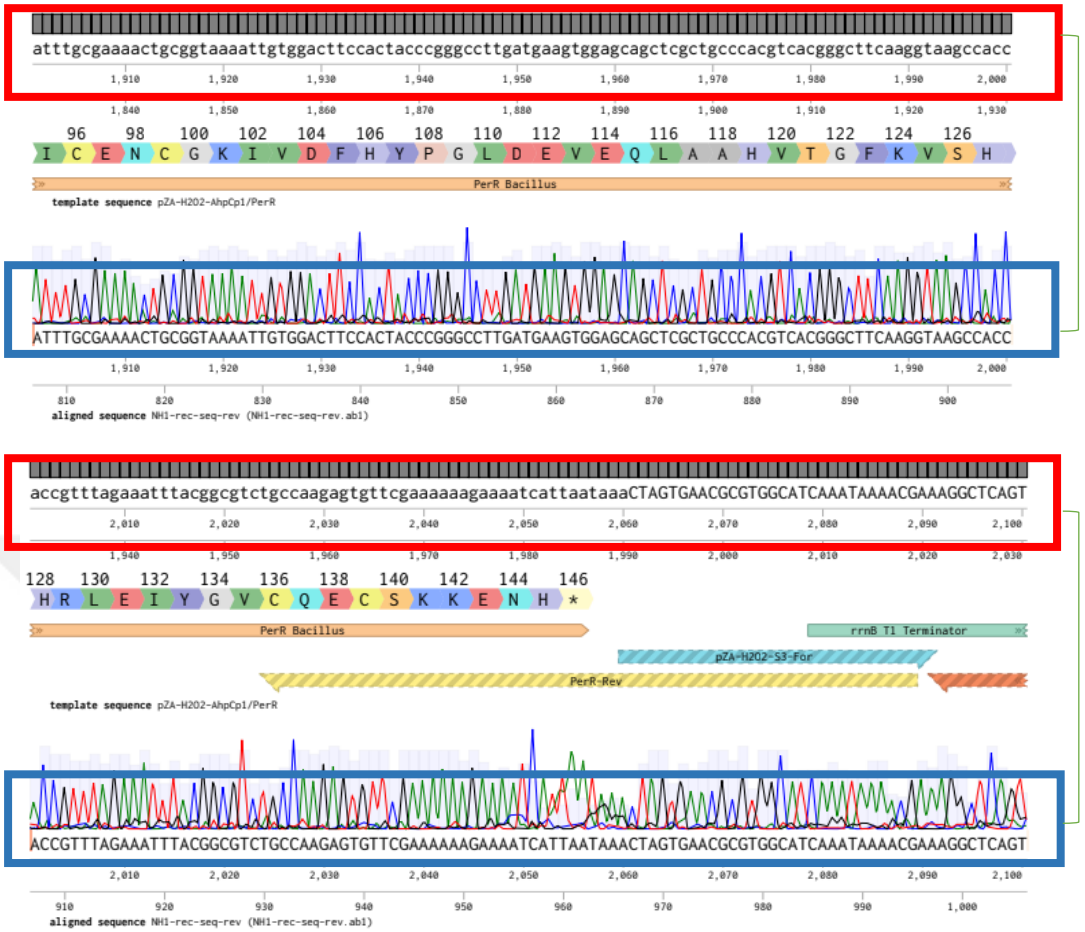

Figure D9: Sequencing result alignment of PerR generated by Benchling.

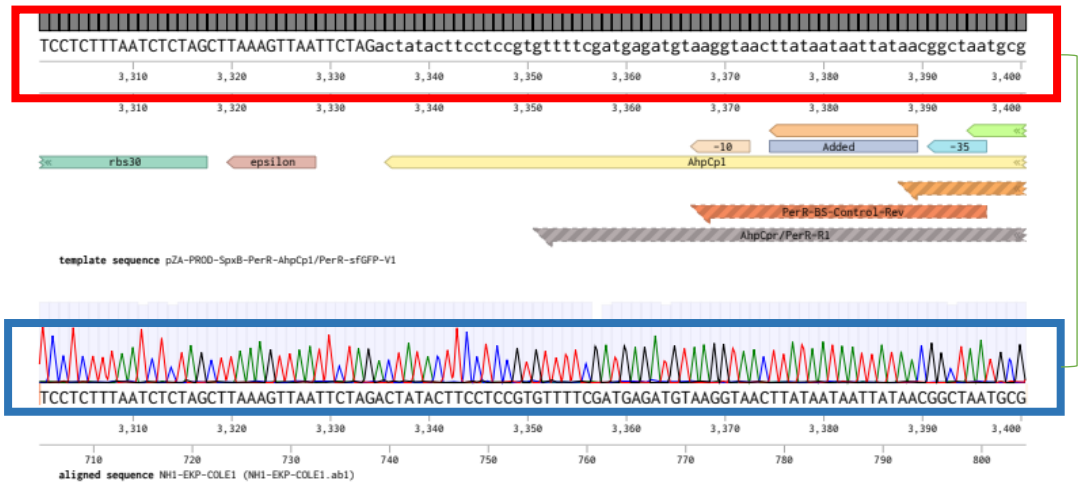

Figure D10: Sequencing result alignment of hybrid Ahp/Per generated by Benchling.


gctggtttccaaccaacacggtaagcagaacctgtcaaaccttcatagttccattcgaaagcttcaaagtttttaccagttgtgatgattggtgctttga
2,510 2,520 2,530 2,540 2,550 2,560 2,570 2,580 2,590 2,600
264 262 260 258 256 254 252 250 248 246 244 242 240 238 236 234 232
A P K W G V R Y A S G T L G E Y N W E F A E F N K G T T I I P A K I
spxB
template sequence pZA-PROD-PerR-AhpCp1/PerR-spxB-sfGFP-V2
GCTGGTTTCCAACCAACACGGTAAGCAGAACCTGTCAAACCNTCATAGTTCCATTCGAAAGCTTCAAAGTTTTTACCAGTTGTGATGATTGGTGCTTTGA
2,510 2,520 2,530 2,540 2,550 2,560 2,570 2,580 2,590 2,600
310 320 330 340 350 360 370 380 390 400
aligned sequence NH5-PTTO (NH5-PTTO.ab1)
ttttacgtgacaattcagtaatcacttcaccagctttaacaccaccaaatccagcatagataactgggcgttcagcattgttcaagatttcaacagcttt
2,610 2,620 2,630 2,640 2,650 2,660 2,670 2,680 2,690 2,700
230 228 226 224 222 220 218 216 214 212 210 208 206 204 202 200 198
K R S L E T I V E G A K V G G F G A Y I V P R E A N N L I E V A K
spxB
template sequence pZA-PROD-PerR-AhpCp1/PerR-spxB-sfGFP-V2
TTTTACGTGACAATTCAGTAATCACTTCACCAGCTTTAACACCACCAAATCCAGCATAGATAACTGGGCGTTCAGCATTGTTCAAGATTTCAACAGCTTT
2,610 2,620 2,630 2,640 2,650 2,660 2,670 2,680 2,690 2,700
410 420 430 440 450 460 470 480 490 500
aligned sequence NH5-PTTO (NH5-PTTO.ab1)
gtcgatttcaacttcgttcaaagcaggagcgatgaatgagcgttcgtatgaacctgaaccgtagtatgagttttcgtcgatttcttggaaaccgaagttt
2,710 2,720 2,730 2,740 2,750 2,760 2,770 2,780 2,790 2,800
196 194 192 190 188 186 184 182 180 178 176 174 172 170 168 166
D I E V E N L A P A I F S R E Y S G S G Y Y S N E D I E Q F G F N
spxB
template sequence pZA-PROD-PerR-AhpCp1/PerR-spxB-sfGFP-V2
GTCGATTTCAACTTCGTTCAAAGCAGGAGCGATGAATGAGCGTNNGTATGAACNTGAACCGTAGTATGAGTTTTCGTCGATTTCTTGGAAACCGAAGTTT
2,710 2,720 2,730 2,740 2,750 2,760 2,770 2,780 2,790 2,800
510 520 530 540 550 560 570 580 590 600
aligned sequence NH5-PTTO (NH5-PTTO.ab1)


template sequence pZA-PROD-PerR-AhpCp1/PerR-spxB-sfGFP-V2
aligned sequence NH5-PTTO (NH5-PTTO.ab1)
template sequence pZA-PROD-PerR-AhpCp1/PerR-spxB-sfGFP-V2
aligned sequence NH5-PTTO (NH5-PTTO.ab1)

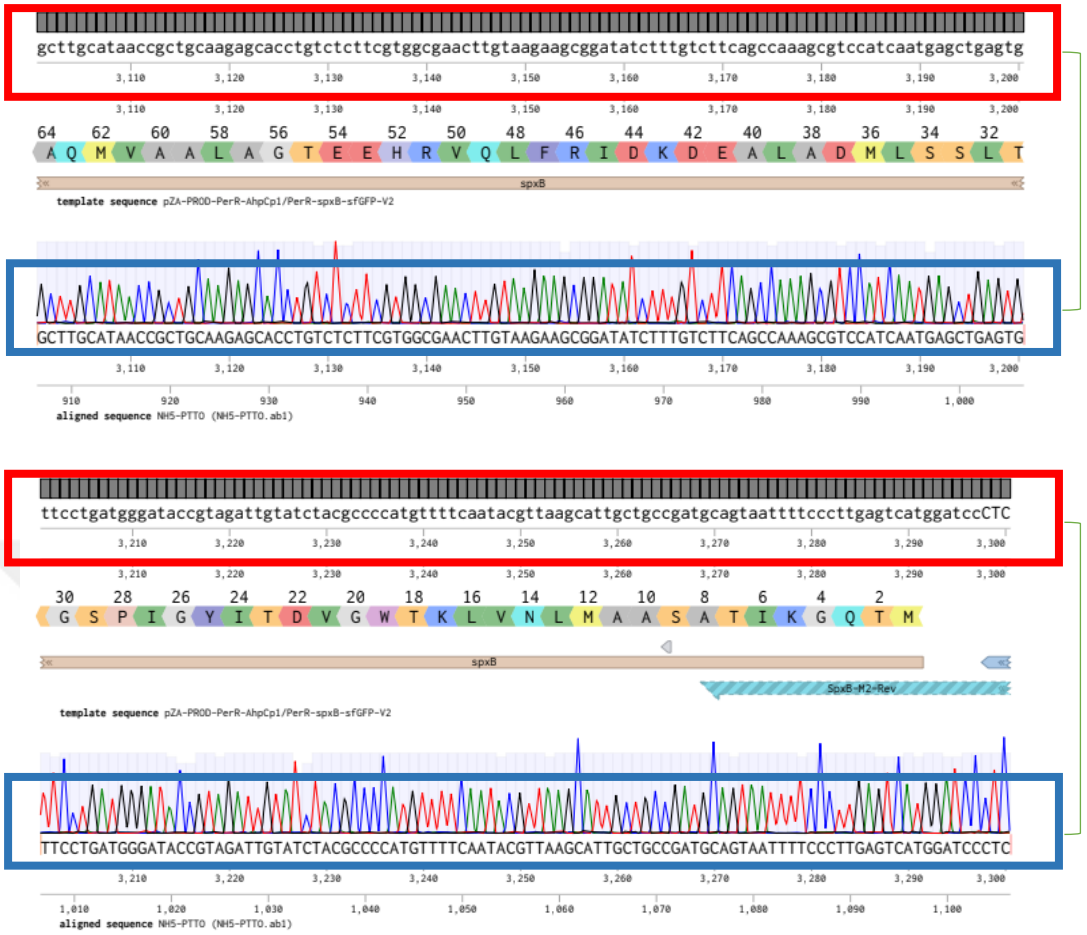

Figure D11: Sequencing result alignment of SpxB initial region generated by Benchling.

APPENDIX E

Additional reaction recipes and methods

LB Medium Recipe for 1 L	
H20	950 mL
Tryptone	10 g
NaCl	10 g
Yeast Extract	5 g
Agar (For LB Agar)	15 g

Table E1: LB and LB Agar medium recipes

TSS Buffer	
PEG 8000	5 g
1M $MgCl_2$	1.5 g
DMSO	2.5 g
Add LB to 50 mL, filter sterilize	

Table E2: TSS Buffer recipe

T4 Ligation Mix 20 µL	
T4 DNA Ligase Buffer (10X)	2 µL
Backbone DNA	50 ng
Insert DNA	37.5 ng
T4 DNA Ligase	1 µL
Add water up to 20 µL	

Table E3: T4 Ligation Mix recipe

Gibson Mix Stock	
Taq ligase (40u/µl)	50µl
5x isothermal buffer	100µl
T5 exonuclease (1u/µl)	2µl
Phusion polymerase	6.25µl
Nuclease-free water	216.75µl

Table E4: Gibson Mix stock recipe

SOC Medium	
Yeast Extract	0.5%
Tryptone	2%
NaCl	10 mM
KCl	2.5 mM
MgCl2	10 mM
MgSO4	10 mM
Glucose	20 mM

Table E5: SOC medium recipe

TAE Buffer (50X)	
EDTA disodium salt	50 Mm
Tris	2 M
Glacial accetic acid	1 M

Table E6: TAE Buffer (50X) recipe

1X PBS (Phosphate Buffered Saline) Buffer, 1 L	
NaCl	8 g
KCl	0.2 g
Na_2HPO_4	1.44 g
KH_2PO_4	0.24 g

Table E7: 1X PBS (Phosphate Buffered Saline) Buffer recipe

GOX Test Buffer	
ABTS	50 mg
D-Glucose	90 mg
HRP	50 mg
PBS	50 mL

Table E8: GOX Test Buffer recipe

TEV Protease Buffer	
Tris-HCl (pH 7.5)	50 mM
DTT	5 mM
EDTA	1 mM
Triton X-100	0.1%
Glycerol	50% (v/v)

Table E9: TEV Protease Buffer recipe

	Stacking Gel	**Resolving Gel (12%)**
30% Acrylamide-Bis	1.98 mL	6 mL
0.5 M Tris-HCl (pH: 6.8)	3.78 mL	-
1.5 M Tris-HCl (pH: 8.8)	-	3.75 mL
10% SDS	150 µL	150 µL
Distilled water	9 mL	5.03 mL
TEMED	15 µL	7.5 µL
10% SDS	75 µL	75 µL
Total volume	15 mL	15 mL

Table E10: 12% SDS-PAGE Gel recipe